Analysis and design of stainless steel reinforced concrete structural elements

By

Musab Mohammad Rabi

A thesis submitted for the degree of Doctor of Philosophy

College of Engineering, Design and Physical Science

Brunel University London

December 2019

Abstract

Stainless steel reinforced concrete has seen a large increase in usage in recent years, in response to the ever-increasing demands for structures and infrastructure to be more durable, efficient and sustainable. Stainless steel has excellent corrosion resistance, as well as many other distinctive properties such as excellent strength and ductility, ready availability and a long, low-maintenance, life cycle. On the other hand, one of the fundamental challenges that dramatically limits the lifetime and reliability of traditional carbon steel reinforced concrete is corrosion of the reinforcement, especially in harsh environments such as coastal, marine or industrial settings. With the increased focus on environmentally conscious and reliable design, stainless steel reinforcement represents an ideal solution for the corrosion and deterioration problems faced by reinforced concrete structures, as well as the associated maintenance issues. However, it is also has a higher initial cost, and therefore needs to be used carefully and efficiently.

The existing material models provided for the structural analysis of reinforced concrete members in current design standards, such as Eurocode 2, are not appropriate for stainless steel reinforced concrete and lead to inaccurate predictions of the section capacity. Generally, there is a lack of data in the public domain regarding the behaviour of concrete beams reinforced with stainless steel, mainly owing to this being a relatively new and novel topic. This is especially true for the important issue of bond strength and the relationship that exists between the reinforcement and the surrounding concrete. Currently, existing design standards advise using the same design rules for stainless steel reinforced concrete as traditional carbon steel reinforced concrete, owing to a lack of alternative information, although this is not based on test or performance data. As such, there is a real need to develop a full and fundamental understanding of the behaviour of stainless steel reinforced concrete, to achieve more sustainable and reliable design methods for reinforced concrete structures.

In this context, this thesis provides a detailed background of the existing information on stainless steel reinforced concrete, as well a discussion on the potential advantages and challenges. Then, attention is given to analysing the behaviour of stainless steel reinforced concrete beams by developing the Continuous Strength Method to predict the bending moment capacity. A finite element model has been developed in order to further assess the performance, and this is also used to conduct a parametric study of the most influential properties. It is concluded that the proposed analytical models provide a reliable solution for predicting the capacity of concrete beams reinforced with stainless steel.

In addition, this thesis investigates the bond behaviour of stainless steel reinforced concrete and compares the performance to traditional carbon steel reinforced concrete, through experimental testing and analysis. It also compares the results to existing design rules in terms of bond strength, anchorage length and lap length. It is shown that stainless steel rebar generally develops lower bond strength with the surrounding concrete compared with equivalent carbon steel reinforcement. Moreover, it is shown that existing design codes are extremely conservative and generally underestimate the actual bond strength by a significant margin. Therefore, following detailed analysis, it is concluded that current design rules can be safely applied for stainless steel rebar, although more accurate and efficient methods can be achieved. Hence, new design parameters are proposed reflecting the bond behaviour of stainless steel rebars, so that more efficient designs can be achieved.

List of publications

The work presented in this thesis has led to a list of publications and conferences, as follows:

Journals

- **Rabi, M.,** Cashell, K. and Shamass, R. (2019) 'Flexural analysis and design of stainless steel reinforced concrete beams', Engineering Structures, 198, pp. 109432.
- **Rabi, M.,** Cashell, K. and Shamass, R. 'Ultimate and serviceability analysis of stainless steel reinforced concrete beams', (Submitted to Structures).
- **Rabi, M.,** Cashell, K., Shamass, R. and Desnerck, P. 'Bond behaviour of stainless steel reinforced concrete', (Submitted to Engineering Structures).

Conferences

- **Rabi, M.,** Cashell, K.A. and Shamass, R. (2019) 'Analysis of concrete beams reinforced with stainless steel'. Proceedings of the fib Symposium 2019: Concrete-Innovations in Materials, Design and Structures, Krakow, Poland, (pp. 690-697).
- **Rabi, M.,** Cashell, K.A. (2019) 'Investigation on the behaviour of concrete beams with stainless steel reinforcement', 21st Young research conference, the institution of structural engineers (IStructE), London, UK.
- **Rabi, M.,** Cashell, K.A. (2019) 'Design of reinforced concrete beams with stainless steel', Civil and Environmental Engineering research conference, London, UK.
- **Rabi, M.,** Cashell, K.A. (2019) 'Novel design approach for stainless steel reinforced concrete beams', Brunel University research student conference, London, UK.

Acknowledgment

First and foremost, I am very grateful and thankful to Allah, the most gracious and merciful, for guiding me to the right path and providing me with countless bounties and blessings through all the stages of my life. Millions of thanks to my supervisor Dr Katherine Cashel for the time, expertise, knowledge and guidance. This thesis could not be accomplished without her feedback and continuous support. I would like to thank Dr Rabee Shamass for providing invaluable comments and insightful suggestions. I also appreciate the PhD studentship received from Jerash University. Exceptional thanks to my parents for their endless support and encouragement, without them I would not be able to achieve this. I would like to express my special thanks to my beloved wife Noor for her spiritual and emotional support and for her always stuck with me in the tough times. Last but not least, many thanks to all my loyal friends and colleagues, namely Dr Mazen Al-Kheetan and Asif Mohammed, who made my time through the PhD journey unforgettable.

Contents

List of Figures

List of Tables

List of notation

This list defines the symbols used in this thesis. However, those are not included here are defined in the text as appropriate.

$\sigma_{0.2}$	0.2% proof strength of reinforcement
σ_u	Ultimate strength of reinforcement
f_y	Yield strength of reinforcement
f_{yk}	Characteristic yield strength of reinforcement
f_{yd}	Design yield strength of reinforcement
f_{cm}	Mean compressive strength of concrete
f_c	Characteristic cylinder compressive strength of concrete
f_t	Ultimate tensile strength of concrete
f_{ctd}	Characteristic design tensile concrete strength
f_{b0}/f_{c0}	Ratio of the strength in the biaxial state to the strength in the uniaxial state
σ_{sd}	Stress in the bar to be anchored by bond over the anchorage length
σ_{true}	True stress
f_{bd}	Design bond strength
$f_{bd,0}$	Basic bond strength
$\tau_{bu,split}$	Bond strength for splitting failure
τ_{bf}	Constant residual bond strength
F_t	Internal tensile forces in the beam
F_c	Internal compression forces in the beam
P	Applied load
E	Young's modulus
E_2	Tangent modulus at the 0.2% proof stress

E_{sh}	Slope of the strain hardening region
E_u	Tangent modulus at the ultimate stress
E_{sec}	Secant modulus of elasticity
E_{tan}	Tangent modulus of elasticity
E_{cm}	Elastic modulus of concrete
ε_u	Ultimate strain
$\varepsilon_{0.2}$	0.2% strain
ε_y	Yield strain
ε_{true}	true strain
ε_{cu}	Compressive ultimate strain of concrete
ε_{c1}	Compressive strain at the peak stress of concrete
ε_c^{in}	Inelastic strain of concrete
ε_{cr}	Tensile ultimate strain of concrete
n	Strain hardening constant
m	Strain hardening constant
A	Reinforcement elongation
A_s	Reinforcement area
$A_{s,cal}$	Designed reinforcement area
$A_{s,ef}$	Actual reinforcement area
ρ	Reinforcement ratio
ρ_{bal}	Balanced reinforcement ratio
ρ_{min}	Minimum reinforcement ratio
d_c	Compressive damage parameter of concrete
d_t	Tensile damage parameter of concrete

d	Position reinforcement from the top fibre of the cross-section
y	Depth of neutral axis
κ_{su}	Limiting curvature for reinforcement failure
κ_{cu}	Limiting curvature for concrete failure
M_{pl}	Plastic bending moment
M_{cr}	Bending moment at cracking load
M_a	Bending moment at service load
δ_{max}	Max deflection
δ_1	Deflection for un-cracked section
δ_2	Deflection for cracked section
ζ	Distribution coefficient represented the tension stiffening phenomenon
β	Loading duration coefficient
I_g	Gross second moment of area
I_{cr}	Second moment of area for cracked section
L	Clear span in the beam
a	The distance between the support and the position of the load
ϕ	Bar diameter
f_P	Relative rib area
F_P	Area of the longitudinal section of a single rib
c	Rib spacing
c_{clear}	Clear distance between adjacent ribs
β°	Rib inclination
I_{bd}	Design anchorage length

$I_{b,rqd}$	Basic anchorage length
$I_{bd,min}$	Minimum design anchorage length
I_0	Design lap length
$I_{0,min}$	Minimum design lap length

Chapter 1: Introduction

1.1 General

In response to growing demands for civil engineering structures and infrastructure to be more durable, sustainable and efficient, stainless steel has emerged as a very attractive material for many applications. It is available in several different forms including sheet, plate and bar products as well as structural sections. Stainless steel elements are corrosion resistant with low or negligible maintenance requirements and also offer excellent strength, ductility, toughness, recyclability and fatigue properties. Of course, they are considerably more expensive than traditional carbon steel and therefore must be used efficiently and in appropriate applications. Until recently, their most common use in load-bearing applications was as bare structural sections such as beams, columns, etc. However, the current thesis is focussed on a relatively new application for stainless steel which as reinforcement in concrete structures.

1.2 Research significance

The subject of durability, resilience and efficiency of structures and infrastructure is highly topical at the current time, especially following the Polcevera Viaduct tragedy in Italy 2018 (Smale, K., 2018). Whilst there are ever-increasing demands for civil engineering structures and infrastructure to be more durable, there are also huge pressures for them to remain in service for long periods without requiring rehabilitative or remedial works, to be more efficient in terms of material usage, and to be more resilient to both natural and man-made environments and scenarios. It is estimated that Western Europe spends around €5 billion annually to repair corroding concrete infrastructure (Markeset et al., 2006), with a corresponding figure of $8.3 billion for the United States (Kalina et al., 2011). In addition, there can be significant further indirect costs associated with important infrastructure being out-of-service. In this context, there is a high demand to improve the life-time performance of reinforced concrete structures, especially for those subjected to sensitive or harsh environments such as bridges, tunnels and marine structures.

There is a huge demand to improve the durability and life-cycle of reinforced concrete structures. The typical approach is to increase the concrete cover or to control the alkalinity of concrete (British Highways Authority, 2003). However, in aggressive conditions, these measures may not be sufficient to prevent a significant corrosion problem. In this context, the use of stainless steel reinforcement represents an ideal solution for exposed reinforced concrete structures. Replacing the traditional carbon steel reinforcement with stainless steel improves the expected life time of these structures and may also significantly reduce the costs associated with expensive inspection and rehabilitation works. Although the initial cost of stainless steel reinforcement is relatively high compared to that of traditional carbon steel, the use of stainless steel reinforcing bar can reduce the overall maintenance costs up to 50% (Cramer et al., 2002).

1.3 Knowledge gap

Current design codes such as Eurocode 2 (EN 1992-1-1, 2004) do not include explicit rules for stainless steel reinforced concrete structures. Moreover, the standards do not incorporate efficient approaches for designing structures with stainless steel reinforcement as the given material models for the reinforcement do not fully exploit the significant strain hardening characteristics and high levels of ductility that are present for stainless steel. The behaviour of stainless steel is quite different from that of carbon steel in that carbon steel has a linear elastic response with a well-defined yield point and yield plateau, followed by a moderate degree of strain hardening. On the other hand, stainless steel exhibits a predominantly non-linear and continuous stress-strain response without a clearly-defined yield point as well as significant levels of strain hardening. However, as stated before, current design approaches do not include specific rules for stainless steel reinforced concrete, and generally suggest using the same criteria as for traditional carbon steel reinforced concrete. The existing material models provided for the structural analysis of reinforced concrete members in current design standards, such as Eurocode 2, are not appropriate for stainless steel reinforced concrete and lead to overly conservative (or indeed unconservative in some cases) predictions of the section capacity.

Additionally, existing design standards advise using the same bond design rules for stainless steel reinforced concrete as traditional carbon steel reinforced concrete, owing to a lack of alternative information, although this is not based on test or performance data. As such, there is a real need to develop a full and fundamental understanding of the bond behaviour of stainless steel reinforced concrete, to achieve more sustainable and reliable design methods for reinforced concrete structures. Given the high initial cost of stainless steel, it is imperative that structurally efficient design solutions are made available which consider and exploit the distinctive and advantageous properties of stainless steel.

1.4 Aims and objectives

There is a real need to develop a full and fundamental understanding of the behaviour of stainless steel reinforced concrete in order to achieve more sustainable and reliable design methods for reinforced concrete structures. The primary aims of this research are to examine the behaviour of stainless steel reinforced concrete beams and to develop a new design approach which incorporates the advantageous material properties. The main research objectives are summarized as follows:

- To conduct a detailed literature study of the existing information on stainless steel reinforced concrete, as well as a discussion on the potential advantages and challenges.
- To assess the design of stainless steel reinforced concrete beams using the current design rules in Eurocode 2 which were developed and validated for carbon steel concrete members.

- To develop a new deformation-based design method that incorporates the distinctive properties of stainless steel and reflects the actual behaviour, in order to predict the bending moment capacity of reinforced concrete beams.
- To develop a finite element model to further assess the performance of the proposed analytical method, and this is also used to conduct a parametric study of the most influential properties.
- To investigate the bond behaviour of stainless steel reinforcement with reference to traditional carbon steels through experimental testing and analysis. These findings will be compared with the existing design guidance provided in both Eurocode 2 and Model Code 2010 (Fédération Internationale du Béton, 2013). Accordingly, proposing new design parameters in the light of the findings of this bond study.

1.5 Thesis outline

This thesis is divided into six further chapters which are summarised below:

Chapter 2 provides a detailed background of the existing information on stainless steel reinforcement including the metallurgical, mechanical and structural aspects as well as the corrosion behaviour and bond performance. In addition an overview of the current code of practice and some design changes that are considered as a result of using stainless steel reinforcement in concrete structures is presented.

Chapter 3 describes the development of the finite element model of a simply reinforced concrete beam using the ABAQUS software package including the solution procedures, materials behaviour, types of mesh and element, and boundary and loading conditions. This chapter also presents the validation of the numerical model using the available data in the literature.

Chapter 4 focuses on the design of stainless steel reinforced concrete beams, and investigates the impact that neglecting strain hardening has on the load-bearing capacity. Additionally, a new deformation-based design method is developed to predict the bending moment capacity for stainless steel reinforced concrete beams. The proposed method is based on the increasingly popular continuous strength method (CSM), which harnesses the advantages of material strain hardening in the design procedure. The design method is developed in two forms, first as a full model in which the whole material response is considered and then as a simplified model incorporating a more simplistic elastic-linear hardening stainless steel constitutive response. Finally, the proposed method is validated by utilising the numerical model developed in the previous chapter.

Chapter 5 further develops and analyses the behaviour and design of stainless steel reinforced concrete beams, using the proposed CSM approach. A comprehensive parametric study is carried out to investigate the effect of the most influential parameters on the performance of stainless steel concrete beams including various concrete strengths and reinforcement grades and different

geometries. Additionally, this chapter aims to provide guidance for selecting an appropriate reinforcement ratio that exploits the strain hardening properties of stainless steel rebar. Moreover, attention is also given to assessing the serviceability limit state of stainless steel reinforced concrete beams through analysing the deflection behaviour compared to the predicted response from Eurocode 2.

Chapter 6 investigates the bond behaviour of stainless steel reinforced concrete and compares the performance to traditional reinforced concrete, through experimental testing and analysis. This chapter proceeds with a background of the information currently available in design standards, following by a detailed description and analysis of a pull-out test experimental programme involving both stainless steel and carbon steel reinforcements. It also compares the results to existing design rules in terms of bond strength, anchorage length and lap length. Finally, suitable bond-slip models for stainless steel and also carbon steel reinforcements are proposed.

Chapter 7 concludes the main findings from this research and identifies the potential future research in this area.

Chapter 2: Literature review

2.1 Introduction

There has been increased interest and application of stainless steel reinforcement in concrete structures in recent years, owing mainly to its excellent corrosion resistance as well as its other distinctive properties such as significant development of strain hardening and high ductility. Giving that stainless steel has excellent corrosion resistance would significantly contribute to improve its life cycle which reflects the advantageous sustainability and economic efficiency. In this chapter, a detailed background of the previous research on the behaviour and design of stainless steel as a structural material is presented. This chapter is divided into three main sections in which the first section gives a background of stainless steel in general including the chemical composition, grade categories, classifications and material properties. The second section provides detailed information about the use of stainless steel as reinforcement in concrete structures, outlining the needs and challenges. It also discusses the behaviour of stainless steel in corrosive environments and under fire conditions as well as its bond performance. Additionally, this section reviews the current applications for stainless steel reinforcement. The third section focusses on the design aspects of stainless steel reinforcement highlighting the differences between stainless steel and carbon steel, particularly the constitutive relationship, and discusses the current codes of practice for concrete members reinforced with stainless steels with an emphasis giving to the durability requirements.

2.2 Stainless steel in structural applications

2.2.1 Background

Stainless steel is widely used for load-bearing applications in structural engineering, largely owing to its excellent corrosion resistance. In addition to durability, it has a long life-cycle, excellent mechanical characteristics, good formability and recyclability and requires little maintenance (Shamass and Cashell, 2018). Stainless steel offers excellent ductility and strain hardening capacity compared with traditional carbon steel, which is particularly desirable in design as a ductile section which provides warning of imminent collapse.

The earliest use of stainless steel in construction was in the 1920's, for roofing and facade applications (Baddoo, 2008). In more recent times, stainless steels have become popular in load-bearing applications where the durability, ductility, stiffness and strength are required, as well as excellent fire resistance. Stainless steels are produced in different forms including sheet, plate, bar, tube, hot-rolled and cold-formed structural sections, fasteners and fixings. Cold-formed sections fabricated from steel plates are the most commonly used products for structural members because they are the most readily available and are reasonably straight-forward to manufacture (Gardner, 2005).

2.2.2 Composition

Stainless steels are defined as a group of corrosion resistant alloying steels which possess a minimum chromium content of 10.5% and a maximum carbon content of 1.2% (EN 10088-1, 2014). The distinctive properties of stainless steel depend on the constituent elements of the stainless steel alloy, and therefore it is important to select the appropriate grade for each application. One of the most important chemical elements in all stainless steel alloys is chromium (Cr) which provides the corrosion resistance through the formation of a thin chromium oxide film on the surface of the material in the presence of oxygen, resulting in a passive protective layer (Evans, 2002). There are other influential alloying elements that play important role in identifying the properties of stainless steel. For example, nickel (Ni) improves the ductility and the formability of the material, molybdenum (Mo) improves the resistance against the uniform and localized corrosion and nitrogen (N) significantly enhances mechanical properties of the material including strength and ductility (Markeset et al., 2006). Additionally, a number of other alloying elements are typically present including manganese (Mn), copper (Cu), carbon (C), silicon (Si), phosphorus (P) and sulphur (S). Detailed information about the chemical composition associated with different stainless steel grades is given in the European Standard EN 10088-1 (2014). Table 2.1 presents the chemical composition of some common stainless steel grades available as reinforcement.

Table 2.1: The chemical composition of some common stainless steel grades (Markeset et al., 2006).

European (EN 10088-1)		American (AISI)	Chemical composition (%)								
Grade	Name	Grade	C Max	Si Max	Mn Max	P Max	S Max	Cr Min/ Max	Ni Min/ Max	Mo Min/ Max	N Min/ Max
1.4301	X5CrNi 18-10	304	0.07	1.0	2.0	0.045	0.03	17.5/ 19.5	8.0/ 10.50	-	max 0.11
1.4401	X5CrNiMo 17-12-2	316	0.07	1.0	2.0	0.045	0.03	16.5/ 18.5	10.0/ 13.0	2.00/ 2.50	max 0.11
1.4429	X2CrNiMoN 17-13-3	316LN	0.03	1.0	2.0	0.045	0.015	16.5/ 18.5	11.0/ 14.0	2.5/ 3.0	0.12/ 0.22
1.4162	X3CrNiMo 22-2-0	LDX 2101	0.03	0.4	5.0	-	-	21.5	1.5	0.3	max 0.22
1.4362	X2CrNiMo 23-4	2304	0.03	1.0	2.0	0.035	0.015	22.0/ 24.0	3.5/ 5.5	0.1/ 0.6	0.05/ 0.20
1.4462	X2CrNiMoN 22-5-3	2205	0.03	1.0	2.0	0.035	0.015	21.0/ 23.0	4.5/ 6.5	2.5/ 3.5	0.10/ 0.22

2.2.3 Classification

There are number of different global classification systems used for stainless steels. The most widely adopted are the European standard and the American Iron and Steel Institution (AISI) specification. The following sub-sections provide more information about these classification systems.

European standard

Stainless steels are classified in the European standard EN 10088-1 (2014) according to their chemical composition. Each grade is given a generic number to identify its group, and then an individual number is specified to refer to the nominal alloy composition. For example, the numbers in grade 1.4436 represent:

- 1 refers to the steel.
- 44 refers to the group of stainless steel.
- 36 refers to the individual material identification.

The grade number is also given a corresponding grade name to provide more information about the chemical composition of a particular grade. For instance, the name of grade 1.4436 is X3CrNiMo 17-13-3 and represents:

- X refers to a high alloy steel.
- 3 represents the percentage of carbon content.
- CrNiMo is the chemical symbols of the main alloying elements.
- 17-13-3 represents the nominal percentage of the main alloying elements.

American Iron and Steel Institute system (AISI)

AISI classifies stainless steels according to the category of stainless steel. For instance, austenitic and ferritic stainless steels are classified as 300 series alloys (e.g. 316, 304) and as 400 series alloys (e.g. 403, 409), respectively. The main limitation of this system is that the details of the chemical composition for a particular grade are not provided. Table 2.1 presents some stainless steel grades available as reinforcement with their European designation and the equivalent American numbers.

2.2.4 Stainless steel categories

There are five main categories of stainless steel which are classified according to their metallurgical structure, including the austenitic, ferritic, duplex, martensitic and precipitation hardened grades. The austenitic and duplex grades are most common in structural applications, including for stainless steel reinforcement. Precipitation hardened stainless steels are also used in construction for particular applications such as tie-bolts. Ferritic stainless steels are more suitable for indoor components. Whereas, the use of martensitic stainless steels is typically limited for applications such as valves and knife blades. A summary of the main advantages and limitations of each category is given below:

Austenitic stainless steel

Austenitic stainless steels are the most commonly used grades in structural applications owing to the excellent mechanical properties and high corrosion resistance. They typically comprise of 17-18% chromium and at least 8-11% nickel (Gardner, 2005). The austenitic grades offer very good weldability and formability and large scale of service temperature (British Stainless Steel Association, 2000). Austenitic stainless steels have been used in various applications such as load-bearing structural members, containers, architectural facades, house wares and industrial piping.

Ferritic stainless steels

The ferritic stainless steels typically have chromium content between 11% and 17% (British Stainless Steel Association, 2000). They comprise less nickel compared to the austenitic stainless steels and have an atomic structure similar to that of carbon steels. Consequently, they have generally limited ductility and toughness and less formability and weldability as well as less corrosion resistance compared to austenitic stainless steels. Ferritic stainless steels are relatively inexpensive because of the limited nickel content, and have fewer price fluctuations. Since ferritic stainless steels are less corrosion resistance compared with other grades, they are more suitable for indoor components such as shop-fittings and handrails or for other household products such as washing machines parts and boilers (Baddoo and Burgan, 2012).

Duplex stainless steel

Duplex stainless steels are also known as austenitic-ferritic stainless steels because of the mixed microstructure between the ferritic and austenitic stainless steels. Typically, duplex stainless steels contain around of 22-23% chromium and 4-5% nickel (Gardner, 2005). These grades exhibit high strength and great ductility properties as well as outstanding corrosion performance. Duplex stainless steels should be used in applications that require high strength materials where the materials are subjected to aggressive or contaminated environments. Accordingly, they are commonly used in offshore structures and chemical industries as tension bars, shafts, valves and pins connection (Baddoo and Burgan, 2012).

Martensitic stainless steels

Martensitic stainless steels contain higher carbon content than the other grades. The microstructure of martensitic stainless steels are similar to that of ferritic stainless steels and carbon steels. These grades exhibit similar level of corrosion resistance to that of ferritic grades. They have limited ductility in comparison with austenitic, duplex and ferritic grades (British Stainless Steel Association, 2000). Additionally, martensitic stainless steels require heat treatment before and after welding. Despite their relative cheapness compared to the other grades of stainless steels, their lower corrosion resistance and weldability requirements limit their use to applications such as valves and knife blades. They are typically not used in load bearing applications.

Precipitation hardened stainless steels

Precipitation hardened stainless steels have a better corrosion resistance than that of ferritic or martensitic stainless steels and similar to the austenitic grades which comprise of 18% chromium and 8% nickel (Baddoo and Burgan, 2012). They generally exhibit excellent strength, good ductility and toughness depending on the heat treatment conditions. These grades are mostly used in oil and gas and aerospace industries, but they are also used in construction for particular applications such as tie-bolts (Baddoo and Burgan, 2012).

2.2.5 Material properties

Stainless steels do not just offer high corrosion resistance but also provide excellent strength, toughness and weldability. The material properties of stainless steel vary depending on several parameters including the chemical composition, material thickness, direction of rolling and level of cold-working. Austenitic and duplex stainless steels have relatively higher strength and significant strain hardening properties compared with carbon steels. These grades typically exhibit large ductility that may reach more than 40%. Ferritic and martensitic stainless steels exhibit relatively lower strength and limited strain hardening. On the other hand precipitation-hardened stainless steels have extraordinarily high strength that may reach more than 1500 N/mm^2, however these grades have low ductility, depending on the heat treatment condition (British Stainless Steel Association, 2000). In general, the modulus of elasticity for different stainless steel categories is quite similar to that of carbon steels. According to the European standard EN 10088-2 (2014), a value of 200000 N/mm^2 maybe used to specify the modulus of elasticity for all grades of stainless steel. Information on the mechanical properties of some common stainless steel grades is presented in Table 2.2.

Table 2.2: Mechanical properties for some common stainless steel grades EN 10088-2 (2014) with reference to carbon reinforcement BS 4449+A3 (2005).

Stainless steel type	Grade	Minimum 0.2% proof strength, $\sigma_{0.2}$ (N/mm^2)	Ultimate tensile strength, σ_u (N/mm^2)	Modulus of elasticity, E (kN/mm^2)	Minimum elongation after fracture (%)
Carbon steel	B500B	485	515-690	200	4
Austenitic	1.4301 (304)	210	520 – 720	200	45
	1.4307 (304L)	200	500 – 650	200	45
	1.4401 (316)	220	520 – 670	200	40
	1.4404 (316L)	220	520 – 670	200	40
Duplex	1.4362 (SAF2304)	400	600 – 850	200	20
	1.4462 (2205)	400	640 – 840	200	20
Ferritic	1.4000 (410S)	220	400-600	200	19
	1.4512 (409)	210	380-560	200	25

2.2.6 Cost

The use of stainless steels in structural applications is inevitably more expensive than that of carbon steels (Sharif et al., 2019; Eladly, 2020). This limits the more widespread of using stainless steel in structural applications. However, the initial cost of the material itself does not reflect the total costs over the lifetime of a structure. There are other factors which must be considered to have a rational comparison including maintenance and inspection costs as well as the immediate costs associated with corrosion and fire protections. If these factors are counted together, stainless steel would represent more efficient option compared to carbon steel especially for those structures subjected to harsh conditions.

2.2.7 Recycling

The construction industry produces a large amount of material waste. Currently, there is a need to minimize the waste in the construction sector by using more environmentally friendly materials. In this context, stainless steels are highly durable materials that retain high residual value of the basic elements including chromium, nickel and molybdenum (British Stainless Steel Association, 2016). It has been shown that about 80% of the new stainless steels produced in western European are made

from the recycled scrap stainless steel (Aalco, 2013). This provides stainless steels with additional economic and environmental advantages.

2.3 Stainless steel reinforcement in concrete structures

2.3.1 General

Reinforced concrete is one of the most common structural solutions found in construction. It is popular because it provides an economic, efficient and versatile solution and there is plenty of guidance and performance criteria available for designers. Stainless steels have recently being included in reinforced concrete structures owing to the exceptional corrosion resistance, excellent durability, long life cycle, significant strain hardening and great ductility. Reinforced concrete (RC) structures are widely used for a range of applications such as multi-storey buildings, tunnels and bridges owing to the efficient use and ready availability of the constituent materials.

2.3.2 Durability

There are increasing demands to improve the durability and the life-cycle cost of reinforced concrete structures because of the high maintenance costs associated with corrosion of the steel reinforcement and carbonation and deterioration of the concrete. This is particularly true for structures subjected to harsh environments such as in marine, coastal or industrial settings. For structures reinforced with traditional carbon steel and subjected to aggressive conditions, corrosion is difficult to avoid. The typical approach to improving the durability of RC structures is to change some of the design parameters such as the thickness of the concrete cover or to control the alkalinity of the concrete mix (British Highways Authority, 2003). However, in aggressive conditions, these measures may not be enough to prevent unacceptable levels of corrosion developing. In this context, the use of stainless steel reinforcement in exposed structures like bridges, retaining walls and tunnels can provide an ideal solution to the deterioration and corrosion problems. This may even result in the structure not requiring expensive inspection and rehabilitation works over its lifetime. Stainless steel reinforcement can also be used for the restoration and rehabilitation of existing concrete structures (Pérez-Quiroz et al., 2008).

2.3.3 Life cycle cost

The initial cost of stainless steel reinforcing bars is relatively high, typically between 3 and 8 times than that of traditional carbon steel rebar, depending on the grade (Nationwide Stainless, 2019; Metals4U, 2019). In some cases, the use of stainless steel reinforcement is limited only to the outer layer of the reinforcement, which is more susceptible to chloride-ingress, due to the high initial costs. In spite of this, it has been shown that stainless steel reinforcement can reduce the overall maintenance costs during the service life by up to 50%, especially for bridges and marine structures (Cramer, 2002). A study conducted by The Arup Research & Development group and supervised by the UK Highways Agency found that using stainless steel reinforcement can significantly increase the

lifetime of structures and also reduce the associated maintenance costs (Gedge, 2003). Implementing stainless steels in concrete structures results in these structures requiring less maintenance and rehabilitation works over their lifetime. These characteristics are extremely important for highways and infrastructure to avoid road closures and highway rerouting as well as the associated delays and carbon emissions.

Additionally, using high corrosion resistant reinforcement such as stainless steel results in further savings due to a potential relaxation of some of the durability requirements including the depth of concrete cover, design crack width and the need for reinforcement coating. Implementing these changes into the design of RC structures may result in significant cost saving especially in mega-projects.

Fig. 2.1 presents an example of the actual life cycle costs for the Oland Bridge in Sweden where both stainless steel and carbon steel reinforcement were used. The data presented in the figure shows that the cost of the bridge incorporating stainless steels remains constant indicating no additional costs over the entire lifetime whereas the cost of the carbon steel reinforced concrete solution significantly increases after around 20 years. Another important observation is that the whole initial construction costs when stainless steel reinforcement is employed instead of carbon steel rebar only increase by around 5-10%. This means that although the initial costs of the bare stainless steel reinforcement are undoubtedly more expensive than that of carbon steel, the variation on the entire construction costs is much less significant. Another study on the Schaffhausen Bridge in Switzerland revealed that the life cycle cost of stainless steel grade 1.4301 is 14% lower than carbon steel reinforcement (McGurn, 1998). This is clear evidence of the long term cost efficiency of using stainless steel reinforcement in infrastructure projects.

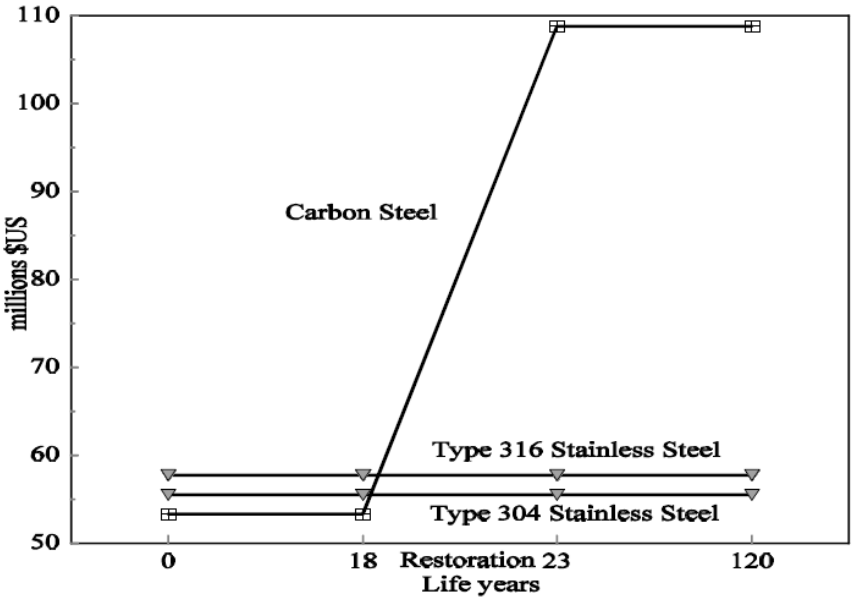

Fig. 2.1: Analysis of the life-cycle cost for Oland Bridge in Sweden (McGurn, 1998).

2.3.4 Common stainless steel reinforcement grades

Stainless steel reinforcement is currently available in the open market in a number of different grades including austenitic grades 1.4311, 1.4307 and 1.4301 and duplex grades 1.4462, 1.4162 and 1.4362. Grade 1.4307 is the most commonly found grade used in construction and is a standard low-carbon austenitic stainless steel whereas grade 1.4311 is also a low-carbon austenitic stainless steel but with improved low-temperature toughness and strength owing to its higher nickel and nitrogen content. Both of these grades are very suitable for low magnetic structural applications. Grade 1.4362 is a duplex stainless steel which offers superior corrosion resistance due to the relatively high nickel content compared to the austenitic grades. In recent years, a new type of duplex stainless steel has been developed which has a relatively low nickel content and these are known as the lean duplex grades. Grade 1.4162 is in this category and offers excellent corrosion resistance whilst also possessing around double the characteristic strength of austenitic stainless steel for almost the same cost, owing to the low nickel content.

2.3.5 Classification and selection of stainless steels reinforcement

It is clear that one of the fundamental advantages for using stainless steel reinforcement is its excellent corrosion resistance. Therefore, classifying stainless steels according to their corrosion resistance may facilitate the selection of the appropriate grade. The most widely used classification method to measure the relative corrosion resistance of metals is the Pitting Resistance Equivalent Number (PREN). The criteria for predicting the corrosion resistance of a metal depends mainly on the contents of chromium (Cr), nickel (Ni) and molybdenum (Mo) in the alloy, as shown in Eq. (2.1) (Markeset et al., 2006).

$$\begin{aligned} &\text{PREN} = \%\,\text{Cr} + 3.3\,(\%\,\text{Mo}) + 16\,(\%\,\text{N}) && \text{For austenitic stainless steels} \\ &\text{PREN} = \%\,\text{Cr} + 3.3\,(\%\,\text{Mo}) + 30\,(\%\,\text{N}) && \text{For duplex stainless steels} \end{aligned} \qquad (2.1)$$

Classifying stainless steels according to their PREN number is quite useful in the selection of the appropriate stainless steel grade for a particular application. However, the PREN does not take into account the chloride threshold of each grade and also ignores the beneficial effects come from the concrete cover on the passivity of stainless steels (Markeset et al., 2006).

A classification example for stainless steel reinforcement is given in Table 2.3. In this example, the reinforcement is classified into four groups according to their PREN, lifetime of the structure and the surrounding environment. Class 0 is recommended for those structures located in a marine environment and subjected to moderate temperature and relative humidity with a design service life between 10 and 30 years. Class 1 is suggested for the same conditions but with a design service life between 50 and 100 years. On the other hand, Class 2 is suitable for those structures subjected to high chloride-ingress and moderate to high temperature and relative humidity with a moderate design

service life. Finally, Class 3 is recommended for those structures located in marine environments and requiring long design service life with high temperature and relative humidity.

Table 2.3: Classification of stainless steel reinforcement according to their corrosion resistance (Markeset et al., 2006).

Corrosion resistance class	Steel Type	Stainless steel grade	PREN
Class 0	Carbon steel	-	-
Class 1	Austenitic stainless steel (without Mo)	1.4301	19
		1.4541	17
Class 2	Austenitic stainless steel (with Mo)	1.4401	25
		1.4429	26
		1.4436	26
		1.4571	25
Class 3	Duplex	1.4462	36

Table 2.4 provides recommendations for selecting the appropriate grade of stainless steel reinforcement based on the exposure conditions as suggested by the Design Manual for Road and Bridges (BA 84/02, 2003) for highways and infrastructures.

Table 2.4: Selection of stainless steel grades (BA 84/02, 2003).

Exposure Condition	Stainless steel grade
Stainless steel reinforcement embedded in concrete with normal exposure to chlorides in soffits, edge beams, diaphragm walls, joints and substructures.	1.4301
As above but where additional relaxation of design for durability is required for specific reasons on a given structure or component i.e. where waterproofing integrity cannot be guaranteed over the whole life of the structure.	1.4436
Direct exposure to chlorides and chloride bearing waters for example dowel bars, holding down bolts and other components protruding from the concrete.	1.4429 1.4436
Specific structural requirements for the use of higher strength reinforcement and suitable for all exposure conditions.	1.4462 1.4429

2.3.6 Mechanical behaviour

Stainless steel reinforcement exhibits excellent mechanical behaviour compared with the traditional carbon steels. A limited number of investigations on the mechanical behaviour of stainless steel reinforcement has been conducted in recent years. It has been shown that austenitic stainless steel reinforcement grades 1.4429 and 1.4311 provide higher strength and hardness characteristics compared with the equivalent carbon steels (Castro et al., 2003). More recently, Medina et al. (2015) investigated the ductility and the mechanical properties of austenitic and duplex stainless steel reinforcement grades 1.4301, 1.4362 and 1.4482 with reference to carbon steel grade B500SD. It was observed that stainless steels show great ductility that can reach three times than that of carbon steels. However, these stainless steels exhibited a lower modulus of elasticity compared to carbon steels by around 15%. This is mainly because stainless steels exhibit nonlinear behaviour from an early stage and therefore the elastic modulus can be harder to quantify. A summary of some of the mechanical properties for different stainless steel reinforcement grades is presented in Table 2.5. It is clear that the stainless steels have excellent tensile strength associated significant strain hardening and great ductility. These characteristics are very desirable in design in order to avoid sudden collapse.

Table 2.5: Summary of the mechanical properties of stainless steel reinforcement (Gardner et al., 2016).

Product form	Grade	Bar diameter (mm)	$\sigma_{0.2}$ (N/mm^2)	σ_u (N/mm^2)	E (kN/mm^2)	ε_u (%)
Plain round bars	1.4307	12	562	796	210.2	39.9
	1.4162	12	805	964	208.7	18.8
	1.4307	16	537	751	211.1	42.4
	1.4362	16	760	860	197.5	22.0
Ribbed bars	1.4311	12	480	764	202.6	48.3
	1.4162	12	682	874	199.1	32.4
	1.4162	16	646	844	195.2	32.9
	1.4311	16	528	717	199.9	47.9
	1.4362	16	608	834	171.4	35.1

2.3.7 Corrosion behaviour

It is now clear that one of the fundamental challenges that is experienced by reinforced concrete structures is corrosion of the reinforcement, especially for members which are exposed to harsh environments (Helland, 2013). Corrosion is a serious problem that results in a reduction in the nominal reinforcement area and weakness in the bond strength between the reinforcement and surrounding concrete which impacts the safety and integrity of concrete structures. Corrosion occurs as a result of chloride penetration or carbonation of concrete. The former is caused by chloride ingress from using de-icing salts in frosty weather or from marine environments. Whereas the latter occurs as a result of carbon dioxide existing in the surrounding air, which attacks the calcium in the concrete. In standard RC design, the corrosion protection of the reinforcement mainly relies on the concrete cover and the durability of the steel passivation layer. For traditional carbon steels, this passivation layers can easily break down and then corrosion develops, especially in a contaminated or harsh environment.

The typical approaches to reducing the potential corrosion risk are to control the alkalinity of concrete, increase the depth of concrete cover or use cement inhibitors or reinforcement coating materials (British Stainless Steel Association, 2003). However, these measures may not be enough to prevent the development of unacceptable levels of corrosion. In this context, the use of stainless steel reinforcement is an ideal solution to solve the inherent corrosion problem. Stainless steels exhibit

outstanding corrosion resistance performance even in aggressive conditions owing to have rich chromium content (i.e. minimum of 10.5%). Chromium provides the corrosion resistance through the formation of a thin self-regenerating chromium oxide film on the surface of the material in the presence of oxygen, resulting in a strong passive protective layer (Evans, 2002; Medina et al., 2015).

It is shown that austenitic stainless steel reinforcement, particularly grades 1.4404 and 1.4301, have corrosion resistance 10 times better than that of carbon steels (Nurnberger, 1996; García-Alonso et al., 2007). Duplex reinforcement generally demonstrates similar or even better corrosion resistance compared to that of the austenitic grade (Bertolini et al., 2002; Bautista et al., 2007; Serdar et al., 2013). Fig. 2.2 demonstrates the corrosion behaviour of different stainless steel grades with reference to that of carbon steels. The influence of chloride concentration is given on the y-axis, whilst the influence of the PH value of concrete is given on the x-axis. It is obvious that carbon steel has poor corrosion resistance even at very low chloride contents. It is also very sensitive to the PH values as it becomes corroded once the PH value drops below 11. On the other hand, stainless steel reinforcement shows exceptional corrosion resistance even at very high chloride contents and low PH values.

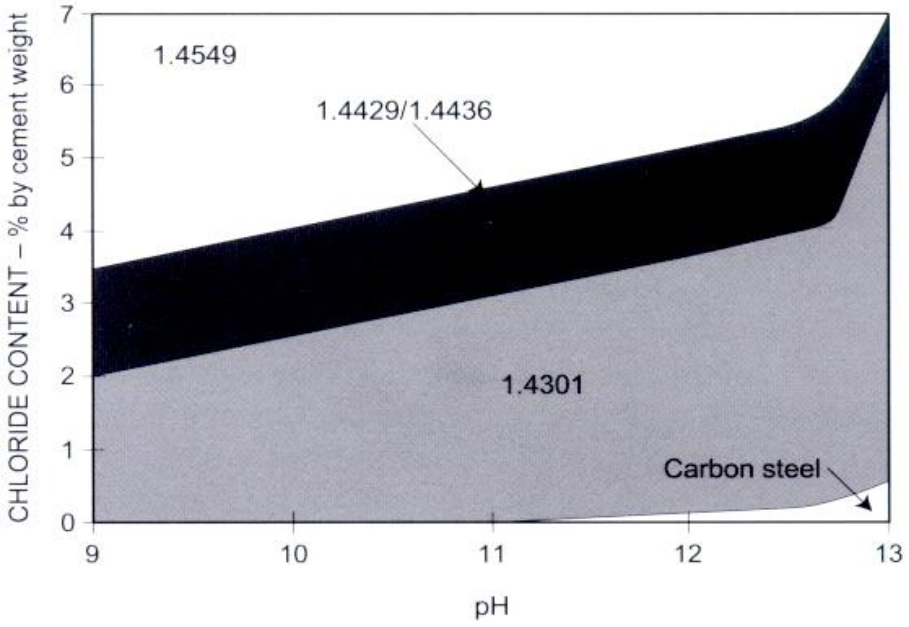

Fig. 2.2: Corrosion behaviour of different stainless steel reinforcements compared with carbon steels (Pietro et al., 1998).

2.3.8 Fire behaviour

One of the fundamental features for achieving fire-resistant structures is the capability of the material to retain stiffness and strength at elevated temperature. Stainless steels exhibit excellent stiffness and strength retention at elevated temperature owing to the advantageous of the chemical composition (Baddoo, 2008). There has been plentiful research into the behaviour of structural stainless steel in fire (e.g. Lopes et al., 2012; Tondini et al., 2013; Huang and Young, 2014; Fan et al., 2016) and much more limited research studies into the behaviour of stainless steel reinforcement at elevated

temperature (e.g. Gardner et al., 2016). Moreover, there is an even greater dearth of research publications on the behaviour of stainless steel reinforced concrete under fire conditions. In fact, none have been found in the available literature.

Fig. 2.3(a) and (b) present a comparison of the strength and stiffness retention factors between stainless steel grade 1.4301 and carbon steel at 0.2% proof stress, respectively. It is clear that stainless steel retains better strength and stiffness at elevated temperature compared with carbon steel. These distinctive features are extremely beneficial in the event of fire which provide the structure with the essential resistance required for a longer period.

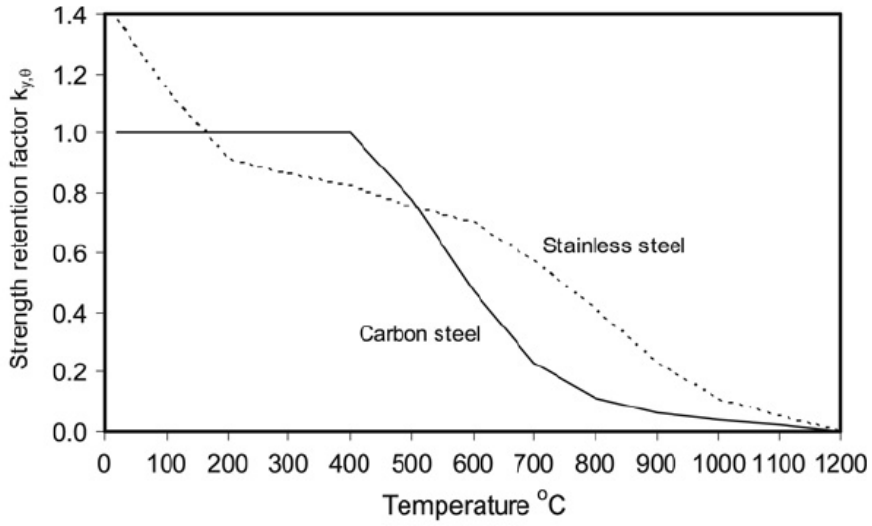

(a)

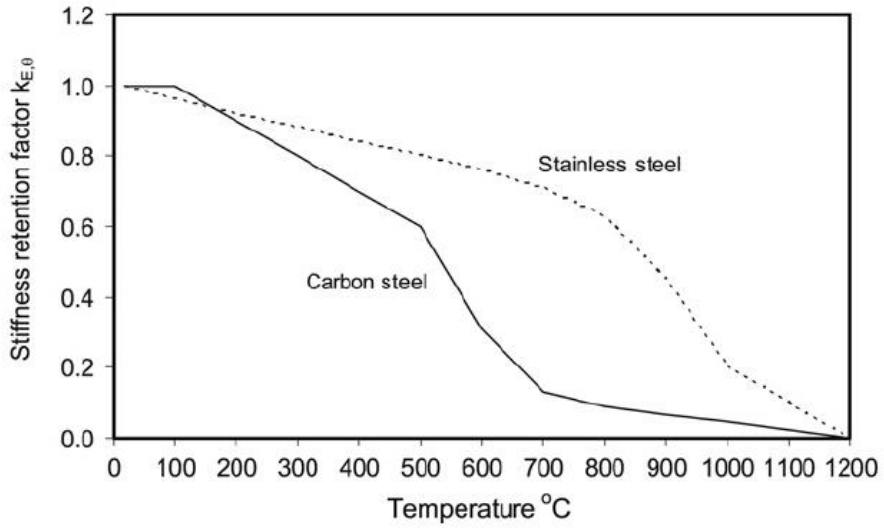

(b)

Fig. 2.3: Comparison of stainless steel and carbon steel (a) strength retention factor (b) stiffness retention factor (Baddoo, 2008).

Fig. 2.4 shows the thermal expansion performance of duplex and austenitic stainless steel reinforcement compared with that of carbon steel, as well as concrete aggregates. It is clear that stainless steels demonstrate higher thermal expansion than that of carbon steel over the entire range of temperature included in this examination, and do not exhibit a phase-change plateau at 750 °C, like occurs for the carbon steel rebar. The thermal expansion performance of concrete is influenced by the type of aggregate. The figure shows that the thermal expansion of siliceous and calcareous aggregates increases gradually with temperature until around 700-800 °C, where it becomes constant owing to the changes in the chemical composition at these temperatures. Given that reinforced concrete elements rely on the effective development of composite action between the two constituent materials, namely concrete and the reinforcement, the greater thermal expansion properties of stainless steel may not be desirable during exposure to elevated temperature. In this scenario, the higher coefficient of thermal expansion of stainless steel reinforcement compared with traditional carbon steel rebars may cause premature loss of bond between the two constituent materials, leading to greater cracking and more concrete spalling

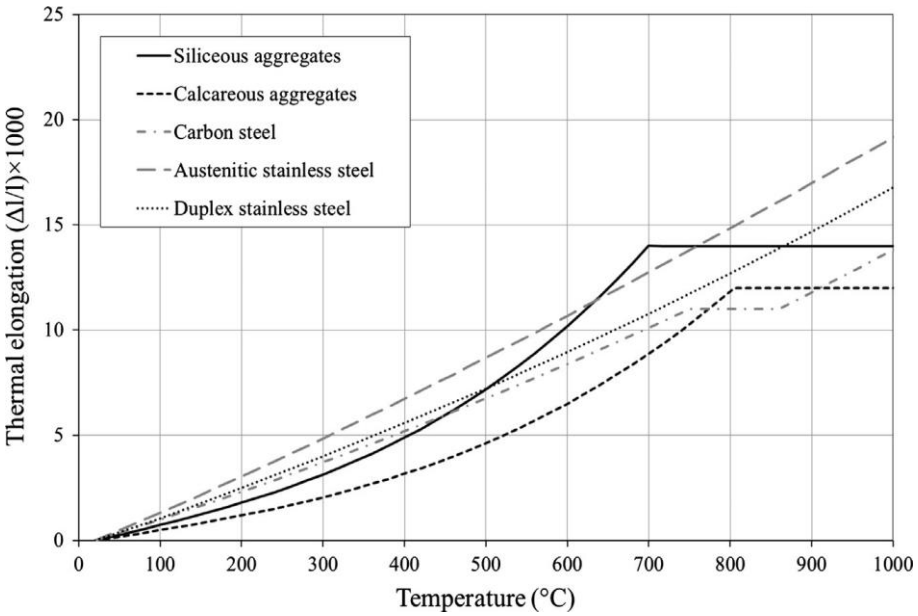

Fig. 2.4: Thermal expansion behaviour of austenitic and duplex stainless steels, carbon steel and aggregates (Gardner et al., 2016).

2.3.9 Bond behaviour

Bond is an essential property in the design of reinforced concrete structures. It is essential for ensuring that the composite action between the two constituent materials is achieved, thereby enabling loads to be efficiently carried. Inadequate steel-concrete bond can cause excessive slippage of the reinforcement resulting in serious cracking of the concrete, ineffective anchorage of the reinforcement bar as well as excessive deflections or rotations. Bond is a complex phenomenon owing to the many inter-related parameters that influence its development. The most influential parameters are the

quality of the concrete and the surface geometry of the reinforcing bar. There are other relevant parameters also including the cover distance, clear space between adjacent bars, bar size, number of reinforcement layers and the direction of casting with respect to the orientation of the bars.

There has been a limited research on the bond behaviour of stainless steel reinforcement in a corrosive environment (e.g. Calderon-Uriszar-Aldaca et al., 2018; Zhou et al., 2017) and very few studies on the bond behaviour of stainless steel reinforcement in normal conditions, and these have even resulted in inconclusive results with one study showing that the bond developed by some austenitic and duplex stainless steel bars is lower than for similar carbon steel reinforcement (Aal Hassan, 2003) whilst other publications have shown the opposite finding (Ahlborn and DenHartigh, 2003; Johnson, 2010). Therefore, further research on the bond behaviour of stainless steel reinforcement in concrete is required.

Most global design standards including Eurocode 2 and MC2010 do not provide specific design rules for bond in stainless steel reinforced concrete structures, and therefore designers typically use the same design rules developed for traditional carbon steel reinforcement when designing stainless steel reinforced concrete structures. Since it is reported that stainless steel may develop lower bond strength compared with carbon steel, this is not necessarily a safe strategy, unless specific experimental evidence is available.

2.3.10 Applications of stainless steel reinforcement

It is now recognised that reinforced concrete with carbon steel reinforcement may not be as durable in all conditions as was previously assumed (British Stainless Steel Association, 2003). In harsh environments such as marine or coastal locations, corrosion of carbon steel reinforcement can result in very expensive, challenging and inconvenient rehabilitation works. In this context, stainless steel reinforcement offers a durable and efficient alternative. One of the earliest examples of the use of stainless steel reinforcement is the Progresso Pier in Mexico, as shown in Fig. 2.5, which was constructed in the early 1940's using grade 1.4301 austenitic stainless steel. It has been in continuous service for over 70 years without any major repair or significant maintenance activities. The benefits of using stainless steel rebar are quite starkly visible in this image as, in the foreground, the remains of a carbon steel reinforced concrete pier are evident. This was built many years after the stainless steel reinforced concrete pier, but is clearly no longer in service.

Stainless steel reinforcement has also been used in a number of other projects, including Stonecutters Bridge in Hong Kong and Sheik Zayed Bridge in Abu Dhabi, as shown in Fig. 2.6 and Fig. 2.7, respectively. These two bridges are reinforced with grade 1.4462 duplex stainless steel. Because of the relatively high initial cost, the stainless steel rebars are strategically placed and only used for the outer layer of the reinforcement in both projects, in the so-called splash zone. Grade 1.4436 stainless steel was used in the Highnam bridge widening project in the UK as well as the Broadmeadow Bridge

in Ireland. One of the most high profile and recent applications of stainless steel rebar is in the Queensferry Crossing in Scotland which opened in 2017. As well as new construction, stainless steel reinforcement has also been used for renovation and restoration purposes. For example, austenitic grade 1.4301 stainless steel reinforcement was used to rehabilitate the pillars and stone arches of the Knucklas Rail Bridge (McGurn, 1998). In summary, the main usage of stainless steels is in applications that require high corrosion resistance and long life cycle owing to aggressive environment such as infrastructures and marine buildings.

Fig. 2.5: The Progresso Pier in Mexico (Nickel Institute, 2018).

Fig. 2.6: Stonecutters Bridge in Hong Kong (Thousandswonder, 2015).

Fig. 2.7: Sheik Zayed Bridge in Abu Dhabi (Edvardsen, 2008).

2.4 Design of RC structures using stainless steel reinforcement

2.4.1 Constitutive relationship of stainless steel

The constitutive behaviour of stainless steel is noticeably different than that of carbon steel, in that stainless steel exhibits a relative initial linear behaviour, particularly at a very early stage, followed by a rounded response, without a clearly defined yield point and with significant strain hardening and high ductility. In contrast, carbon steel exhibits a more linear relationship in the elastic range with a well-defined yield point, which is then followed by a moderate (even negligible) degree of stain hardening, as shown in Fig. 2.8. In the absence of a visible yield point, the typical value adopted in design is the 0.2% proof stress ($\sigma_{0.2}$).

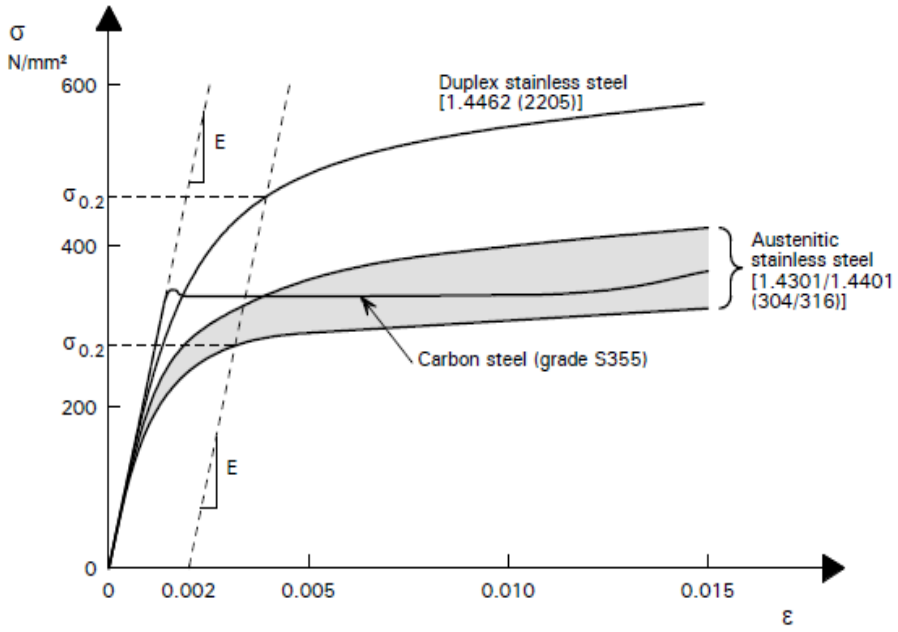

Fig. 2.8: Typical stress-strain curves for carbon steel and stainless steel (Baddoo and Burgan, 2012).

The modified Ramberg-Osgood (R-O) stainless steel material model (Mirambell and Real, 2000; Rasmussen, 2003), which is an extension of the original version proposed in 1943 (Ramberg and Osgood, 1943), is commonly used to represent stainless steels. It includes the two expressions presented in Eqs. (2.2) and (2.3), for the elastic and non-elastic stages of the behaviour, respectively:

$$\varepsilon = \frac{\sigma}{E} + 0.002\left(\frac{\sigma}{\sigma_{0.2}}\right)^{n} \qquad \text{for} \quad \sigma \leq \sigma_{0.2} \tag{2.2}$$

$$\varepsilon = \varepsilon_{0.2} + \frac{\sigma-\sigma_{0.2}}{E_2} + \left(\varepsilon_u - \varepsilon_{0.2} - \frac{\sigma_u-\sigma_{0.2}}{E_2}\right)\left(\frac{\sigma-\sigma_{0.2}}{\sigma_u-\sigma_{0.2}}\right)^{m} \qquad \text{for} \quad \sigma_{0.2} < \sigma \leq \sigma_u \tag{2.3}$$

In these expressions, ε and σ are the engineering strain and stress, respectively, E_2 is the tangent modulus at the 0.2% proof stress point, σ_u and ε_u are the ultimate stress and corresponding strain, respectively, $\varepsilon_{0.2}$ is the strain corresponding to $\sigma_{0.2}$ and n and m are model constants related to the strain hardening behaviour.

2.4.2 Current design of practice

Currently, the majority of global design standards including Eurocode 2 do not incorporate an efficient design approach for RC members with stainless steel. In particular, they generally only include inappropriate material models for the reinforcement, such as an elastic-plastic stress-strain idealisation, which does not exploit the significant strain hardening and high ductility characteristics of stainless steel. This means that any contribution to the load capacity after the steel yield strength has been reached, is not considered in design. Although, this assumption could be acceptable for design traditional concrete structures reinforced with carbon steel, it results in inaccurate predictions for stainless steel RC members. It has been shown that design of stainless steel reinforced concrete members using the current design rules in Eurocode 2 can be either over- or under-conservative (Technical Research Centre of Finland, 2011). This is particularly because stainless steel exhibits a relatively nonlinear response in the elastic stage followed by significant strain hardening. Therefore, designing RC structures with stainless steel using the current design rules, which have been developed and verified for carbon steel reinforced concrete, is neither efficient nor accurate.

2.4.3 Deformation-based design

The continuous strength method (CSM) is a deformation-based design approach which harnesses the advantages of material strain hardening. A brief description of the method and its evolution in recent years is covered in this section while more details are presented in Chapter 4, where the method is further analysed and expanded. The CSM is based on replacing traditional cross-section classification with an assessment of the deformation capacity of the section, using a realistic material model. As such, the method predicts the cross-sectional resistance of the member depending on two main components: (1) a base curve that defines the relationship between the limiting strain at the ultimate load and the cross-section slenderness, and (2) a material model that allows for strain hardening (Theofanous et al., 2016). The approach was originally developed for stainless steel structural

members with non-slender cross-sections (Gardner and Nethercot, 2004) and has been developed many times over the last 15 years to account for different conditions (e.g. Ashraf et al., 2008; Gardner et al., 2011; Lan et al., 2018). In recent years, the method has been adapted for composite construction including carbon steel-concrete composite beams (e.g. Gardner et al., 2017) and stainless steel-concrete composite members with either a full and partial shear connection (e.g. Shamass and Cashell, 2018).

2.4.4 Design changes for durability requirements

The main objective of considering the durability requirements in the design of concrete structures reinforced with carbon steel is to protect the reinforcement against aggressive conditions. Given the exceptional corrosion performance of stainless steel reinforcement, it is possible that these requirements may be relaxed including a reduction in the required concrete cover, an increase in the allowable design crack widths as well as illuminating the use of cement inhibitors and reinforcement coating during construction. Relaxing these requirements may result in a significant cost saving especially in large scale projects, as well as a more efficient use of materials. A number of modifications of the durability requirements have already been implemented in the design of highways structures and bridges (BA 84/02, 2003), as summarized in Table 2.6.

Table 2.6: Design changes for durability requirements in highways structures and bridges (BA 84/02, 2003).

Design condition	Relaxation
Cover	Cover for durability can be relaxed to 30 mm where stainless steel reinforcement is used irrespective of the concrete quality or exposure condition.
Design crack width	Allowable crack width increased to 0.3 mm
Silane treatment	Not required on elements with stainless steel reinforcement.

2.5 Concluding remarks

This chapter presents the state-of-the-art for the use of stainless steel as a structural material, and provides the context for the work in this thesis. It is shown that stainless steel is an exceptional construction material that has become an increasingly attractive choice for reinforced concrete structures owing principally to its excellent corrosion resistance, favourable mechanical properties, great ductility, long life cycle and recyclability. There are a number of inhibitors to stainless steel reinforcement not being more commonly employed in every-day reinforced concrete structures. Firstly, there is a perception amongst engineers that stainless steel reinforcement is prohibitively expensive. Although the initial cost of stainless steel is undoubtedly more expensive than carbon steel, over the life time of a structure if maintenance and rehabilitation costs are considered, then stainless

steel provides a very competitive and efficient design option. Secondly, there is a lack of design guidance and performance data available in the public domain, mainly owing to this being a relatively new topic in structural engineering terms.

Given the high initial cost of stainless steel, it is imperative that structurally efficient design solutions are made available which consider and exploit the distinctive and advantageous properties of stainless steel. However, current design codes such as Eurocode 2 do not incorporate an efficient approach for designing structures with stainless steel reinforcement and instead include inappropriate material models for the rebar which does not utilise the distinctive characteristics of stainless steel. Although, this assumption may be acceptable for carbon steel reinforced concrete, it gives very inaccurate predictions when stainless steel reinforcement is employed. This is mainly because stainless steel exhibits nonlinear behaviour from an early stage and also significant strain hardening. Therefore, designing stainless steel reinforced concrete members using the existing design rules which have been validated for carbon steel reinforced concrete structures is neither efficient nor accurate.

It has also been observed that the bond behaviour of stainless steel reinforcement is barley discussed in the literature with very limited research, and inclusive and conflicting results. The current design standards such as Eurocode 2 and MC2010 do not include specific bond design rules for stainless steel reinforced concrete, and generally suggest using the same criteria as for traditional carbon steel reinforcement. Since it has been reported that stainless steel reinforcement may develop lower bond strength than carbon steel reinforcement, using the current bond design rules for designing stainless steel reinforced concrete structures without proper experimental data may not be a safe option.

Chapter 3: Development and validation of the finite element model for simply supported reinforced concrete beams

3.1 General

Numerical modeling and computational power have advanced rapidly in recent years, making it the best choice to simulate complex experiments with minimum cost and time. Numerical modeling can handle arbitrary loading conditions, boundary conditions, non-linearities and time dependence with emphasis on the geometric complexities and material characteristics (Jamali et al., 2013). It provides a better understanding of reinforced concrete structures as it shows the deformation shape, load factor and crack pattern (Otieno, et al., 2011). It also provides high flexibility as parameters can be changed easily and salient parameters identified and studied.

A finite element model has been developed using the general purpose finite-element analysis software Abaqus (Dassault Systèmes, 2016) in order to examine the behaviour of stainless steel reinforced concrete beams, and to conduct further parametric studies. Abaqus offers a number of different solution strategies for complex nonlinear problems and in the current work, an implicit dynamic solution procedure is selected following a detailed literature survey (e.g. Shamass and Cashell, 2017; Cotsovos, 2013; Chen et al., 2015; Sunayana and Barai, 2019). It was found that this method can be used efficiently for quasi-static applications and has been shown to provide excellent convergence behaviour.

Developing such numerical model typically involves serious challenges related to convergence problems owing to the complexity of the nonlinear behaviour of the composite materials. In order to overcome such problems, the following measures have been implemented:

- An implicit dynamic solution is rather than general static.
- A power stress-strain relationship is selected to model the softening tensile behaviour in concrete (this will be further discussed in next section).
- The maximum numbers of iterations and the number of increments are taken as 15 and 1000000, respectively.
- Additionally, the initial increment size was taken as 0.01 with the minimum value of 1×10^{-15}.

In this chapter, details of the development and validation of the finite element model are discussed.

3.2 Material behaviour

3.2.1 Concrete

A number of concrete material models are available in Abaqus including the smeared crack concrete model and the concrete damage plasticity (CDP) model. The former is based on reducing the stiffness of concrete elements when the stresses exceed the maximum tensile stress, while the latter considers the inelastic behaviour of concrete by defining damage factors in both compression and tension. The CDP model is selected in this study for simulating the concrete behaviour as it is more desirable in

applications where the concrete is subject to static loads and has been used widely for similar applications in the literature (e.g. Earij et al., 2017; George et al., 2017; Solhmirzaei et al., 2017; Fan et al., 2018).

The CDP model is based on continuum damage mechanics and considers two failure modes, namely cracking of the concrete in tension and crushing in compression. The material behaviour is defined in terms of the elastic, plastic, compressive and tensile properties. In the current work, Poisson's ratio and density of concrete are taken as 0.15 and 2400 kg/m^3, respectively. For the compression behaviour, the model given in Eurocode 2 (EN 1992-1-1, 2004) is adopted, given as:

$$\sigma_c = \left(\frac{k\eta - \eta^2}{1 + (k-2)\eta}\right) f_{cm} \qquad \text{for} \quad 0 \le \varepsilon_c \le \varepsilon_{cu} \tag{3.1}$$

In this expression, ε_{cu} is the nominal ultimate strain and f_{cm} is the ultimate compressive strength of concrete (in MPa), given by:

$$f_{cm} = f_c + 8 \tag{3.2}$$

where f_c is the characteristic cylinder strength. The parameters k and η are determined from Eqs. (3.3) and (3.4), respectively:

$$k = 1.05 E_c \frac{\varepsilon_{c1}}{f_{cm}} \tag{3.3}$$

$$\eta = \frac{\varepsilon_c}{\varepsilon_{c1}} \tag{3.4}$$

in which E_c is the elastic modulus of concrete (in MPa) and ε_{c1} is the strain at the peak stress, determined from Eqs. (3.5) and (3.6):

$$E_c = 22(0.1 f_{cm})^{0.3} \tag{3.5}$$

$$\varepsilon_{c1} = 0.7(f_{cm})^{0.31} \le 2.8 \tag{3.6}$$

The nominal ultimate strain (ε_{cu}), as a percentage, is given by:

$$\varepsilon_{cu} = 2.8 + 27[(98 - f_{cm})/100]^4 \quad \text{for} \quad f_c \ge 50\ \text{N/mm}^2, \text{ otherwise } 3.5 \tag{3.7}$$

The CDP model requires the compressive damage parameter (d_c) to be defined at each inelastic strain increment (ε_c^{in}), ranging from 0, for un-damaged material, to 1, when the concrete completely loses its load-bearing capacity. As shown in Fig. 3.1, this parameter is calculated for the descending branch of the stress-strain curve of concrete in compression as follows:

$$d_c = 0 \qquad \text{for} \quad \varepsilon_c < \varepsilon_{c1} \tag{3.8}$$

$$d_c = \frac{f_{cm} - \sigma_c}{f_{cm}} \qquad \text{for} \quad \varepsilon_c \geq \varepsilon_{c1}$$

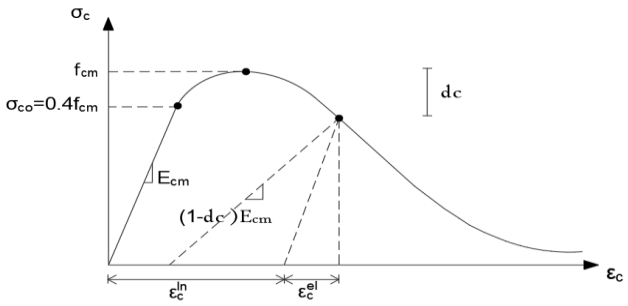

Fig. 3.1: CDP model for concrete in compression (Dassault Systèmes, 2016).

In tension, the concrete stress-strain behaviour is modelled as a linear relationship up to the ultimate tensile strength (ε_{cr}) followed by a gradually descending branch, which inherently incorporates the effects of tension stiffening (Fig. 3.2). The effect of the bond between the rebar and the concrete is approximated within this tension stiffening branch. Tension stiffening refers to the phenomenon whereby concrete continues to carry some tensile load even after cracking has taken place, though the tensile strength gradually decreases with increasing tensile strain. This is captured within the descending branch of the concrete stress-strain model which, in Abaqus, can be described using a linear, bilinear or nonlinear relationship. In this study, the power stress-strain relationship proposed by Wang and Hsu (2001) is employed for the descending branch, as described in Fig. 3.2 and presented in Eq. (3.9). This nonlinear formula is found to be capable for providing accurate predictions of the experimental response and has also been used by other researchers in the literature (e.g. Kmiecik and Kamiński, 2011; Dede and Ayvaz, 2009):

$$\begin{aligned} \sigma_t &= E_c \varepsilon_t \qquad \text{if} \quad \varepsilon_t \leq \varepsilon_{cr} \\ \sigma_t &= f_t \left(\frac{\varepsilon_{cr}}{\varepsilon_t}\right)^{0.4} \qquad \text{if} \quad \varepsilon_t > \varepsilon_{cr} \end{aligned} \tag{3.9}$$

The tensile strength (f_t) can be obtained as follows (EN 1992-1-1., 2004):

$$f_t = 0.3(f_c)^{2/3} \tag{3.10}$$

Similar to the compression behaviour, the CDP model requires the tensile damage parameter (d_t) to be defined as follows:

$$\begin{aligned} d_t &= 0 \qquad \varepsilon_t < \varepsilon_{cr} \\ d_t &= \frac{f_t - \sigma_t}{f_t} \qquad \varepsilon_t \geq \varepsilon_{cr} \end{aligned} \tag{3.11}$$

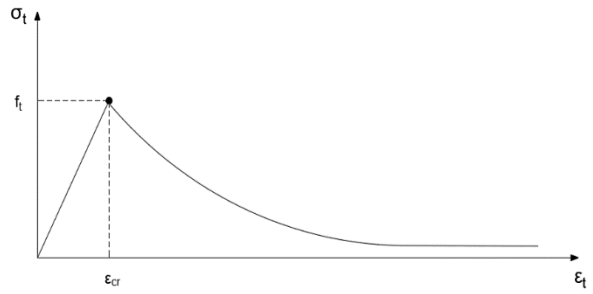

Fig. 3.2: Post-failure stress-strain relationship proposed by (Wang and Hsu, 2001).

In addition to the compressive and tensile constitutive relationships, the model makes use of the yield function of Lubliner et. al. (1989), with the modifications proposed by Lee and Fenves (1998), to account for different evolution of strength under tension and compression. The evolution of the yield surface is calculated by defining the ratio of the strength in the biaxial state to the strength in the uniaxial state (f_{b0}/f_{c0}) and the parameter K. The recommended default values in Abaqus manual are 1.16 and 0.667 for (f_{b0}/f_{c0}) and K, respectively. A number of other parameters are required in order to define the CDP model including the eccentricity, viscosity parameter and dilation angle.

Eccentricity is a parameter defines the rate at which the function approaches the asymptote (the flow potential tends to a straight line as the eccentricity tends to zero). A defualt value of 0.1 is selected for the eccentricity parameter.

Viscocity parameter, also known as the viscous regularisation, is an internal property of a fluid that offers resistance to flow. This parameter is used in the FE analysis in order to minimize the computational time and suppress numerical instabilities due to convergence difficulties by permitting stresses to be outside of the yield surface (Dassault Systèmes, 2016). However, the viscous regularisation must be used with extream cuation as the results might become quite inaccurate if a relatively large value is used. Hence, a defult value of zero is selected for the viscocity parameter.

The dilation angle is the angle of internal friction of the material and is also related to the mechanisms of crack propoagations in the concrete during the plastic period. The dilitaon angle is taken as 36° following other researchers in the literature (e.g. Shamass et al., 2014; Earij et al., 2017; Bypour et al., 2019; Farzad et al., 2019).

3.2.2 Reinforcement

The stainless steel material is represented in the model using the modified Ramberg-Osgood material model described in Chapter 2 and presented in Fig. 3.3. On the other hand, the carbon steel material is modelled using an elastic perfectly-plastic model, as shown in Fig. 3.3. As stainless steel does not exhibit a clearly defined yield point, the 0.2% proof stress is used to define the yield stress. The stress-strain relationships described in Eqs. (2.2) and (2.3) are employed to model the stainless steel constitutive relationship in Abaqus.

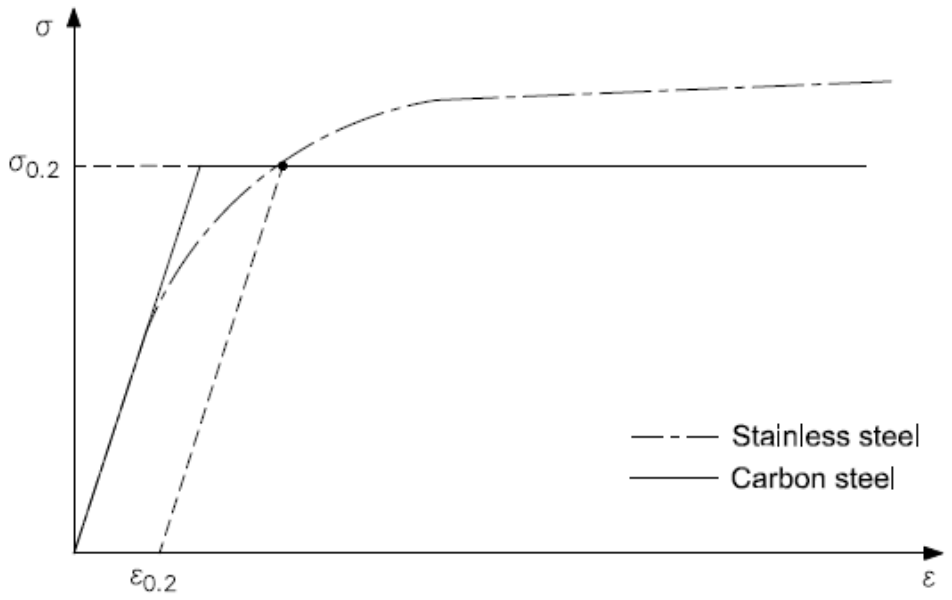

Fig. 3.3: Typical material model for stainless steel and carbon steel reinforcements.

Abaqus requires that the material properties are specified in terms of true stress (σ_{true}) and strain (ε_{true}) which can be derived from the engineering stress-strain curves as follows:

$$\sigma_{\text{true}} = \sigma(1 + \varepsilon)$$
$$\varepsilon_{\text{true}} = \ln(1 + \varepsilon) \quad (3.12)$$

3.3 Element types and mesh

In the model, the concrete elements are represented using 3D eight-node hexahedral elements which are known as C3D8 in the Abaqus library whereas the reinforcement is simulated using 2-node beam elements (B3). The reinforcement is embedded in the concrete. This means that if a node lies on the reinforcement which is embedded in the host element (e.g. concrete), the translational degrees of freedom at this node are eliminated and the node becomes "embedded node". Thus, the translational degrees of freedom at each node of the reinforcement are constrained to the interpolated values of the corresponding degrees of freedom of the concrete element (Dassault Systèmes, 2016). A mesh sensitivity study has been conducted to select the most appropriate size and it was found that elements which are 15 mm in size are the most appropriate in terms of achieving both computational accuracy and efficiency. For relatively small beams, a smaller element size of 10 mm is used. The mesh sensitivity study is discussed in more details in Section 3.6.

3.4 Boundary and loading conditions

The beam model is designed to simulate a four-point bending test arrangement where the loads are applied through a 3 cm wide surface in displacement control in order to avoid the local stress

concentration, as shown in Fig. 3.4. There are pinned boundary conditions and therefore the beam ends are restrained against vertical displacement but allow movement at the other degrees of freedom. As the beam is symmetrical about both its longitudinal axis and along the length, it is only necessary to model a quarter of the beam, and use symmetrical boundary conditions along the length and also around the x-axis and z-axis at the mid-span to reduce the computational time and cost.

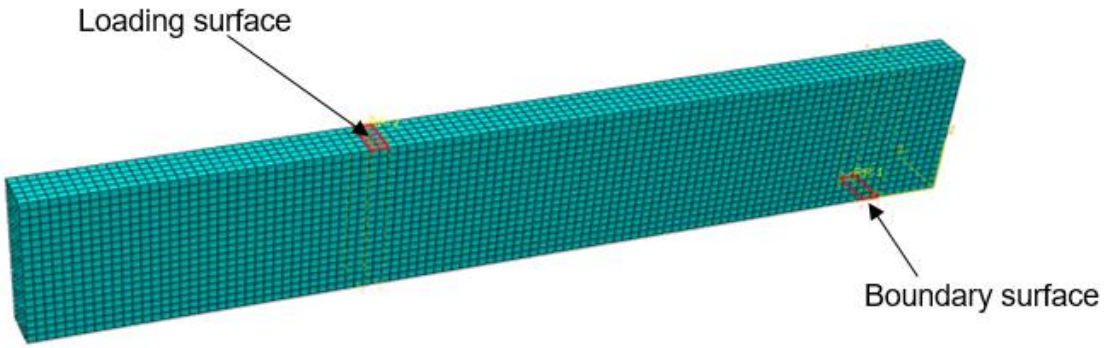

Fig. 3.4: Position of the boundary and load surface on the model.

3.5 Experimental results for validation

The FE model is validated using five reinforced concrete beams from different experimental programmes, as presented in Table 3.1. Beams SS and B3 were reinforced with austenitic and duplex stainless steel rebars in grade 1.4311 and 1.4362, respectively. As these are the only two stainless steel reinforced concrete beam tests which have been found in the literature, three other beams containing carbon steel reinforcement are also included in the validation exercise for additional robustness. The details of geometry and reinforcement of these beams are shown in Fig. 3.5.

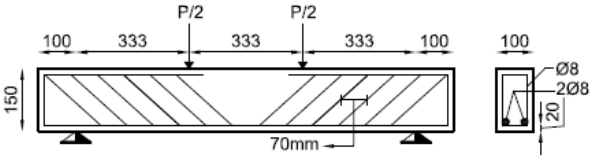

(a)

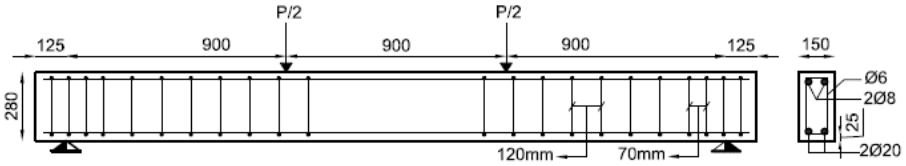

(b)

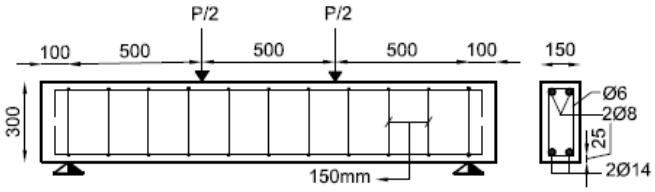

(c)

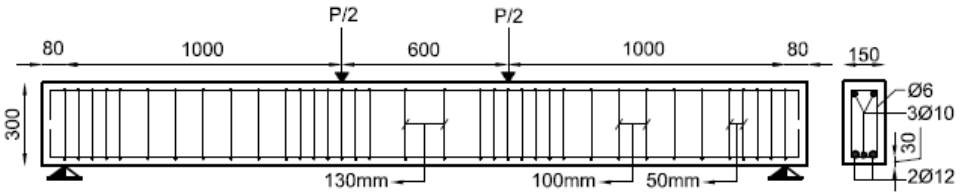

(d)

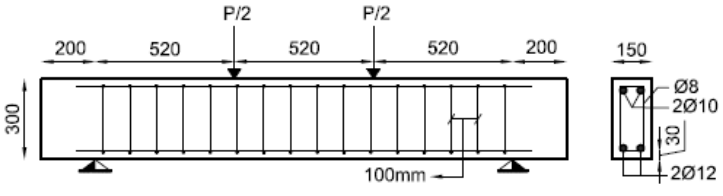

(e)

Fig. 3.5: Geometrical and reinforcement details of the beams used in the validation study, including (a) B3 (Medina et al., 2015) (b) SS (Alih and Khelil, 2012), (c) SR6 (Dong et al., 2013), (d) U2 (Alfano et al., 2011) and (e) O (Obaidat et al., 2011).

All of the beams were tested under monotonic loading, in displacement control. Beams B3, SR6 and O were loaded continuously until failure. On the other hand, beam U2 was loaded until cracking occurred and then unloaded to zero before being reloaded up to failure. Beam SS was subjected to loading up to 80 kN before the test was stopped (the reason for stopping the test at this point is not known but it was possibly owing to the test machine capacity being reached). Table 3.1 presents the material properties of the concrete and the reinforcement for each of these beams, as provided in the literature. The elastic modulus and tensile strength of the concrete can be calculated using Eq. (3.5) and Eq. (3.10), respectively, for beams where this data was not provided. For beam SS, the exponent of 0.4 in Eq. (3.9 is changed to 0.3 in order to obtain better depiction of the experimental response. This is most likely because this grade of stainless steel reinforcement has a different bond relationship with the surrounding concrete compared with carbon steel rebar.

Table 3.1: Material properties of the RC beams reported by (Medina et al., 2015; Alih and Khelil, 2012; Dong et al., 2013; Alfano et al., 2011 and Obaidat et al., 2011.

Beam	Reinforcement					Concrete	
	Material	Diameter (mm)	Young's modulus E (kN/mm^2)	Yield strength $\sigma_{0.2}$ (N/mm^2)	Ultimate strength σ_u (N/mm^2)	Young's modulus E_c (N/mm^2)	Compressive strength f_c (N/mm^2)
B3	Duplex stainless Steel 1.4362	8	189	1003	1066	Not provided	27 (cylinder)
SS	Austenitic stainless steel 1.4311	20	177	480	773	37.6	50.0 (cylinder)
SR6	Carbon steel	14	200	410	Not provided	Not provided	31.3 (cube)
U2	Carbon steel	12	205	380	Not provided	26.0	19.4 (cube)
O	Carbon steel	12	209	507	Not provided	Not provided	30.0 (cylinder)

3.6 Mesh sensitivity analysis

In numerical modelling, it is imperative to select a sufficiently fine mesh for achieving accurate results. A fine mesh provides more precise results than the coarse one but at higher computational cost. Therefore, it is extremely important to select an appropriate mesh size that provides accurate results at minimal computational costs. Hence a mesh sensitivity study is carried out through comparing the load-displacement curves form the numerical model with their corresponding experimental responses. Three experimental beam tests are selected for this purpose, two beams were reinforced with stainless steel (e.g. SS and B3) and one beam with carbon steel (e.g. SR6).

Fig. 3.6 and Fig. 3.7 present the load-displacement curves obtained numerically for beams SR6 and SS, respectively, using three different mesh sizes (namely 10 mm, 15 mm and 20 mm) in comparison with their corresponding experimental responses. It is observed that the overall load-displacement responses obtained using these different meshes are generally in good agreement with experimental response. However, the coarse mesh tends to provide slightly stiffer response compared with the others in the early stages. It is found that mesh size 15 mm provides accurate predictions which are quite similar to that of 10 mm mesh size, and therefore elements which are 15 mm in size have been selected in order to keep the computational cost to the minimum.

Fig. 3.8 shows the moment-displacement curves obtained numerically for beam B3 using three different mesh sizes in comparison with the corresponding experimental response. It is observed that there is no considerable difference between the responses obtained using the three meshes in terms of the cracking load, initial stiffness and the ultimate load. However, in the post-failure region, it is observed that the models with mesh size 20 mm and 15 mm fail to capture the experimental response whilst the model with mesh size 10 mm exhibits a very good agreement with the experimental response, and therefore it has been selected for beams with relatively short span.

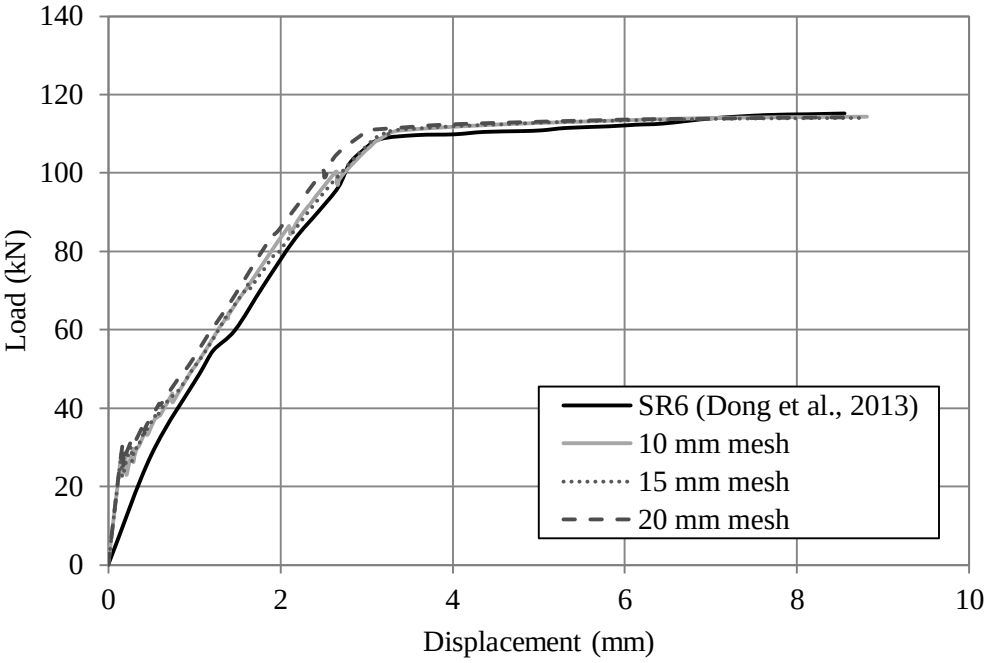

Fig. 3.6: Mesh sensitivity analysis for beam SR6.

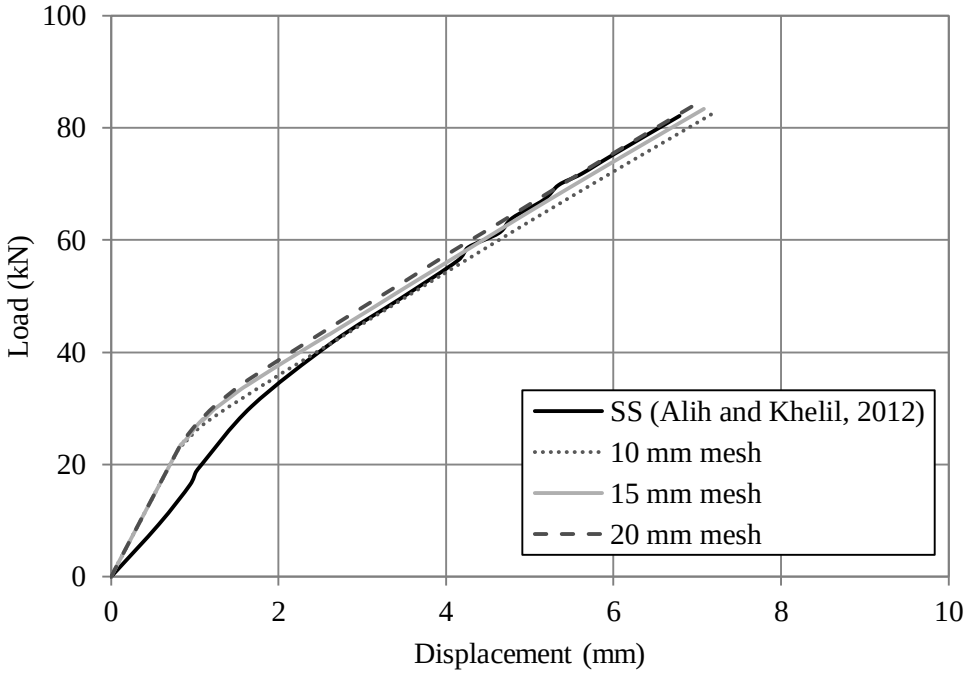

Fig. 3.7: Mesh sensitivity analysis for beam SS.

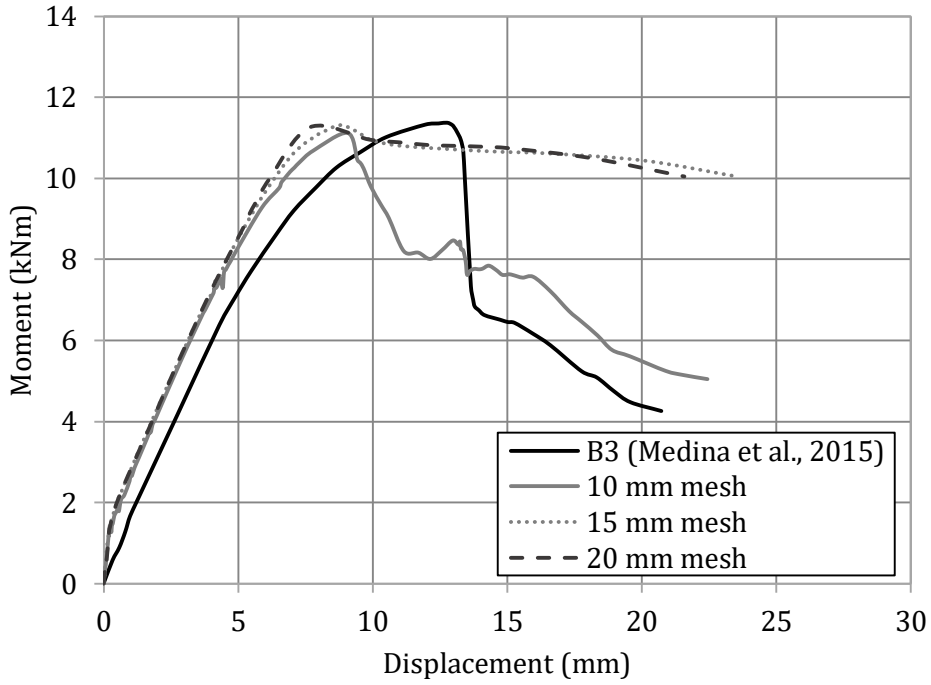

Fig. 3.8: Mesh sensitivity analysis for beam B3.

3.7 Failure criteria

In the numerical analysis, it is typically assumed that ultimate failure of a normally reinforced concrete beam occurs when the outer fibre of the concrete in compression reaches the ultimate crushing strain (usually taken as 0.003 or 0.0035). This is likely to occur when the reinforcement material exhibits elastic perfectly-plastic stress-strain properties, because the compressive strain in the concrete at the top surface is reached after the reinforcement yields so the steel no longer contributes towards the ultimate bearing capacity of the section. However, this behaviour is different when the reinforcement is made from stainless steel rather than carbon steel, owing to the significant levels of strain hardening and ductility in the stainless steel, and the lack of a distinct yield point. Even when the concrete reaches the crushing strain at the top surface, the stainless steel reinforcement is still contributing towards the ultimate bearing capacity of the section. In addition, it is difficult to predict exactly when the concrete has crushed and therefore, it is necessary to make an assumption regarding the exact point at which the concrete is assumed to have failed (e.g. once the first node at the top surface reaches the assumed strain limit or all nodes on the top surface). In order to avoid this uncertainty, in the current work the maximum capacity of the section is taken at the ultimate load capacity of the section, in the same manner that this is commonly determined experimentally.

3.8 Validation of the finite model

3.8.1 Load-displacement response

Fig. 3.9 presents the load-displacement curves obtained for beams SS, SR6, U2 and O from the FE model, together with the corresponding experimental data. Fig. 3.10 presents the moment-displacement curve for beam B3, as this is the manner in which the experimental data is published (Medina et al., 2015). With reference to Fig. 3.9, it is observed that the model presents an excellent depiction of the overall behaviour in all cases. The key features such as initial stiffness, cracking point, and ultimate strength are in very good agreement. For all of the beams, the initial stiffness of the beams is slightly greater in the FE model data compared with the experimental response, most likely due to some localised cracking in the experiment which is not captured in the numerical simulations. For beam U2, the loading-unloading-reloading path is reasonably well simulated by the model although there is some disparity between the residual displacements (i.e. the displacements when the applied load returns to zero following the unloading phase) predicted (around 3.9 mm) and those that occurred in the test (1.53 mm). This is possibly due to differences in the way that the tensile behaviour of concrete is represented in the model, compared with the experimental performance.

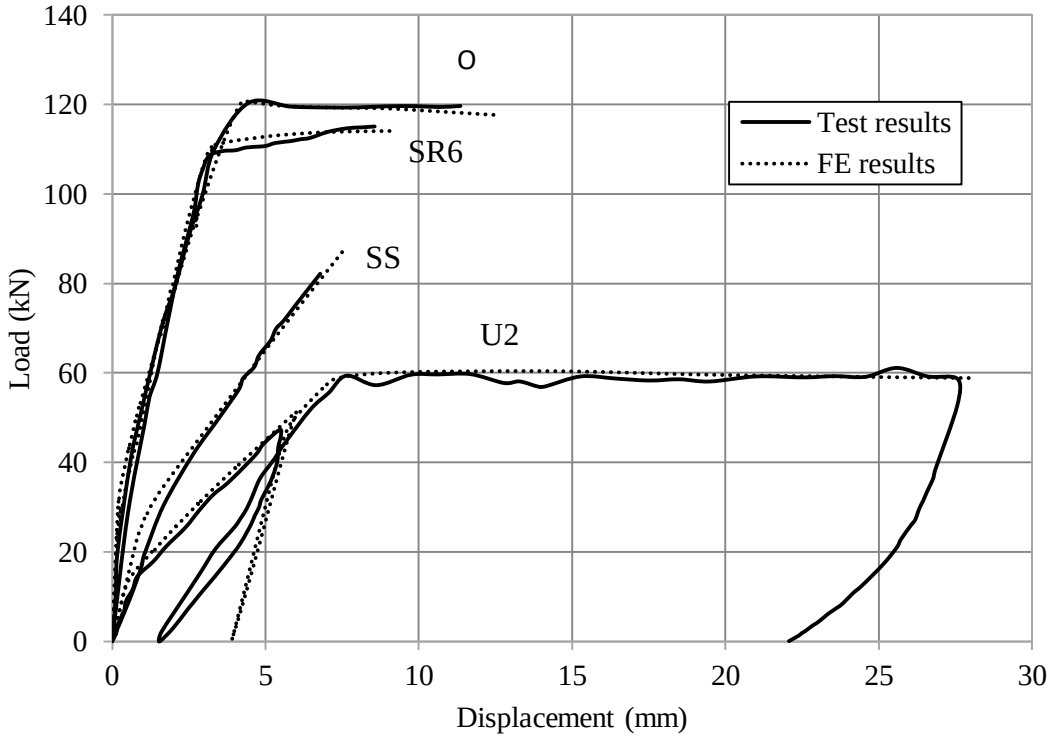

Fig. 3.9: Comparison between experimental and numerical load-displacement curves for beams SS (Alih and Khelil, 2012), SR6 (Dong et al., 2013), U2 (Alfano et al., 2011) and O (Obaidat et al., 2011).

The results for beam B3 presented in Fig. 3.10 demonstrate that the FE model captures the ultimate moment quite well, with the disparity between the model predictions and the experimental data being around 2%. However, the stiffness response obtained numerically is greater than occurred during the experiment, which is most likely due to localised cracking again that is not captured exactly by the model. It is observed in the numerical model that the beam exhibits a sudden failure in the post-failure region owing to concrete crushing, this result is in line with the experimental response. In conclusion, a good agreement has been shown between the numerical load-displacement response and the experimental data.

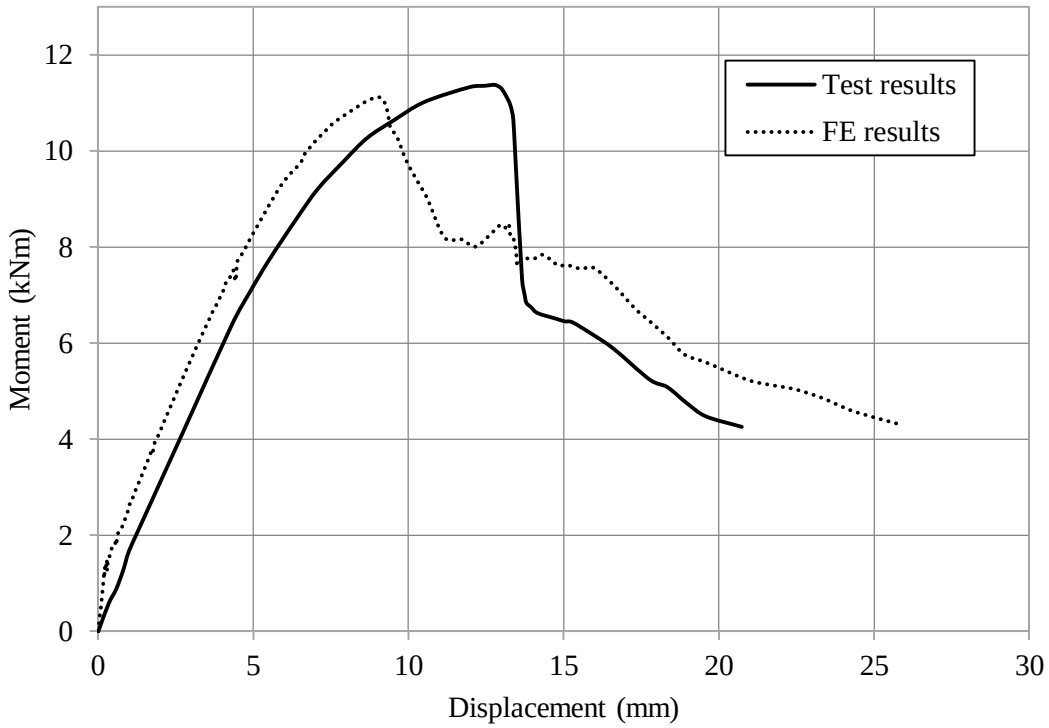

Fig. 3.10: Comparison between experimental and numerical moment-displacement curves for beam B3 (Medina et al., 2015).

3.8.2 Crack pattern

Fig. 3.11 (a) and (b) show the crack patterns obtained numerically and experimentally, respectively, for beam SR6 at the ultimate load, which occurred at a displacement of 3.7 mm (it is noteworthy that the FE model captures the opposite side of the beam than that is represented in Fig. 3.11 (b). This beam is selected for demonstration purposes and similar comparisons have been found for all of the other beams in this validation study, where the data is available in the literature. In the legend for Fig. 3.11 (a), the term “PE Max Principle” as outputted by Abaqus refer to the tensile plastic strain values in the concrete which represent tensile cracks in the beam. In the FE analysis, two cracks develop in the constant-moment region (i.e. the region between the middle of the beam and the application of the

point load), comprising a large crack near the middle of the beam and another under the applied load. In addition, a number of cracks merge into one large diagonal crack in the high shear region (i.e. the area between the support and the application of the point load). Similarly, in the experimental image, one vertical crack formed in the constant-moment region, another short crack occurred below the applied load and a diagonal crack developed in the high shear region.

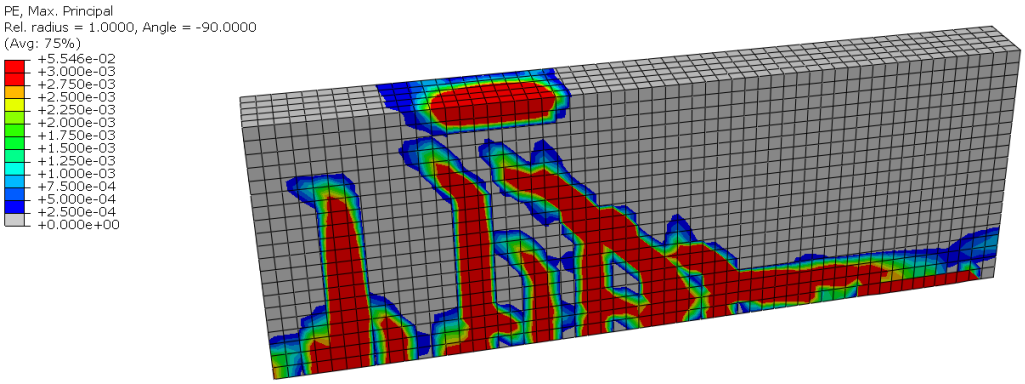

(a)

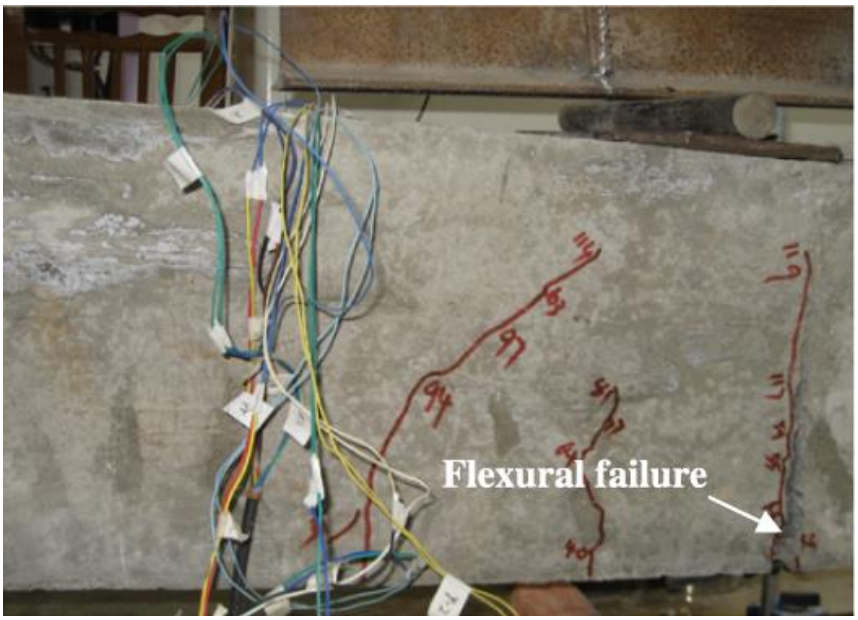

(b)

Fig. 3.11: Crack patterns of beam SR6 obtained by the (a) numerical analysis and (b) experiment (Dong et al., 2013).

Fig. 3.12 and Fig. 3.13 present the crack patterns obtained numerically for the beams SS and B3, respectively, which are the beams reinforced with stainless steel; the experimental patterns are not included in the literature for these beams. With reference to beam SS, it is observed that a large number of cracks developed, which are well distributed along the length of the beam. On the other hand, in Fig. 3.13 for beam B3, it is shown that two cracks developed in the constant-moment region, one crack beneath the load point and four cracks in the shear region. The fewer number of cracks in this case, compared with SS, are mainly due to the shorter member length.

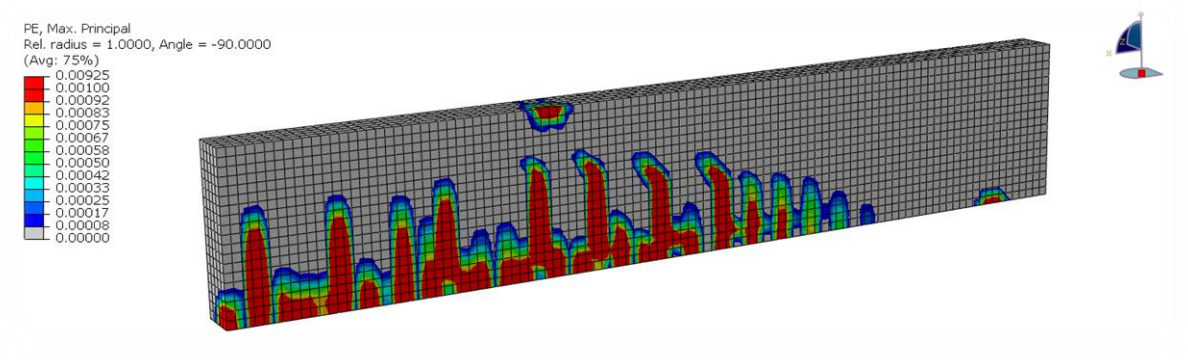

Fig. 3.12: Crack patterns of beam SS obtained numerically.

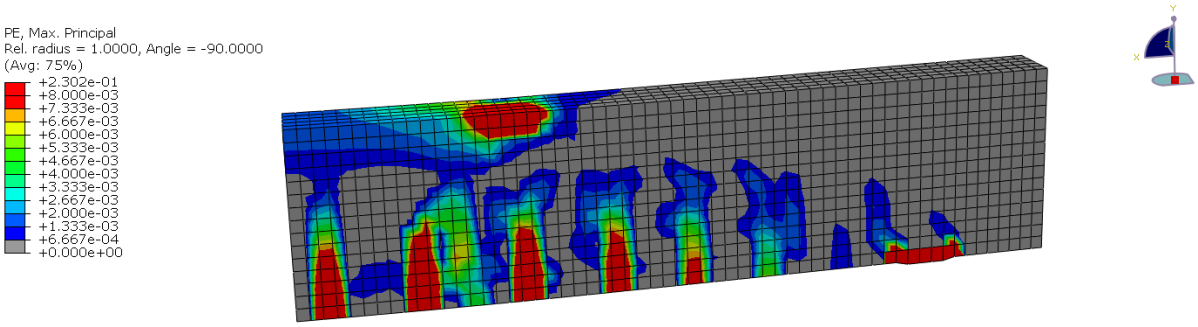

Fig. 3.13: Crack patterns of beam B3 obtained numerically.

3.9 Concluding remarks

In this chapter, the FE model has been developed using Abaqus software and validated using the available data in the literature. On the basis of data presented in the previous sections, it is concluded that the FE model developed in this study is capable of providing a good prediction of the behaviour of stainless steel and carbon steel reinforced concrete beams in terms of the ultimate load, load-displacement response and crack propagation. There are some very small differences in terms of initial bending stiffness, but this is most likely due to localised cracking in the test which cannot be accurately assessed in the numerical model.

Chapter 4: A new design method for stainless steel reinforced concrete beams

4.1 Introduction

One of the great advantages of stainless steel compared with carbon steel is the greater ductility and strain hardening capacity. Currently, the vast majority of global design standards, including Eurocode 2, do not include an efficient design model for concrete structures with stainless steel reinforcement as they neglect the ductility and strain hardening characteristics of stainless steel. Although this assumption is acceptable for carbon steel reinforced concrete, it gives inaccurate predictions when stainless steel reinforcement is employed. Extensive research into the behaviour of structural stainless steel has been reported in the literature including the flexural behaviour (e.g. Yang et al., 2016; Hassanein and Silvestre, 2013; Wang et al., 2014), compressive behaviour (e.g. Gardner and Theofanous, 2008; Huang and Young, 2014; Afshan and Gardner, 2013) and the mechanical characteristics (e.g. Ramberg and Osgood, 1943; Rasmussen, 2003). Although there has been extensive research in recent years into the behaviour of structural stainless steel, most of this has been on bare stainless steel sections, rather than reinforced concrete. Therefore, the aim of this chapter is to assess the behaviour and design of stainless steel reinforced concrete beams and to investigate the impact of neglecting strain hardening in the design roles given in Eurocode 2 on the load-bearing capacity. The novel contribution of this chapter is to develop and validate a new deformation-based design approach for stainless steel reinforced concrete beams including full and simplified analytical models in order to exploit the distinctive strain hardening properties of stainless steel reinforcement.

4.2 Design of reinforced concrete beams in Eurocode 2

In the design of reinforced concrete beams, Eurocode 2 assumes that the compression forces are resisted entirely by the concrete whereas the steel reinforcement carries the tension. The tensile strength of concrete is difficult to measure accurately and represents only about 10% of the compressive strength, so its contribution is usually ignored. Fig. 4.1 shows (a) a typical simple RC cross-section together with the corresponding (b) strain and (c and d) stress distributions, as assumed in Eurocode 2. In these figures, b and h are the width and depth of the beam, respectively, and y and d are the locations of the neutral axis and steel reinforcement from the top fibre of the beam, respectively. The strain in the concrete at the outer fibre is ε_c whereas ε_s is the reinforcement strain, and f_c and σ_s are the characteristic compressive stress of the concrete and tensile stress in the reinforcement, respectively. The failure mechanisms considered are either crushing of the concrete (i.e. when the strain at the outer fibre of the concrete reaches the ultimate crushing strain) or yielding of the reinforcement (i.e. when the strain in the steel reinforcement reaches its yield value). In accordance with the stress blocks presented in Fig. 4.1(d), any contribution to the load capacity after the steel yield strength has been reached, is not considered in design. Giving that the majority of

global design standards including Eurocode 2 implement an elastic-plastic idealisation, the significant levels of strain hardening and great ductility of stainless steels would not be utilised.

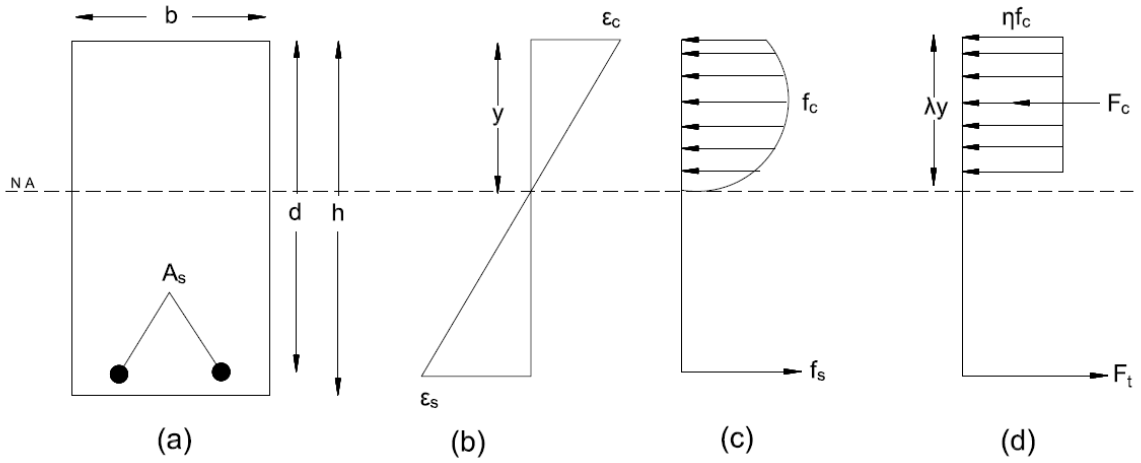

Fig. 4.1: Strain and stress distribution diagrams for a singly reinforced concrete beam including (a) the cross-section (b) the strain distribution through the section, (c) the stress distribution and (d) an equivalent stress distribution in the section, simplifying the concrete stress block.

4.3 Stainless steel constitutive stress–strain relationships

As stated previously, the stress-strain behaviour of stainless steel is quite different from that of carbon steel. Carbon steel has a linear elastic response with a well-defined yield point and yield plateau, followed by a moderate degree of strain hardening. On the other hand, stainless steel exhibits a predominantly non-linear and continuous stress-strain response without a clearly-defined yield point as well as significant levels of strain hardening. In the absence of a visible yield point, the typical value adopted is the 0.2% proof stress ($\sigma_{0.2}$) which is determined by drawing a line with a slope equal to the elastic modulus (E) between 0.2% strain on the x-axis and the stress-strain curve.

The relationships proposed by Ramberg-Osgood (1943) and updated by Mirambell & Real (2000) and Rasmussen (2003), are employed to represent the stress-strain relationship of stainless steel, as presented in Eq. (4.1), to define the stress-strain relationship of stainless steel up to the proof stress followed by Eq. (4.2) for greater levels of stress.

$$\varepsilon = \frac{\sigma}{E} + 0.002\left(\frac{\sigma}{\sigma_{0.2}}\right)^n \qquad \text{for} \quad \sigma \leq \sigma_{0.2} \tag{4.1}$$

$$\varepsilon = \varepsilon_{0.2} + \frac{\sigma-\sigma_{0.2}}{E_2} + \left(\varepsilon_u - \varepsilon_{0.2} - \frac{\sigma_u-\sigma_{0.2}}{E_2}\right)\left(\frac{\sigma-\sigma_{0.2}}{\sigma_u-\sigma_{0.2}}\right)^m \quad \text{for} \quad \sigma_{0.2} < \sigma \leq \sigma_u \tag{4.2}$$

In these expressions, ε and σ are the engineering strain and stress, respectively, E_2 is the tangent modulus at the 0.2% proof stress point, σ_u and ε_u are the ultimate stress and corresponding strain,

respectively, $\varepsilon_{0.2}$ is the strain corresponding to $\sigma_{0.2}$ and n and m are model constants related to the strain hardening behaviour.

4.3.1 Constitutive relationship comparison

In order to build a greater understanding of the stress-strain characteristics of stainless steel reinforcement and to evaluate the deficiencies in current design rules, the experimental data presented in the literature (Gardner et al., 2016) is compared to the relationships obtained using the material model presented in equations (4.1) and (4.2), as well as the elastic-plastic material model currently provided in Eurocode 2. A number of different grades of austenitic and lean duplex stainless steel are considered, including grades 1.4162, 1. 4307 and 1.4311. Fig. 4.2 presents the experimental stress-strain curves for stainless steel reinforcement tested by Gardner et al. (2016). The previously-discussed nonlinear relationship is clear, with no defined yield point and a high degree of strain hardening. All of the tested grades exhibited excellent strength and ductility.

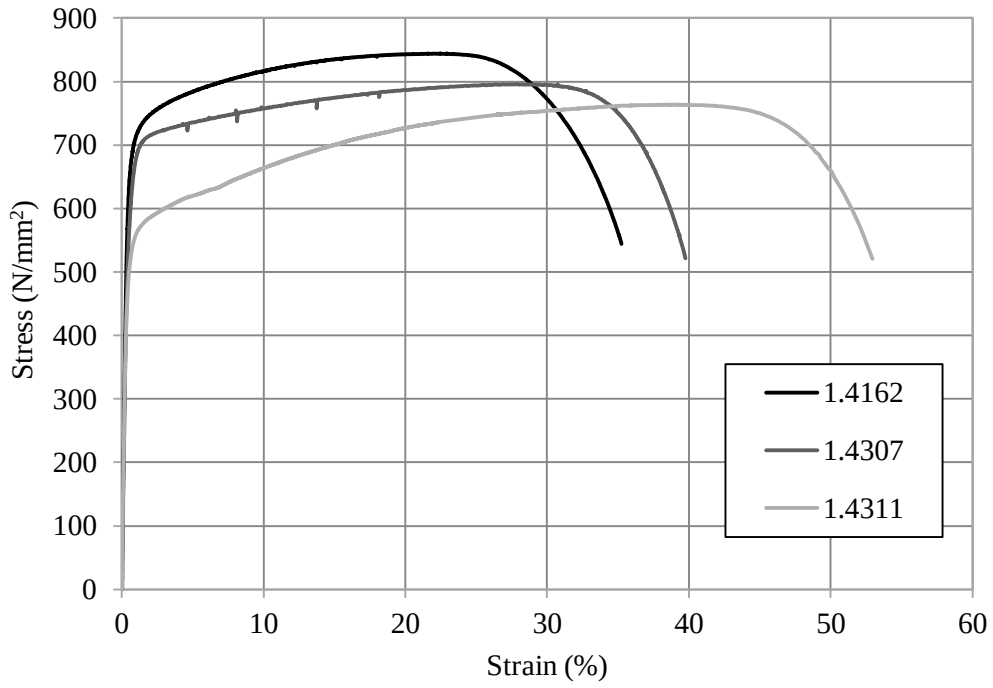

Fig. 4.2: Stress-strain curves for different grades of stainless steel (Gardner et al., 2016).

Fig. 4.3, Fig. 4.4 and Fig. 4.5 present the same experimental stress-strain curves as presented in Fig. 4.2 (Gardner et al., 2016), together with the relationships obtained using the modified Ramberg-Osgood material model and Eurocode 2, for grades 1.4162, grade 1.4307 and 1.4311, respectively. In these figures, both the overall response is presented as well as a closer view of the elastic portion of the behaviour. The parameters for these stress-strain curves are presented in Table 4.1. It is noteworthy that the steels are listed giving their European designation (i.e. 1.4XXX) as well as the commonly used AISI names, in brackets. Generally, it is shown that the modified Ramberg-Osgood

model provides a better representation of the experimental behaviour for all stainless steel grades compared with Eurocode 2. Clearly, ignoring strain hardening in the material response leads to significant errors in the stress-strain curve. The modified Ramberg-Osgood (RO) model provides an excellent depiction of stainless steel grade 1.4311, however it slightly overestimates the stresses for lean duplex grade 1.4162, and slightly underestimates the response of austenitic stainless steel grade 1.4307.

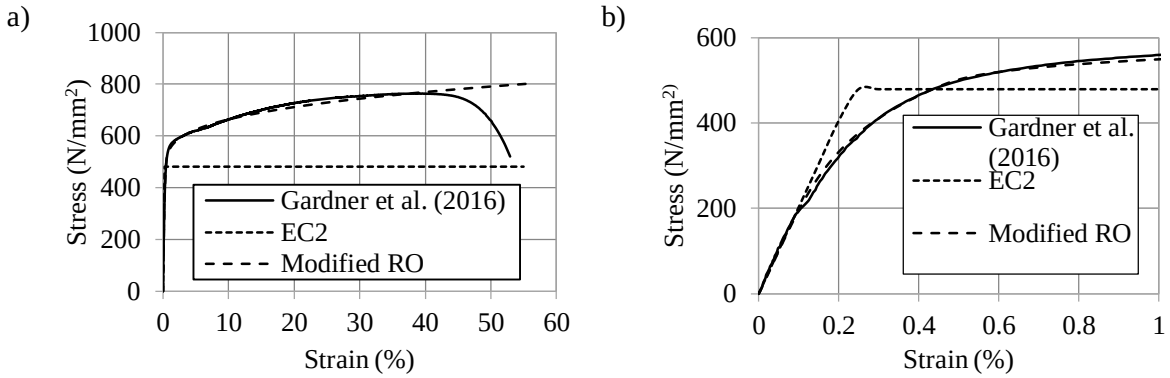

Fig. 4.3: Stress-strain curves obtained experimentally and analytically for grade 1.4311 (a) full curve and (b) more detailed view of the elastic region.

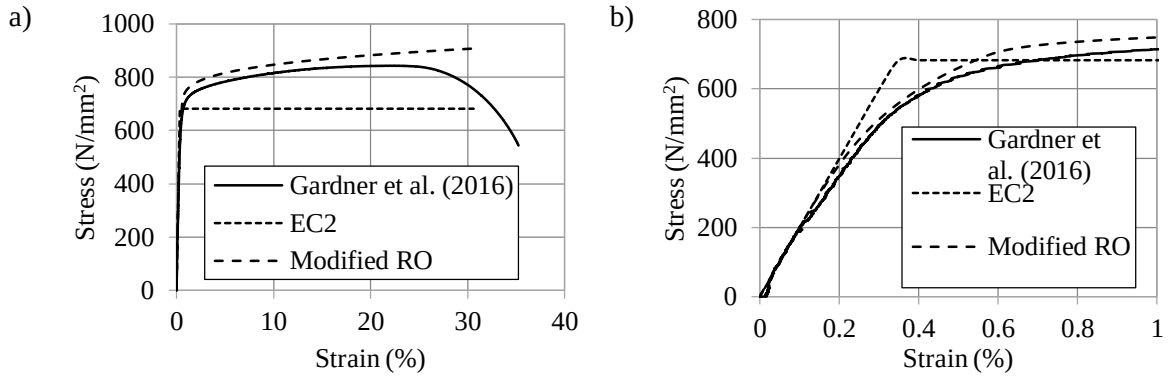

Fig. 4.4: Stress-strain curves obtained experimentally and analytically for grade 1.4162 (a) full curve and (b) more detailed view of the elastic region.

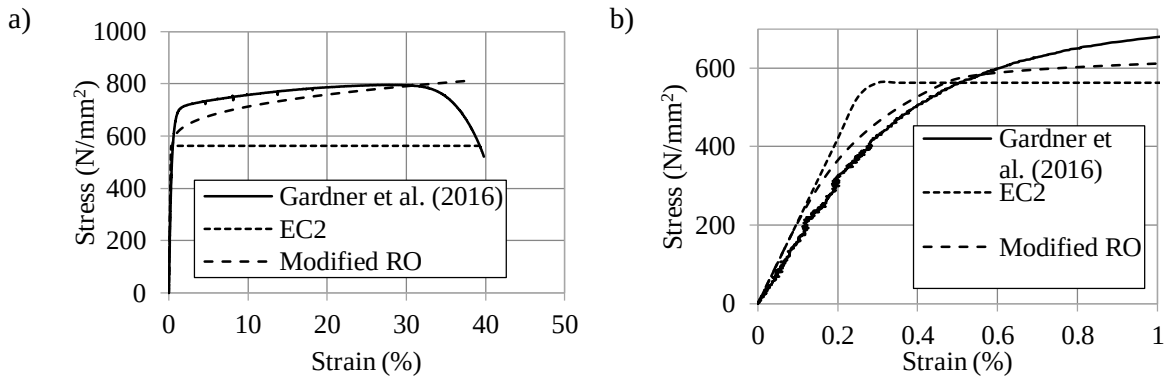

Fig. 4.5: Stress-strain curves obtained experimentally and analytically for grade 1.4307 (a) full curve and (b) more detailed view of the elastic region.

Table 4.1: Material properties of stainless steel (Gardner et al., 2016).

Stainless steel type	Grade	Bar diameter (mm)	$\sigma_{0.2}$ (MPa)	σ_u (MPa)	E (MPa)	ε_u (%)	n	m
Austenitic	1.4311 (304LN)	12	480	764	202600	38.6	4.7	4.8
Lean duplex	1.4162 (LDX2101)	12	682	874	199100	20.4	5.3	5.0
Austenitic	1.4307 (304L)	12	562	796	210200	30.7	4.7	4.8

4.3.2 Effect of neglecting strain hardening on the load-bearing capacity

In this section, the validated FE model described in the previous chapter is utilized to investigate the effect of neglecting strain hardening on the load-bearing capacity of concrete beams with stainless steel reinforcement by implementing the elastic-perfectly plastic material model provided currently in Eurocode 2 as well as the modified Ramberg-Osgood model which captures the strain hardening contribution. The numerical model is then used to study the influence of different stainless steel grades and concrete strengths on the overall behaviour. Beam SS is utilised herein for illustrative purposes as it was reinforced with stainless steel. The material properties of the stainless steel grades are given in Table 4.1.

Fig. 4.6 presents the load-displacement curves obtained from the FE model using both material models. It can be clearly observed that there is an excellent agreement in all cases in terms of the initial stiffness and the cracking point, regardless of the model used for the stainless steel rebar. However, later in the response, there is a considerable difference in terms of the plastic behaviour as the simulation which employed the modified Ramberg-Osgood model exhibits significant strain hardening, whilst the response generated using the elastic-perfectly plastic material model from Eurocode 2 has a well-defined yield point followed by no strain hardening. The effect of including strain hardening in the analysis is clearly demonstrated by the significant difference in the ultimate loads. The beams reinforced with stainless steel grades 1.4311, 1.4162 and 1.4307 and depicted using the modified Ramberg-Osgood material model have load capacities which are 48.6, 24 and 37.17% greater than those modelled with the material model in Eurocode 2, respectively. These results emphasize the deficiency of the design rules in Eurocode 2 in predicting the load capacity for concrete beams with stainless steel mainly because of neglecting the significant strain hardening characteristic. However, there are other important parameters that govern design including deflections and safety factors, therefore a serviceability limit state analysis must be considered too.

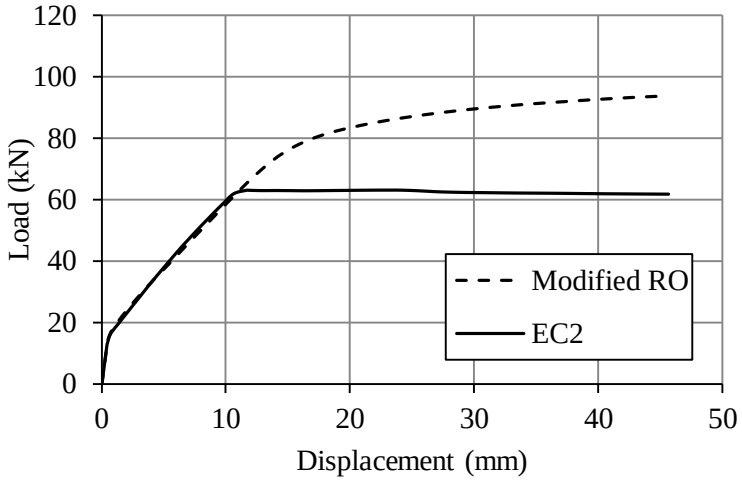

(a)

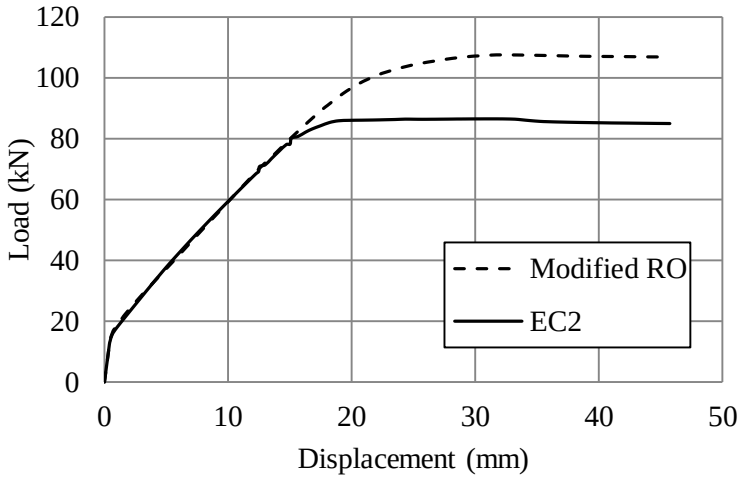

(b)

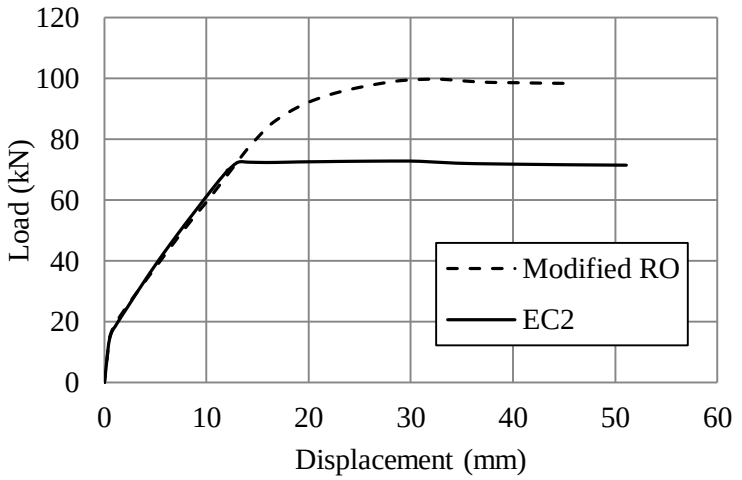

(c)

Fig. 4.6: The influence of the stainless steel material model on the load-displacement response for beams reinforced with (a) grade 1.4311, (b) grade 1.4162 and (c) grade 1.4307 stainless steel.

Table 4.2 presents a comparison of the ultimate loads obtained numerically using either the reinforcement material model in Eurocode 2 or the modified RO material model for different grades of stainless steel and a range of concrete strengths. For all cases, the beams modelled in accordance with the modified Ramberg-Osgood model have an average of a 33% greater ultimate load capacity compared with those modelled using the Eurocode 2 approach. Moreover, using higher concrete strength results in an increase in the load capacity of the beams as illustrated in the final column in Table 4.2, owing to the improvement in compression capacity in concrete. These results emphasise that the design rules suggested by Eurocode 2 provide overly-conservative results and underestimate the capacity of the concrete beams reinforced with stainless steel. For this reason, designing stainless steel RC structures using the existing design rules is neither efficient nor reflective of the real behaviour. It is in this context that the current work is undertaken and a new approach for the design of reinforced concrete structures with stainless steel rebar is developed.

Table 4.2: Comparison between the ultimate loads obtained numerically by implementing Eurocode 2 and modified RO material models using beam SS with a width of 150 mm and a depth of 280 mm.

Stainless steel grades	Concrete grades	Ultimate load using Eurocode 2 material model (kN)	Ultimate load using Modified RO material model (kN)	Modified RO / Eurocode 2 (%)
1.4311	30	59.6	78.9	+32.4
	40	62.2	91.4	+47.0
	50	63.1	93.7	+48.6
1.4162	30	84.9	101.5	+19.5
	40	86.3	104.9	+21.5
	50	86.6	107.4	+24.0
1.4307	30	71.2	94.1	+32.2
	40	71.9	97.1	+35.0
	50	72.7	99.7	+37.2

4.4 New design method of stainless steel reinforced concrete beams

4.4.1 Background to the Continuous Strength Method

The Continuous Strength Method (CSM) is a deformation-based design method which has been developed in recent years to enable material strain hardening properties to be exploited, thus resulting in more accurate capacity predictions and more efficient design. The CSM was originally developed for the design of stainless steel members with non-slender cross-sections (Gardner and Nethercot, 2004). Since then, it has been extended many times to cover the design of structural members made from stainless steel (e.g. Afshan and Gardner, 2013; Ashraf et al., 2008, carbon steel (e.g. Gardner, 2008; Gardner et al., 2011; Liew and Gardner, 2015), aluminium (Su et al., 2016) and high strength steel (Lan et al., 2018). In recent years, the method has been adapted for composite construction including carbon steel-concrete composite beams (Gardner et al., 2017) and stainless steel-concrete composite members with either a full and partial shear connection (Shamass and Cashell, 2018).

In the current work, a similar approach is adopted to develop a deformation-based design method for reinforced concrete beams with stainless steel rebar, allowing for the true stainless steel constitutive relationship. This is developed in two forms, first as a full model in which the whole material response is captured and then as a simplified model incorporating a more simplistic elastic-linear hardening stainless steel constitutive response.

4.4.2 Material models

The full and simplified version of the proposed CSM design model use two different material models for representing the stainless steel reinforcement. The modified Ramberg-Osgood stainless steel material model presented previously in Eqs. (4.1) and (4.2) and depicted in Fig. 4.7, is used for the full CSM analysis. Whilst, the simplified CSM employs a bilinear, elastic-linear hardening stress-strain relationship for the stainless steel rebar, as shown in Fig. 4.7, in order to avoid the need to solve complex nonlinear equations. In this approach, the yield point is identified as the 0.2% proof stress and the corresponding yield strain (i.e. $\sigma_{0.2}$ and $\varepsilon_y = \frac{\sigma_{0.2}}{E}$, respectively). The slope of the strain hardening region (E_{sh}) is obtained from the line passing through the yield point (ε_y, $\sigma_{0.2}$) and the defined ultimate point ($C_2\varepsilon_u$, σ_u), as defined in Eq. (4.3). It has been found that a value of 0.15 is an appropriate value for the constant C_2 in the current work, in agreement with previous CSM developments (Afshan and Gardner, 2013).

$$E_{sh} = \frac{\sigma_u - \sigma_{0.2}}{C_2\varepsilon_u - \varepsilon_y} \tag{4.3}$$

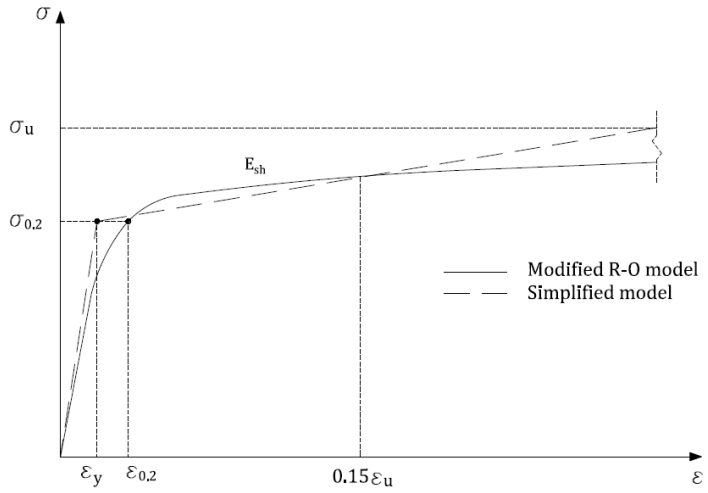

Fig. 4.7: The simplified material model for stainless steel with reference to the modified R-O model.

4.4.3 Flexural capacity of stainless steel reinforced concrete beams

4.4.3.1 Full analytical model

In this section, the continuous strength method (CSM) is developed to analyse the behaviour of stainless steel reinforced concrete beams, using the modified Ramberg-Osgood relationship described in Eqs. (4.1) and (4.2) to model the rebars. The plastic bending moment capacity is obtained by locating the neutral axis (NA) and then applying the equilibrium of internal force equations to the cross-section of the beam. In order to idealise the behaviour, the following assumptions are made in the analytical model, in accordance with Eurocode 2:

[1] The nominal ultimate strain of the concrete (ε_{cu}) is assumed to be 0.0035 for material with a compressive strength less than 50 N/mm^2, otherwise it is determined using Eq. (4.4):

$$\varepsilon_{cu} = 2.6 + 35[(98 - f_{cm})/100]^4 \quad (4.4)$$

[2] As presented in Fig. 4.1(d), an equivalent rectangular stress distribution is assumed for the concrete in compression. The effective strength of the concrete is $0.85f_c$, where f_c is the characteristic compressive strength of the concrete, and the effective height of the compression zone is 0.8y, where y is the distance from the NA to the top fibre of the cross-section.

The material model for stainless steel given in Eqs. (4.1) and (4.2) provides strain as a function of stress. However, in order to implement the material model in conjunction with the design method, it is necessary to identify the stress as a function of strain, which requires a numerical procedure. In the current work, the approximate inversion relationship proposed by Abdella (2006) for the full stress-strain relationship of stainless steel is employed to describe the stress (σ) as an explicit function of strain (ε), as presented in the Eqs. (4.5) and (4.6):

$$\sigma_1(\varepsilon) = \sigma_{0.2}\frac{r\left(\frac{\varepsilon}{\varepsilon_{0.2}}\right)}{1+(r-1)\left(\frac{\varepsilon}{\varepsilon_{0.2}}\right)^p} \quad \text{for} \quad \varepsilon \leq \varepsilon_{0.2} \tag{4.5}$$

$$\sigma_2(\varepsilon) = \sigma_{0.2}\left[1 + \frac{r_2\left[\frac{\varepsilon}{\varepsilon_{0.2}}-1\right]}{1+(r^*-1)\left(\frac{\frac{\varepsilon}{\varepsilon_{0.2}}-1}{\frac{\varepsilon_u}{\varepsilon_{0.2}}-1}\right)^{p^*}}\right] \quad \text{for } \varepsilon > \varepsilon_{0.2} \tag{4.6}$$

where the material parameters are:

$$\varepsilon_{0.2} = \frac{\sigma_{0.2}}{E} + 0.002 \qquad r = \frac{E\,\varepsilon_{0.2}}{\sigma_{0.2}}$$

$$E_2 = \frac{E}{1 + 0.002\,n/e} \qquad p = r\frac{1-r_2}{r-1}$$

$$e = \frac{\sigma_{0.2}}{E} \qquad m = 1 + 3.5\frac{\sigma_{0.2}}{\sigma_u}$$

$$\sigma_u = \sigma_{0.2}\frac{1-0.0375(n-5)}{0.2+185e} \qquad E_u = \frac{E_2}{1+(r^*-1)m}$$

$$r_2 = \frac{E_2\,\varepsilon_{0.2}}{\sigma_{0.2}} \qquad r_u = \frac{E_u(\varepsilon_u - \varepsilon_{0.2})}{\sigma_u - \sigma_{0.2}}$$

$$\varepsilon_u = \min\left(1 - \frac{\sigma_{0.2}}{\sigma_u}, A\right) \qquad p^* = r^*\frac{1-r_u}{r^*-1}$$

$$r^* = \frac{E_2(\varepsilon_u - \varepsilon_{0.2})}{\sigma_u - \sigma_{0.2}}$$

In these expressions, A is the stainless steel elongation, E_2 and E_u are the slope of the stress-strain curve at $\varepsilon_{0.2}$ and ε_u, respectively, and r, r_2, r*, r_u, p, p* and m are parameters that need to be determined.

For calculating the bending moment capacity of a singly reinforced beam, there are two possible cases. Case 1 is when the tensile strain of the reinforcement is less than the total strain corresponding to $\sigma_{0.2}$ (i.e. $\varepsilon_s \leq \varepsilon_{0.2}$) and Case 2 is when the tensile strain of the reinforcement is greater than the total strain corresponding to $\sigma_{0.2}$ (i.e. $\varepsilon_s > \varepsilon_{0.2}$). The internal tensile and compressive forces in the cross-section are calculated based on the full stainless steel stress-strain material model and the equivalent rectangular compressive stress distribution in the concrete, together with the strain distribution in the

section. In order to determine the tensile stress in the reinforcement at failure of the beam, the strain can be calculated from the strain distribution in Fig. 4.1(d), as follows:

$$\varepsilon_s = \kappa(d - y) \tag{4.7}$$

$$\kappa = \min(\kappa_{su}, \kappa_{cu}) \tag{4.8}$$

where κ_{su} is the limiting curvature for stainless steel failure and κ_{cu} is the limiting curvature for concrete failure (i.e. when the strain at the top fibre of the beam reaches the ultimate strain of concrete). There are two possible failure modes, defined by κ_{su} and κ_{cu}. If $\kappa_{su} < \kappa_{cu}$, the beam fails due to rupture of the stainless steel reinforcement whereas if $\kappa_{su} > \kappa_{cu}$, the reinforced beam fails due to concrete crushing. The values of κ_{su} and κ_{cu} are determined as:

$$\kappa_{su} = \frac{\varepsilon_u}{d - y}$$

$$\kappa_{cu} = \frac{\varepsilon_{cu}}{y} \tag{4.9}$$

From equilibrium of the internal forces in the beam, the sum of the tensile forces (F_t) and the compression forces (F_c) must equal zero:

$$F_c - F_t = 0 \tag{4.10}$$

The tension force is determined as the product of the steel area (A_s) and the stress in the stainless steel (σ_s):

$$F_t = A_s \sigma_s \tag{4.11}$$

and the compression force is found using the equivalent rectangular stress block presented in Fig. 4.1(d), to give:

$$F_c = 0.85 f_c (0.8y) b \tag{4.12}$$

Substituting Eq. (4.12) and Eq. (4.11) into Eq. (4.10) gives:

$0.68 f_c y\, b - A_s \sigma_s = 0$ or

$$y = \frac{A_s \sigma_s}{0.68 f_c\, b} \tag{4.13}$$

When the stainless steel strain is less than $\varepsilon_{0.2}$ (i.e. $\varepsilon_s \leq \varepsilon_{0.2}$), the tensile stress in the reinforcement at d is determined by substituting Eq. (4.7) into Eq. (4.5) to give:

$$\sigma_s = \sigma_1(y) = \sigma_{0.2} \frac{r\left(\frac{\kappa(d-y)}{\varepsilon_{0.2}}\right)}{1+(r-1)\left(\frac{\kappa(d-y)}{\varepsilon_{0.2}}\right)^p} \tag{4.14}$$

which can be used together with Eq. (4.13) to obtain y, the depth of the neutral axis measured from the top fibre of the beam. Since the stress $\sigma_1(y)$ is a nonlinear function of the variable y, Eq. (4.13) and Eq. (4.14) create a nonlinear problem which must be solved using an iterative method. Once the position of the neutral axis, y, is located, the assumption of $\varepsilon_s \leq \varepsilon_{0.2}$ must be checked by calculating the strain in the stainless steel using Eq. (4.7). If the assumption is correct, the plastic bending moment capacity of the beam is calculated by taking moments about the position that the compressive internal force in the concrete acts, as follows:

$$M_{pl} = A_s \sigma_s (d - 0.4y) \tag{4.15}$$

where σ_s is the tensile stress in the stainless steel calculated from Eq. (4.14) and corresponding to the obtained neutral axis depth, y.

If the stainless steel strain is higher than the strain corresponding to $\sigma_{0.2}$ (i.e. $\varepsilon_s > \varepsilon_{0.2}$), the tensile stress of the reinforcement can be obtained by substituting Eq. (4.7) into Eq. (4.6) to give:

$$\sigma_s = \sigma_2(y) = \sigma_{0.2}\left[1 + \frac{r_2\left(\frac{\kappa(d-y)}{\varepsilon_{0.2}}-1\right)}{1+(r^*-1)\left(\frac{\frac{\kappa(d-y)}{\varepsilon_{0.2}}-1}{\frac{\varepsilon_u}{\varepsilon_{0.2}}-1}\right)^{p^*}}\right] \tag{4.16}$$

The position of the neutral axis (y) can then be obtained, as before, using the equilibrium of internal forces (i.e. Eq. (4.13)) and substituting the tensile stress obtained from Eq. (4.16) into Eq. (4.13). Once the position of neutral axis is known, the plastic bending capacity is calculated by taking moments about the position of the compression force, and is given in the Eq. (4.15). As before, σ_s is the tensile stress in the stainless steel calculated from Eq. (4.16) and corresponding to the calculated value of y. A flow chart presenting the full procedure for determining the neutral axis and the plastic bending moment capacity is given in Fig. 4.8.

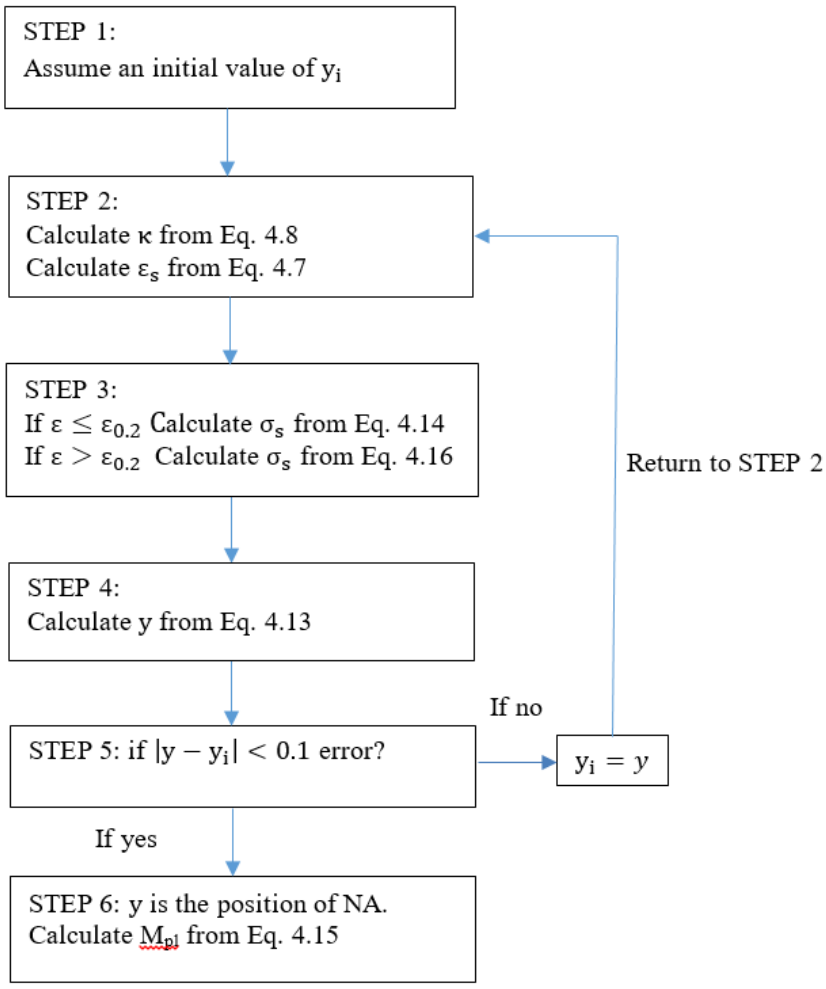

Fig. 4.8: Flow chart of the solution procedure for a singly reinforced concrete beam.

4.4.3.2 Simplified analytical model

In the previous section, a detailed analytical solution was presented to predict the plastic bending moment capacity of stainless steel reinforced concrete beams, incorporating the full stress-strain behaviour of the stainless steel material. This method involves a solution of complex nonlinear equations requiring iterative methods to obtain the position of the neutral axis, which may not be a straightforward procedure for designers. Therefore, in this current section, a simplified analytical solution is developed based on a simpler material model for the stainless steel, as described in Section 4.4.2 and Fig. 4.7. The other initial assumption in the simplified model is that the section always fails due to concrete crushing (i.e. $\kappa_{su} > \kappa_{cu}$), which is a legitimate assumption for concrete beams reinforced with stainless steel rebar owing to its ductility. Hence, the tensile strain of the reinforcement at the failure of the section is determined from the strain distribution in Fig. 4.1(b) as follows:

$$\varepsilon_s = \frac{\varepsilon_{cu}}{y}\,(d - y) \tag{4.17}$$

The tensile stress of the stainless steel can be calculated from the simplified material model presented in Fig. 4.7, in accordance with Eqs. (4.18) and (4.19) hereafter:

$$\sigma_s = E\varepsilon_s \qquad \varepsilon_s \le \varepsilon_y \tag{4.18}$$

$$\sigma_s = \sigma_{0.2} + E_{sh}(\varepsilon_s - \varepsilon_y) \qquad \varepsilon_s > \varepsilon_y \tag{4.19}$$

There are two possible cases for prediction of the bending moment capacity of reinforced beam. Case 1 is when the tensile strain of the reinforcement is less than the yield strain (i.e. $\varepsilon_s \le \varepsilon_y$) and Case 2 is when the tensile strain of the reinforcement is higher than the yield strain (i.e. $\varepsilon_s > \varepsilon_y$). For Case 1, when the strain in the stainless steel is less than ε_y (i.e. $\varepsilon_s \le \varepsilon_y$), the tensile stress in the reinforcement at d is determined by substituting Eq. (4.17) into Eq. (4.18) to give:

$$\sigma_s = E\frac{\varepsilon_{cu}}{y}\,(d - y) \tag{4.20}$$

which can be used together with Eq. (4.13) to give:

$$0.68 f_c\, y\, b - A_s E \frac{\varepsilon_{cu}}{y}\,(d - y) = 0 \tag{4.21}$$

This can be simplified to Eq. (4.22):

$$0.68 f_c b y^2 + A_s \varepsilon_{cu} E y - A_s \varepsilon_{cu} d E = 0 \tag{4.22}$$

Once the position of the neutral axis (y) is located by solving this quadratic equation, the assumption of $\varepsilon_s \le \varepsilon_y$ must be checked by calculating the strain in the stainless steel using Eq. (4.17). If the assumption is correct, the plastic bending moment capacity of the beam is calculated by taking moments about the position of the compressive internal force in the concrete using Eq. (4.15) where σ_s is the tensile stress in the stainless steel calculated from Eq. (4.20).

If the stainless steel strain is higher than the yield strain (i.e. $\varepsilon_s > \varepsilon_y$), the tensile stress of the reinforcement can be obtained by substituting Eq. (4.17) into Eq. (4.19) to give:

$$\sigma_s = \sigma_{0.2} + E_{sh}\left(\frac{\varepsilon_{cu}}{y}\,(d - y) - \varepsilon_y\right) \tag{4.23}$$

As before, the position of the neutral axis is located using the equilibrium of the internal forces by substituting the tensile stress obtained from Eq. (4.23) into Eq. (4.13) to give:

$$0.68f_c y\, b - A_s\left(\sigma_{0.2} + E_{sh}\left(\frac{\varepsilon_{cu}}{y}(d-y) - \varepsilon_y\right)\right) = 0 \tag{4.24}$$

This can simplified, as follows:

$$0.68f_c b\, y^2 + \left(E_{sh}\varepsilon_{cu} + E_{sh}\varepsilon_y - \sigma_{0.2}\right)A_s\, y - A_s E_{sh}\varepsilon_{cu} d = 0 \tag{4.25}$$

Once the position of the neutral axis is located using Eq. (4.25), the plastic bending moment capacity is calculated as given in Eq. (4.15) where σ_s is the tensile stress in the stainless steel calculated from Eq. (4.23). In both cases, the assumption of $\kappa_{su} > \kappa_{cu}$ must be checked to ensure that the beam section fails due to concrete crushing.

In the case that the limiting curvature for stainless steel is less than that of the concrete (i.e. $\kappa_{su} < \kappa_{cu}$), the beam fails due to the rupture of stainless steel reinforcement, which should be very rare in reality or even impossible. In this scenario, the tensile strain of the reinforcement at failure of the section is its ultimate tensile strain, as given in Eq. (4.26):

$$\varepsilon_s = \varepsilon_u \tag{4.26}$$

The tensile stress of the stainless steel is determined by substituting Eq. (4.26) in to Eq. (4.19) to give:

$$\sigma_s = \sigma_{0.2} + E_{sh}(\varepsilon_u - \varepsilon_y) \tag{4.27}$$

As before, the position of the neutral axis is located by applying the equilibrium of internal forces criteria, and substituting the tensile stress obtained from Eq. (4.27) into Eq. (4.13) to give:

$$0.68f_{ck} y\, b - A_s\left(\sigma_{0.2} + E_{sh}(\varepsilon_u - \varepsilon_y)\right) = 0 \tag{4.28}$$

Again, once the position of the neutral axis is located using Eq. (4.28), the plastic bending moment capacity is calculated as given in Eq. (4.15) where σ_s is the tensile stress in the stainless steel calculated from Eq. (4.27).

4.5 Validation of the proposed analytical models

Both the full and simplified analytical models described previously are validated herein using the FE model, by comparing the predicted bending capacities. In order to obtain a robust validation, both of the reinforced concrete beams which included stainless steel rebar, i.e. SS and B3, are studied. A number of different concrete strengths are used in the analysis (i.e. C26, C30, C40, C50). Additionally, three different grades of stainless steel are investigated using the data presented by Gardner et al. (2016), which is presented in Table 4.1. Both beams B3 and SS are selected for further analysis in which a number of different geometric properties are varied, in order to assess their influence on the response. These parameters are detailed in Table 4.3.

Table 4.3: Range of geometrical parameters included in the study.

Width (mm)	Depth (mm)	Bar diameter (mm)
100-150	125-255	8-12

Table 4.4 and Table 4.5 present the bending moment capacity obtained from the proposed full analytical method (AM), the simplified analytical method (SM) and the numerical analysis (FE) as well as the values determined using the design method provided in Eurocode 2 (EC2), for beam SS and B3, respectively. In the Eurocode calculation, it is assumed that the stainless steel material model is elastic-perfectly plastic. In addition, the bending moment capacity predicted using both the full and the simplified analytical solutions are presented together in Fig. 4.9. This figure also includes the equation for the tendency of the data, as well as the R^2 (coefficient of determination).

Table 4.4: Comparison between the ultimate bending moment capacity of the numerical and that of the analytical analysis for beam SS.

Stainless steel grade	Bar diameter (mm)	Concrete strength	EC2 (kNm)	AM (kNm)	FE (kNm)	SM (kNm)	EC2 / FE (%)	AM / FE (%)
1.4311 (304LN)	12	30	26.15	31.95	39.56	30.20	-33.89	-19.23
		40	26.53	33.44	41.11	32.25	-35.47	-18.67
		50	26.76	34.49	42.20	34.04	-36.59	-18.27
1. 4162 (LDX2101)	12	30	36.23	40.01	45.79	39.35	-20.88	-12.62
		40	37.00	41.78	47.21	41.88	-21.63	-11.51
		50	37.47	42.92	48.37	44.01	-22.54	-11.27
1.4307 (304L)	12	30	30.30	35.13	42.36	33.76	-28.48	-17.07
		40	30.83	36.66	43.71	35.88	-29.47	-16.13
		50	31.15	37.69	44.87	37.70	-30.58	-16.01

Table 4.5: Comparison between the ultimate bending moment capacity of the numerical and that of the analytical analysis for beam B3.

Stainless steel grade	Diameter (mm)	Concrete strength	EC2 (kNm)	AM (kNm)	FE (kNm)	SM (kNm)	EC2 / FE (%)	AM / FE (%)
1.4362 (AIS 2304)	8	27	10.45	9.79	11.12	10.45	-6.03	-11.92
		40	11.61	11.84	12.32	11.68	-5.76	-3.90
1.4311 (304LN)	12	27	11.51	11.37	11.54	11.65	-0.26	-1.49
		40	12.38	13.50	15.11	12.94	-18.06	-10.64
1. 4162 (LDX2101)	12	27	13.11	12.33	11.43	13.11	14.70	7.88
		40	16.55	15.98	17.32	16.69	-4.43	-7.73
1.4307 (304L)	12	27	12.95	11.98	11.22	12.98	15.42	6.81
		40	14.15	14.78	17.02	14.52	-16.86	-13.16

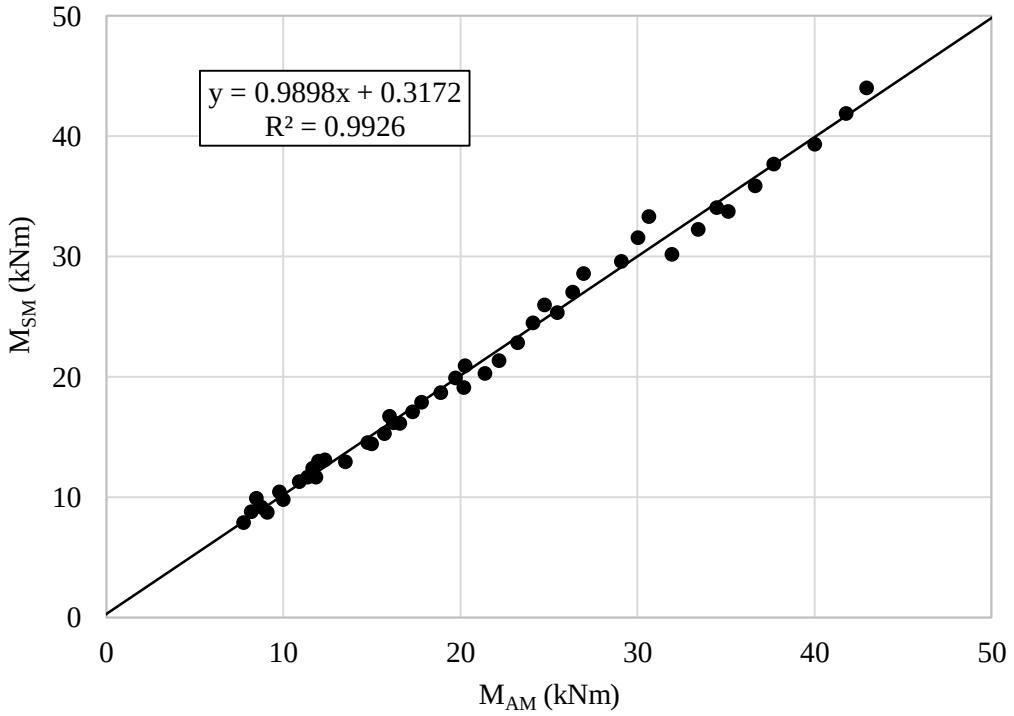

Fig. 4.9: Comparison between the results obtained using the full and simplified analytical solution.

Based on the data presented in Table 4.4 and Table 4.5 and Fig. 4.9, the following general observations are made:

- A very good agreement is obtained between the numerical analysis and the proposed full analytical method in almost all cases, with the maximum and average AM/FE values being -19% and -15.6%, respectively, for beam SS and -13% and -4.3%, respectively, for beam B3. These same values using the Eurocode 2 design rules (EC2/FE) are -37% and -28.8% for SS and -18% and -2.7% for B3. Clearly, the full analytical design method, based on determination of limiting deformations, provides more accurate and realistic moment capacities.
- For beam SS (Table 4.4) the full analytical method underestimates the bending moment capacity in all cases, similarly for beam B3 (Table 4.5), the predicted analytical results are below the numerical results in all cases, except two values.
- For beam SS, it can be seen that the proposed full analytical method improves the bending capacity of the section in average by around 19.0% compared to the current design approach in EC2 whilst no improvement is found for beam B3. In the latter case, the relatively lower prediction using the analytical model rather than existing design rules in some cases is due to the fact that the stresses in the rebar are lower than their proof stress, as shown by the values presented in Table 4.6, when the beam reaches to the maximum loading capacity. Therefore, these beams were not designed to exploit the strain hardening qualities of the stainless steel as concrete failure dominates.
- With reference to Fig. 4.9, it is observed that the predictions of the bending moment capacity obtained using the simplified analytical solution are in very good agreement with those obtained using full analytical solution. In all cases, the simplified predictions fluctuate above and below the prediction of the full analytical model. Therefore, it is concluded that the simplified solution is adequate for predicting the bending moment capacity for stainless steel RC beams.

By implementing these proposed analytical solutions for the design of concrete beams reinforced with stainless steel, the distinctive strain hardening properties of stainless steel are exploited, thus improving the capacity and ductility of the beams in design. At ultimate load capacity, the beam section is more likely to fail by the crushing of concrete rather than the rupture stainless steel. Hence, the strain hardening capacity of the stainless steel reinforcements would not be fully exploited compared with stainless steel structural elements. Nevertheless, the results presented in Table 4.4 and Table 4.5 illustrate the capability of the proposed methods for providing a more accurate and efficient bending moment capacity over a wide range of concrete strengths and stainless steel grades, compared to the traditional design method.

Table 4.6: Rebar stresses compared to their proof stresses for beam B3.

Grade of stainless steel	Reinforcement diameter (mm)	Concrete grade	Stress in the reinforcement (N/mm^2)	Reinforcement proof strength (N/mm^2)
1.4362 (AIS 2304)	8	27	879.88	1003
		40	1023.88	1003
1.4311 (304LN)	12	27	472.79	480
		40	529	480
1. 4162 (LDX2101)	12	27	525.63	682
		40	652.72	682
1.4307 (304L)	12	27	505.74	562
		40	590.24	562

4.6 Concluding remarks

This chapter has presented a detailed study on the behaviour of stainless steel reinforced concrete beams. It is now clear that the design rules in Eurocode 2 ignore the significant strain hardening characteristics and high levels of ductility that stainless steel offers. This design approach provides over-conservative and inaccurate predictions of the section capacity. Therefore, a new deformation-based design method is proposed including full and simplified approach which incorporates the distinctive strain hardening characteristics of stainless steel in design of reinforced concrete beams. The proposed methods have been validated and shown to be effective design tools for stainless steel reinforced concrete beams.

Chapter 5: Parametric study

5.1 Introduction

This chapter further develops and analyses the behaviour and design of stainless steel reinforced concrete beams with reference to the current design provisions in Eurocode 2. Building on the previous chapter, the CSM approach is examined over an extensive range of parameters, with emphasis given to the geometry of the section, reinforcement ratio and also deflections, in the context of the nonlinear stress-strain behaviour. Around 100 numerical simulations have been conducted to investigate the influence that the design parameters have on the exploitation of strain hardening and ductility of the stainless steel reinforcement in the section. Moreover, the serviceability limit state is also explored through a detailed analysis of the deflection behaviour.

5.2 Range of parameters

All of the members in this study are assumed to be simply supported beams under four-point loading conditions and have a clear span of 3300 mm in order to avoid shear failure in the beam. The full range of parameters examined is presented in Table 5.1. Four different concrete strengths are used in the analysis (i.e. C20, C30, C40 and C50). In addition, three different grades of stainless steel, including two austenitic grades (1.4311 and 1.4311) and one lean duplex stainless steel (grade 1.4162), are studied using the material data presented by Gardner et al. (2016). This data is given in Table 4.1, including the n and m parameters required for application of the modified Ramberg-Osgood material model.

Table 5.1: Range of geometrical parameters included in the study.

Parameter	Range examined
Concrete grade	C20, C30, C40, C50
Grade of stainless steel reinforcement	1.4311, 1.4162 and 1.4307
Width/height (b/h) ratio of the beam	0.55 to 1
Diameter of the reinforcement	12 mm and 20 mm
Reinforcement ratio (%)	0.187 – 5.2 %

5.3 Bending moment capacity predictions

Fig. 5.1, Fig. 5.2 and Fig. 5.3 present the bending moment predictions obtained from the proposed full analytical model (AM), the simplified analytical model (SM) and the numerical model (FE) as well as those obtained using the design method provided in Eurocode 2 (i.e. elastic-perfectly-plastic behaviour of the material is assumed), for beams reinforced with stainless steel grades 1.4311, 1.4162, 1.4307, respectively. The results are presented in terms of bending moment versus concrete strength (f_c), to highlight how this parameter influences the behaviour.

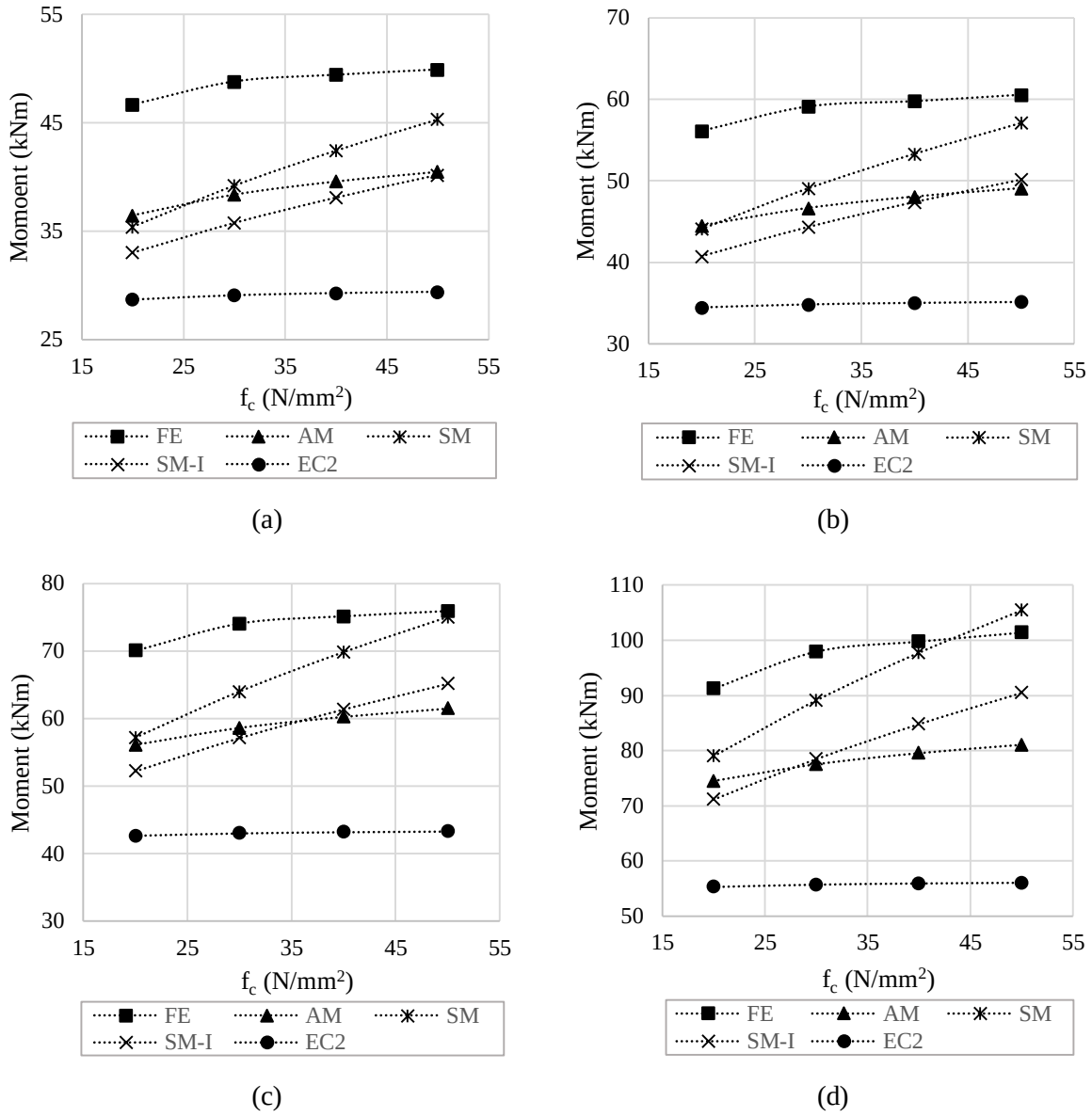

Fig. 5.1: Bending moment predictions for beams with grade 1.4311 austenitic stainless steel using a b/h ratio of (a) 1.00 (b) 0.85 (c) 0.70 and (d) 0.55.

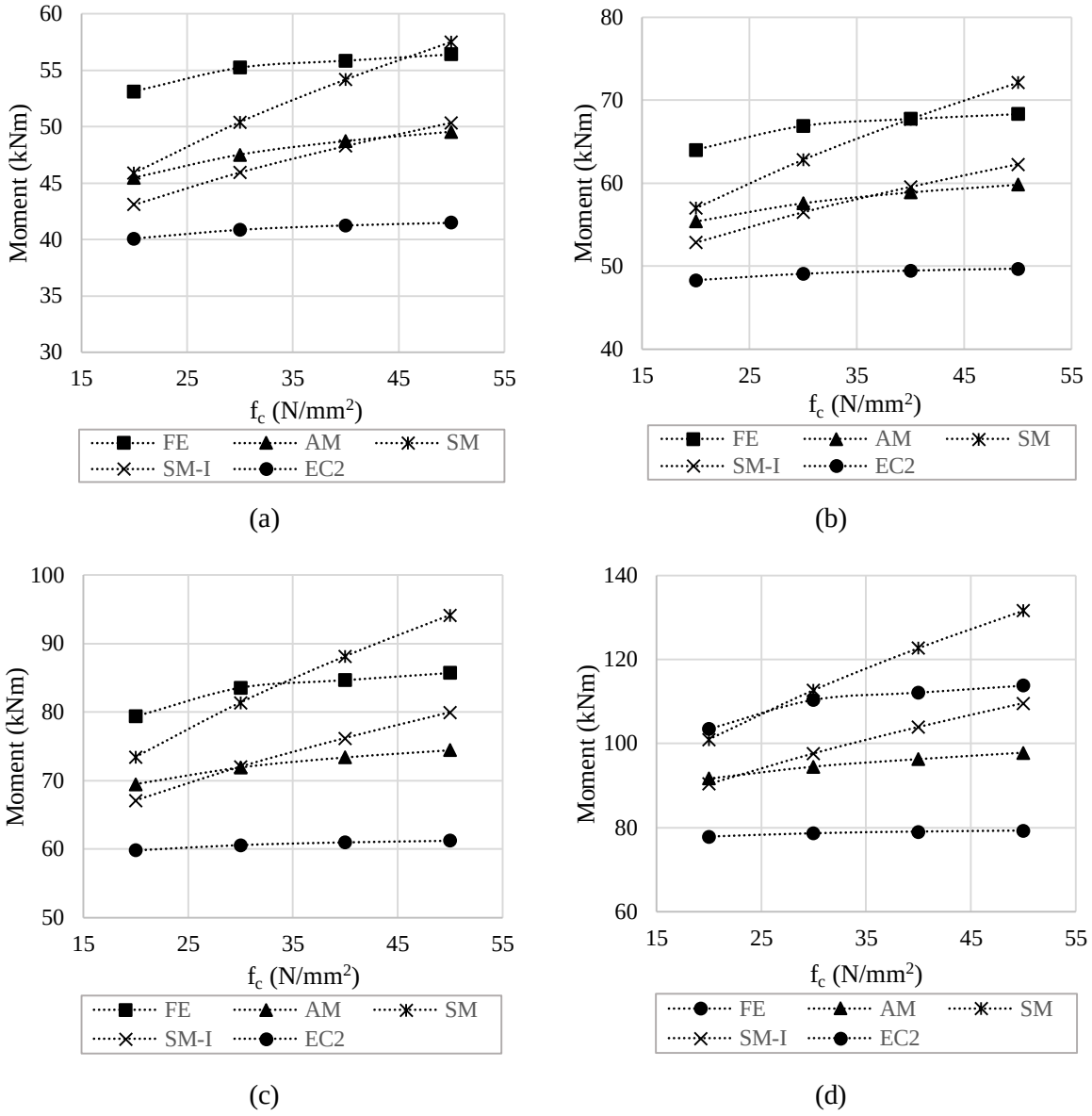

Fig. 5.2: Bending moment predictions for beams with grade 1.4162 duplex stainless steel using a b/h ratio of (a) 1.00 (b) 0.85 (c) 0.70 and (d) 0.55.

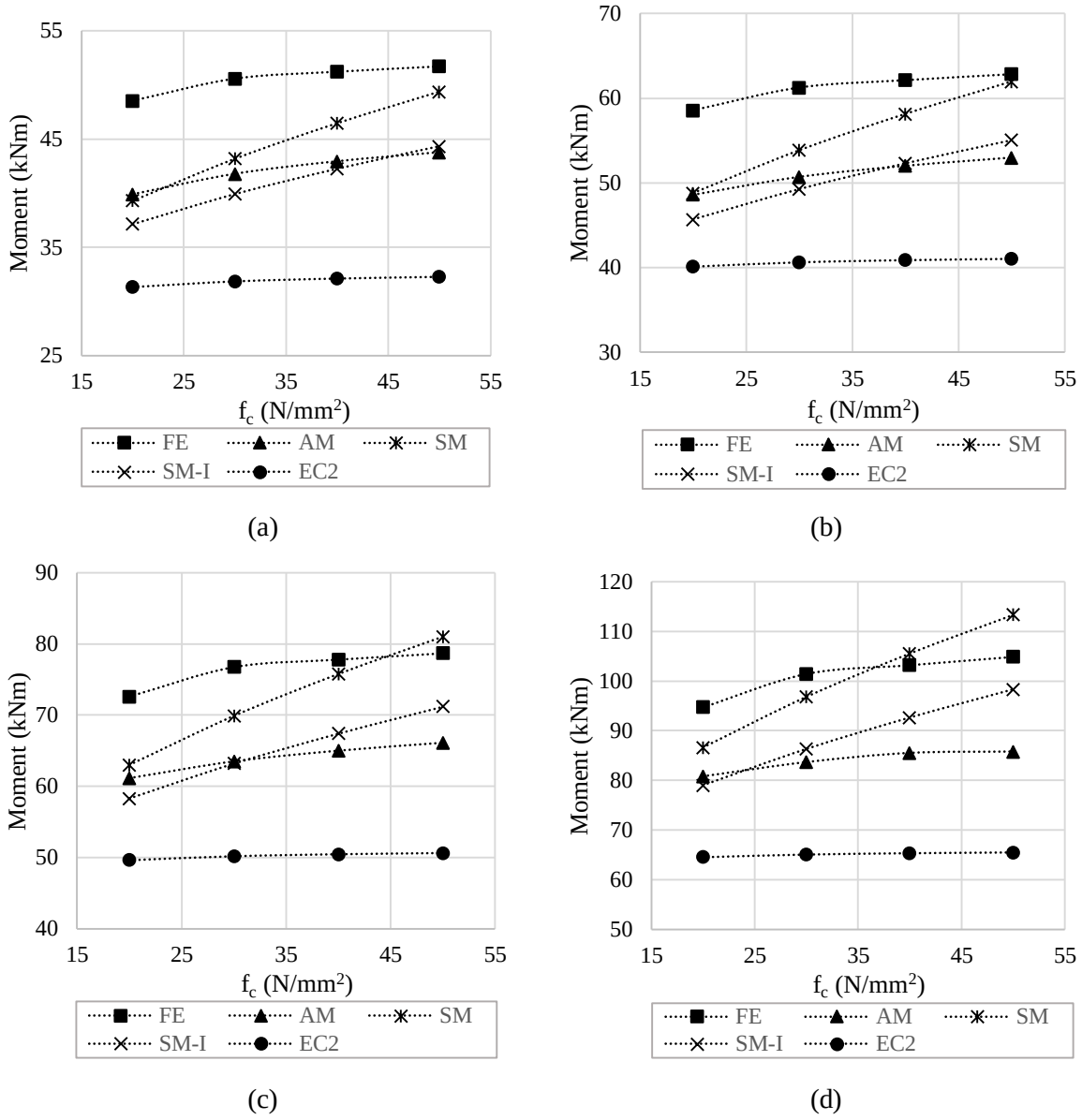

Fig. 5.3: Bending moment predictions for beams with grade 1.4307 austenitic stainless steel using a b/h ratio of (a) 1.00 (b) 0.85 (c) 0.7 and (d) 0.55.

The figures show a good agreement between the results obtained numerically with those calculated using the full proposed analytical model with average and maximum AM/FE values being -14.9% and -22.3% whilst these same values obtained using the Eurocode 2 design rules are -28.3% and -44.77%, respectively. It is noteworthy that a negative value for the AM/FE ratio indicates a conservative result from the analytical model. Clearly, the Eurocode 2 design rules provide an overly conservative prediction of the ultimate bending moment capacity, whereas the full analytical design model provides less conservative yet more accurate and realistic results. There is still some disparity between the analytical and numerical results, which is most likely owing to some of the simplifications in the analytical model. These include the assumption that concrete does not contribute to the load carrying

capacity in tension and also the idealisation of rectangular stress blocks. Nevertheless, the results are better than the existing design provisions, and remain on the conservative side consistently.

The simplified analytical model which incorporates the bilinear stress-strain curve for the stainless steel, also provides conservative predictions for the bending moment capacity in most cases with the average and maximum SM/FE values being -9.9% and -26.8%, respectively. It is noteworthy that the simplified analytical model provides less conservative results overall compared with the full analytical model mainly because the simplified material model has greater slope in the strain hardening portion. In addition, in a small number of cases when beams have a relatively low b/h ratio and are made using high strength concrete and grade 1.4162 stainless steel, the simplified analytical model tends to overestimate the bending moment capacity compared with the numerical results, which slightly skews the average and maximum SM/FE values given before. Therefore, it is necessary to recalibrate the simplified method in order to achieve better agreement with full method predictions, and to provide conservative predictions for all cases, as discussed in the following section.

5.3.1 Proposed modifications into the simplified analytical model

In this section, the slope of the strain hardening portion of the stainless steel constitutive relationship is modified to improve the accuracy of the simplified analytical model, especially for the cases highlighted in the previous section where slightly unconservative results were obtained. This is achieved by recalibrating the C_2 parameter in Eq. (4.3) based on the extensive range of the full analytical data obtained. Since different stainless steel grades have their own mechanical properties, an optimization study for the C_2 parameter is conducted individually for each material type. Consequently, it has been found that the most accurate bending moment predictions for the full range of parameters examined in the current study are achieved using a C_2 value of 0.25 for beams with austenitic stainless steel grades 1.4311 and 1.4307, and 0.3 for beams with lean duplex stainless steel grade 1.4162. This is reasonably acceptable as a higher value of C_2 results in a lower E_{sh} value and hence lower strain hardening capacity, as is the case for lean duplex stainless steel compared with the austenitic grades.

The results of the simplified analytical model predicted using the new proposed values for C_2 (denoted as SM-I) are presented in Fig. 5.1, Fig. 5.2 and Fig. 5.3, for beams made using grade 1.4311, 1.4162 and 1.4307 stainless steel, respectively. The figure also presents the data from the previous C_2 value of 0.15 (SM in the figures). It is observed that the simplified analytical model predictions with the newly proposed C_2 values are in excellent agreement with the predictions of the full analytical model. The average and maximum SM-I/AM ratios are -2.8% and -17.2%, respectively, whilst these same values for SM/AM are 5.9% and 34.5%, respectively. This also ensures that the simplified predictions are below that of the numerical model, for all examined cases. Therefore, the proposed

values for C_2 parameter are implemented in the simplified analytical model for all the results presented in the following sections.

5.4 Influence of concrete strength

The results presented in Fig. 5.1, Fig. 5.2 and Fig. 5.3 exhibit the influence that concrete strength has on the ultimate bending moment capacity for a range of beam geometries and different grades of stainless steel. It is observed that the ultimate bending moment capacity obtained using the numerical model and the full analytical model improves by around 8% on average, respectively, when the concrete strength is increased from 20 to 50 MPa, for all cases considered. Whilst this same value for the simplified analytical model is 21.5%. Clearly, the ultimate bending moment calculated from the simplified analytical model is more influenced by the strength of concrete compared with those obtained using the numerical or the full analytical models. This is perhaps owing to the simplified bi-linear material behaviour of the stainless steel employed in the simplified material model which, for beams made from a relatively higher concrete strength, enables the reinforcement to carry further tensile forces prior concrete crushing failure. Despite this, all the predictions of the simplified method are currently lower than the numerical values, considering the new proposed values for the C_2 parameter.

The effect of concrete strength on the load-displacement response is illustrated in Fig. 5.4, Fig. 5.5 and Fig. 5.6 for beams made using stainless steel reinforcement in grade 1.4311, 1.4162 and 1.4307, respectively. The section used in this analysis is 300 mm in width and 545 mm in height (i.e. the b/h ratio is 0.55). The concrete strength is varied between 20 and 50 MPa. It is clear that as expected, the initial bending stiffness, crack load (i.e. identified as the load in which the slope of the load-displacement curve begins to change) and ultimate load of the beam is improved by increasing the strength of concrete, for all cases. For example, increasing the strength of concrete from 20 MPa to 50 MPa enhances the cracking load and the ultimate load by around 43% and 11% on average, respectively. Beams with C20 concrete exhibit a softer bending stiffness, lower cracking load and ultimate load compared with the responses obtained using the other concrete strengths.

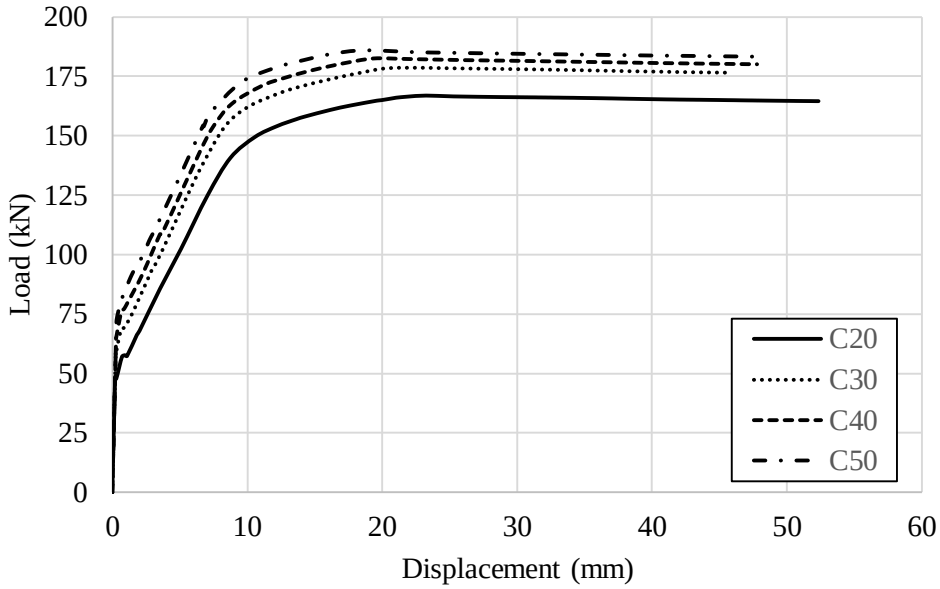

Fig. 5.4: Load-displacement curves obtained numerically using various concrete strength for beams with stainless steel grade 1.4311.

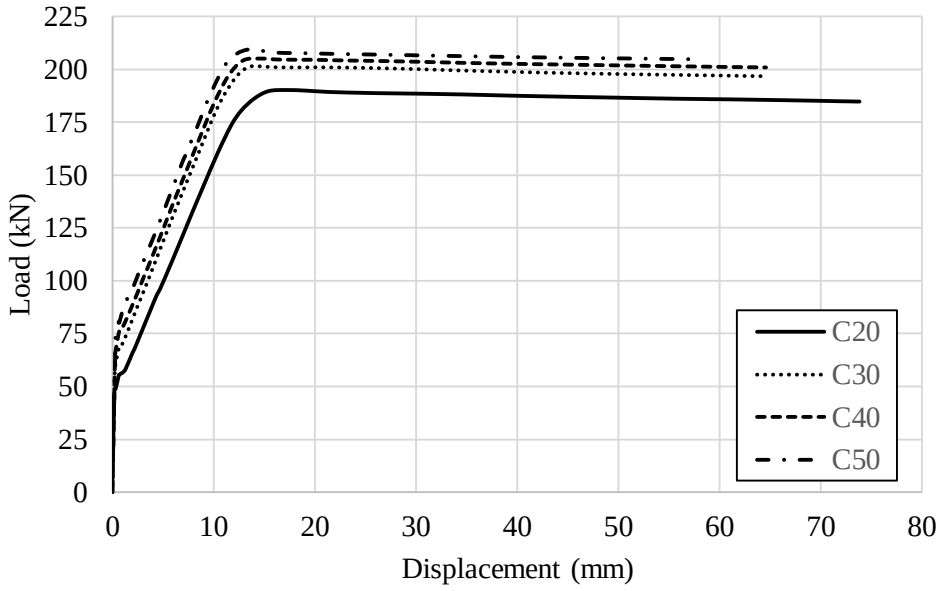

Fig. 5.5: Load-displacement curves obtained numerically using various concrete strength for beams with stainless steel grade 1.4162.

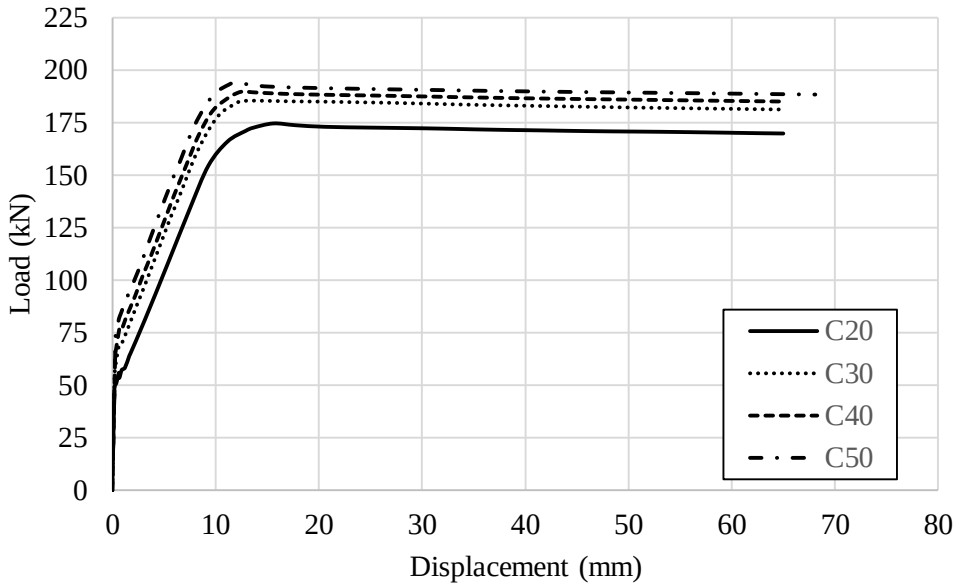

Fig. 5.6: Load-displacement curves obtained numerically using various concrete strength for beams with stainless steel grade 1.4307.

5.5 Stainless steel grade

The effect that stainless steel grade has on the load-displacement response is illustrated in Fig. 5.7. For illustrative purposes, a beam with C50 concrete is considered in this study which is 300 mm in width and 353 mm in height (i.e. b/h ratio of 0.85). It is evident from the figure that using different stainless steel grades shows no significant effect on the cracking load or the initial bending stiffness of the beams mainly owing to having similar modulus of elasticity. However, using stainless steel grades 1.4162 and 1.4307 improves the ultimate load capacity by around 13.7% and 4.3%, respectively, compared to grade 1.4311. It is noteworthy that grade 1.4162 has the highest yield strength of the grades examined in this study, and therefore the beam with reinforcement made from this material is expected to reach a higher load capacity.

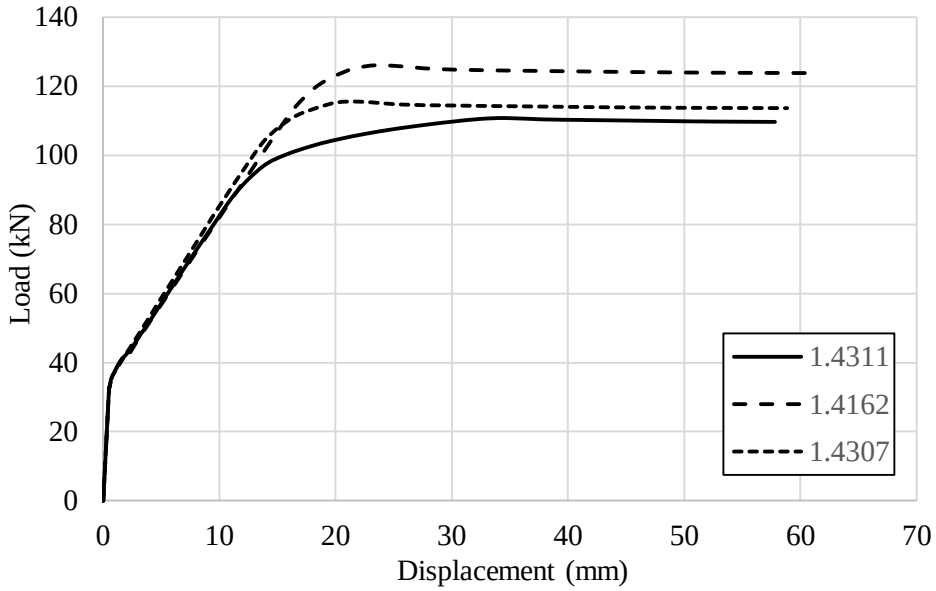

Fig. 5.7: Load-displacement curves obtained numerically for different stainless steel grades.

The other important observation is that the deflection at the ultimate load of the beam is influenced by the grade of stainless steel, as shown in Fig. 5.7. For the purpose of comparison, the deflection values corresponding to the maximum load are selected here mainly because the main concern is the ultimate capacity of the section. For instance, the beam with grade 1.4311 stainless steel reinforcement deflects to 34.7 mm at the ultimate load whereas the corresponding deflections for beams with grades 1.4162 and 1.4307 are 23.5 and 22.1 mm, respectively. Given that grade 1.4311 has the highest strain hardening capacity of the stainless steels examined herein, it is clearly intuitive to conclude that the ductility of the section is improved by using reinforcement with a greater ultimate strain.

In order to analyse the accuracy of the full and simplified analytical models when different stainless steel grades are used, Table 5.2 shows a comparison of the bending moment predictions obtained numerically and analytically with reference to the predictions of Eurocode 2. The results are obtained for two different sections with width to height (b/h) ratios of 0.85 and 0.70. The results demonstrate that both the full and simplified models as well as the Eurocode 2 tend to provide less conservative bending moment predictions compared with the numerical values when a grade of stainless steel with a relatively higher strength is used.

Table 5.2: Comparison between the ultimate bending moment predictions obtained numerically and analytically for different stainless steel grades.

b/h ratio	Grade	FE (kNm)	AM (kNm)	SM-I (kNm)	EC2 (kNm)	AM/FE %	SM-I/FE %	EC2/FE %
0.7	1.4311	75.9	61.4	65.1	43.3	-19.0	-14.1	-42.9
	1.4162	85.8	74.5	80.0	61.2	-13.2	-6.8	-28.6
	1.4307	78.7	66.1	71.2	50.6	-16.0	-9.5	-35.7
0.85	1.4311	60.5	49.1	50.1	35.1	-18.9	-17.2	-41.9
	1.4162	68.3	59.8	62.2	49.7	-12.5	-8.9	-27.3
	1.4307	62.9	53.0	55.1	41.1	-15.7	-12.4	-34.7

5.6 Geometry

In order to investigate the effect that the geometry of the section has on the behaviour of stainless steel RC beams, beams with different b/h ratios ranging from 1.00 to 0.55 are considered in the current section. The results presented are obtained for beams made from C50 concrete. Fig. 5.8, Fig. 5.9 and Fig. 5.10 illustrate the relationship between the bending moment predictions obtained from the numerical and analytical models, and b/h ratios for beams with stainless steel grades 1.4311, 1.4162 and 1.4307, respectively. It is clear that the ultimate bending moment significantly increases for beams with a relatively lower b/h ratio, as expected since these beams would have a greater second moment of area. The simplified analytical model tends to provide a higher prediction compared with the full analytical model for beams with a lower b/h ratio. However, the bending moment predictions obtained from the simplified analytical model are lower than those obtained numerically in all cases, therefore providing a conservative prediction. It is noteworthy that the full analytical method improves the accuracy of the bending capacity of the section by around 41%, 21% and 32% on average, compared with the current design approach in Eurocode 2, for the results presented in this section and obtained using stainless steel grades 1.4311, 1.4162 and 1.4307, respectively.

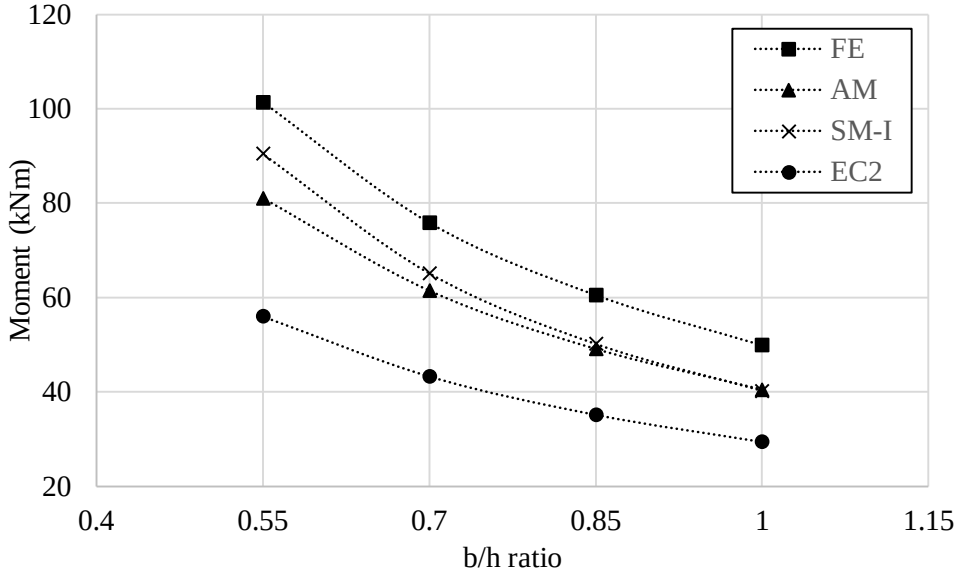

Fig. 5.8: Effect of the beam geometry on the bending moment predictions for beams with austenitic stainless steel grade 1.4311.

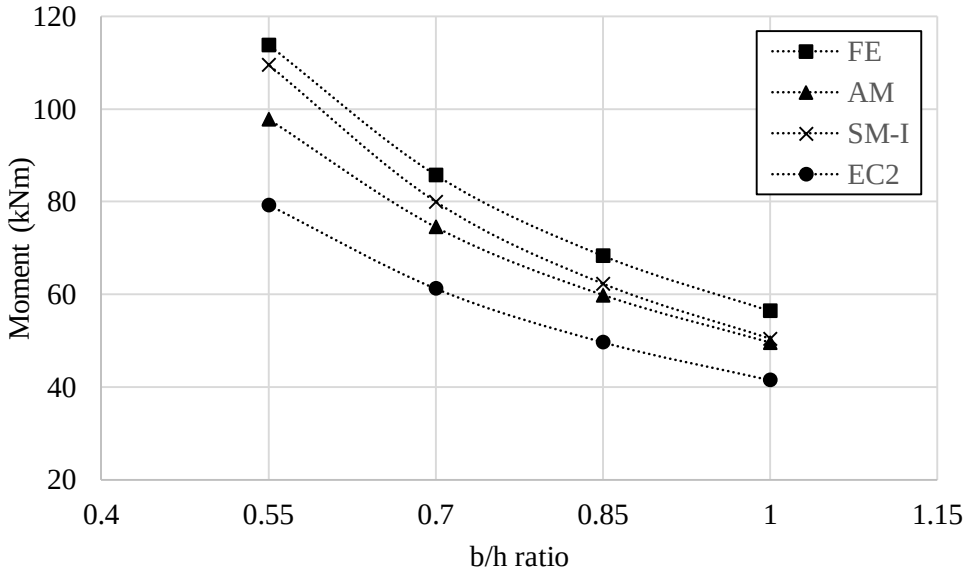

Fig. 5.9: Effect of the beam geometry on the bending moment predictions for beams with lean duplex stainless steel grade 1.4162

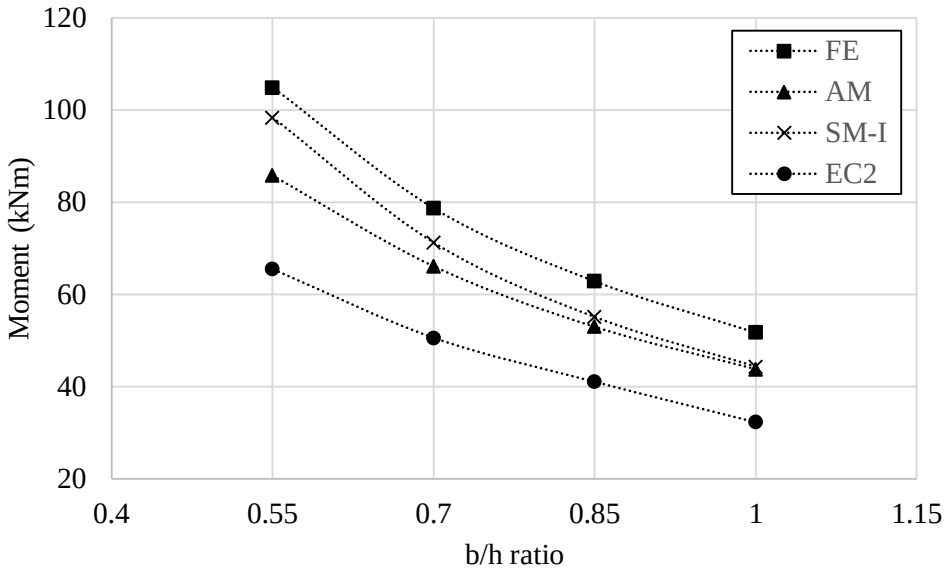

Fig. 5.10: Effect of the beam geometry on the bending moment predictions for beams with austenitic stainless steel grade 1.4307.

Fig. 5.11 presents the relationship between the beam geometry and the ability of the section to exploit the strain hardening capabilities of the stainless steel, using the full analytical model. It is shown that the geometry of the beam has a relatively small influence on the exploitation of strain hardening. For example, a beam with a b/h ratio of 0.55 develops around 4.2%, 2.9% and 2.2% more stress in the reinforcement for grades 1.4311, 1.4162 and 1.4307, respectively, compared with members with a b/h ratio of 1.00. In general, it is observed that beams reinforced with 1.4162 grade lean duplex stainless steel reinforcement exhibit greater exploitation of the strain hardening capacity in the stainless steel, compared with beams reinforced with the austenitic grades 1.4307 and 1.4311.

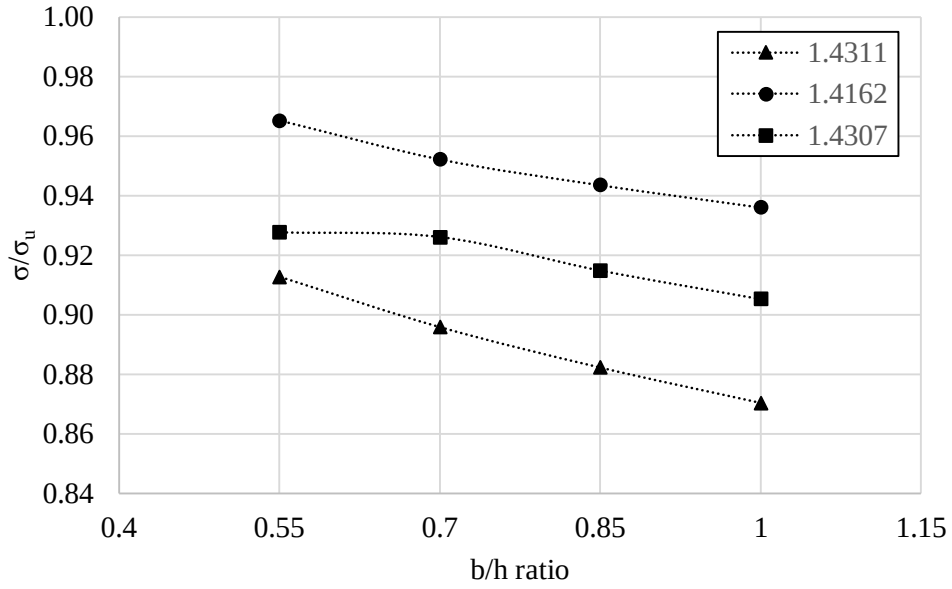

Fig. 5.11: Effect of the beam geometry on the exploitation of strain hardening.

5.7 Reinforcement ratio

Reinforcement ratio is an important parameter in the design of reinforced concrete sections as it dictates not only the load carrying capacity but also the failure mode. In this section, the influence of reinforcement ratio on the behaviour of stainless steel RC beams, in particular the exploitation of strain hardening in the reinforcement, is assessed. The results presented are obtained for beams with concrete strength C40 and a b/h ratio of 0.70.

Fig. 5.12, Fig. 5.13 and Fig. 5.14 illustrate the effect that reinforcement ratio (ρ) has on the bending moment capacity values obtained numerically and analytically for beams made using stainless steel reinforcement in grades 1.4311, 1.4162 and 1.4307, respectively. The results demonstrate that both the full and simplified analytical models underestimate the bending moment capacities obtained numerically in almost all cases, which is conservative and in line with previous findings. The numerical analyses show that the bending moment capacity improves as the reinforcement ratio increases until it reaches a specific ratio (i.e. around 0.032 in the cases presented herein) after which no further improvement in the bending capacity is observed. The reason for this is most likely due to the greater depth of the neutral axis when a higher reinforcement ratio is employed which increases the compressive stress in the concrete until it crushes, and no further improvement can be achieved. Moreover, both the simplified analytical model and the Eurocode 2 design rules provide identical predictions, as expected, when a higher reinforcement ratio is used since both models are based on the same constitutive behaviour for the stainless steel in the elastic range. It is also observed that for beams with a relatively higher reinforcement ratio, the moment capacities predicted by the full analytical model are below those from the simplified analytical model and also Eurocode 2. This is owing to the nonlinearity of the material model which starts from an early stage.

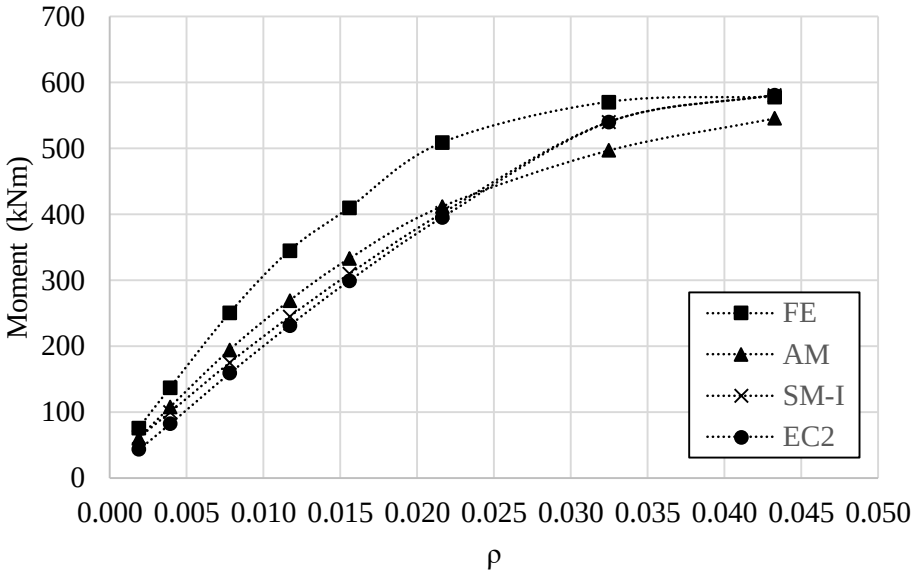

Fig. 5.12: Effect of the reinforcement ratio (ρ) on the bending moment capacity for beams made using grade 1.4311 austenitic stainless steel.

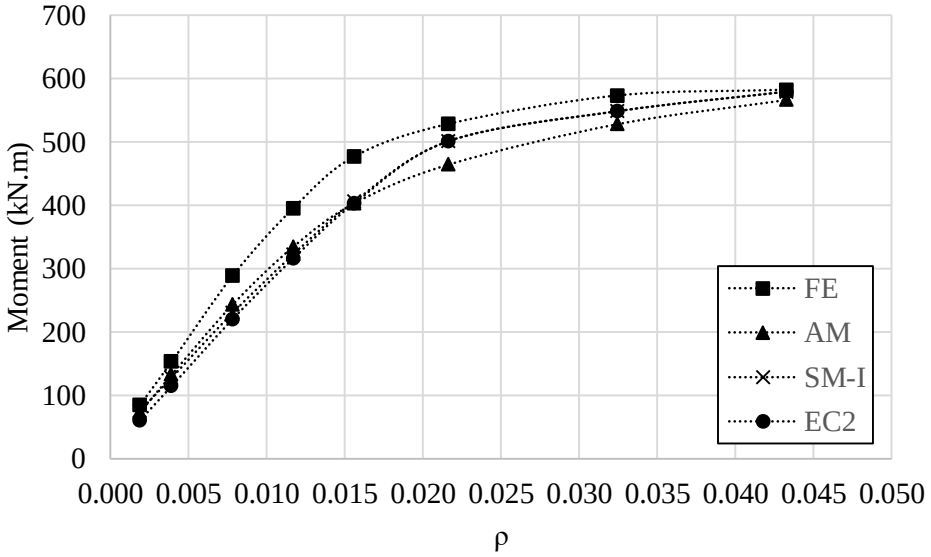

Fig. 5.13: Effect of the reinforcement ratio (ρ) on the bending moment capacity for beams made using grade 1.4162 lean duplex stainless steel.

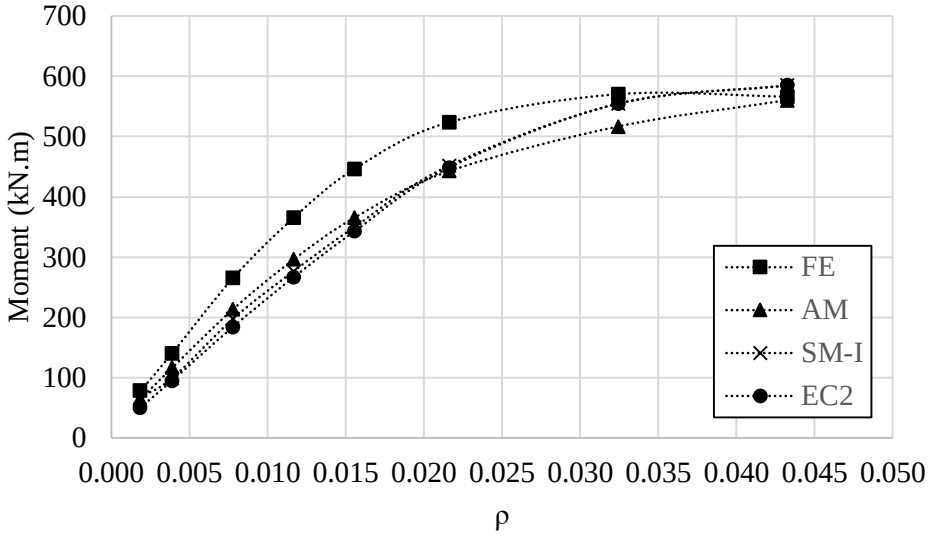

Fig. 5.14: Effect of the reinforcement ratio (ρ) on the bending moment capacity for beams made using grade 1.4307 austenitic stainless steel.

Fig. 5.15, Fig. 5.16 and Fig. 5.17 demonstrate the influence of reinforcement ratio on the exploitation of strain hardening in the rebar for beams with stainless steel reinforcement in grades 1.4311, 1.4162 and 1.4307, respectively. These results are obtained using the full analytical model, for a range of different concrete strengths. The figures illustrate the amount of stress in the rebars that can be exploited when calculating the ultimate bending moment capacity of the section. The horizontal solid line in each of the figures represents the yield limit for that particular grade of stainless steel (i.e. $\sigma_{0.2}/\sigma_u$).

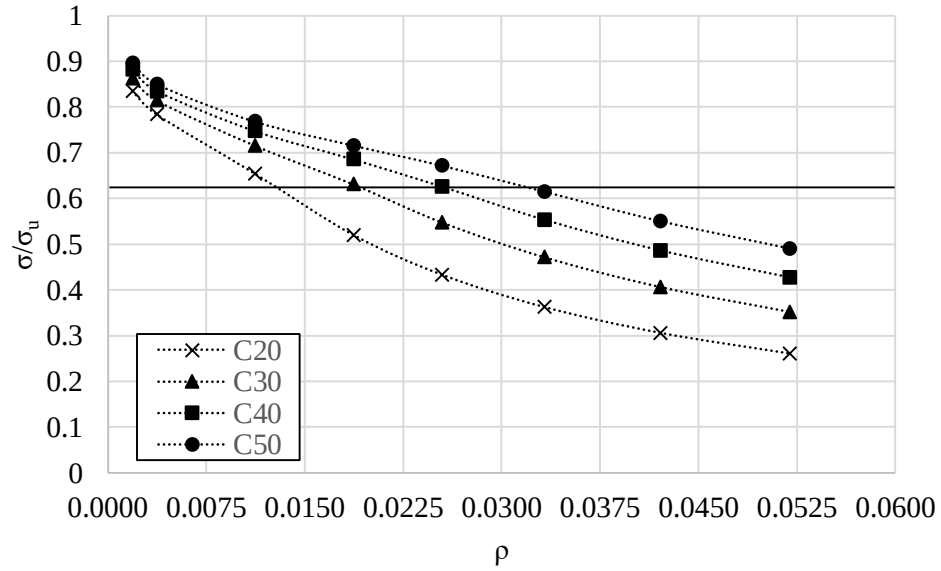

Fig. 5.15: Effect of reinforcement ratio on the exploitation of strain hardening for beams reinforced with grade 1.4311 austenitic stainless steel.

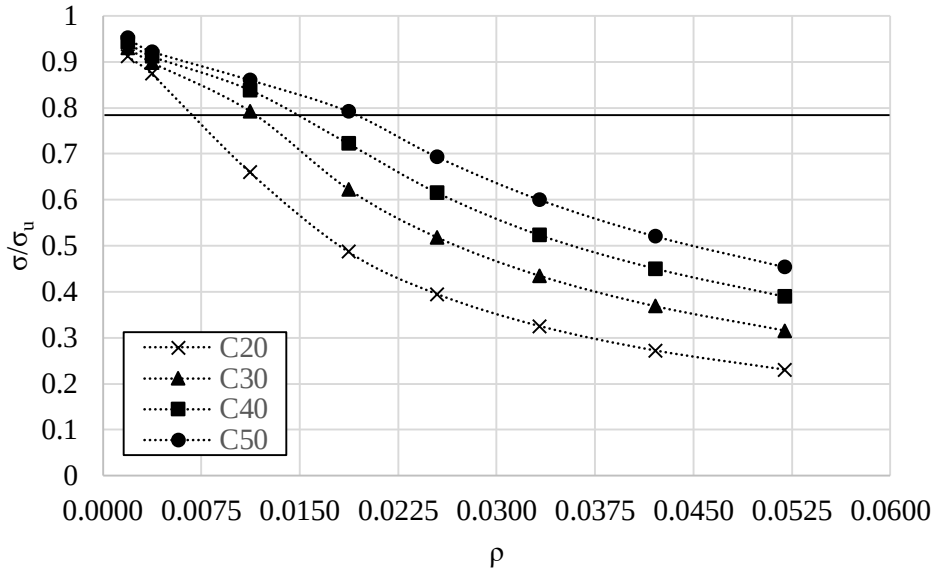

Fig. 5.16: Effect of reinforcement ratio on the exploitation of strain hardening for beams reinforced with grade 1.4162 lean duplex stainless steel.

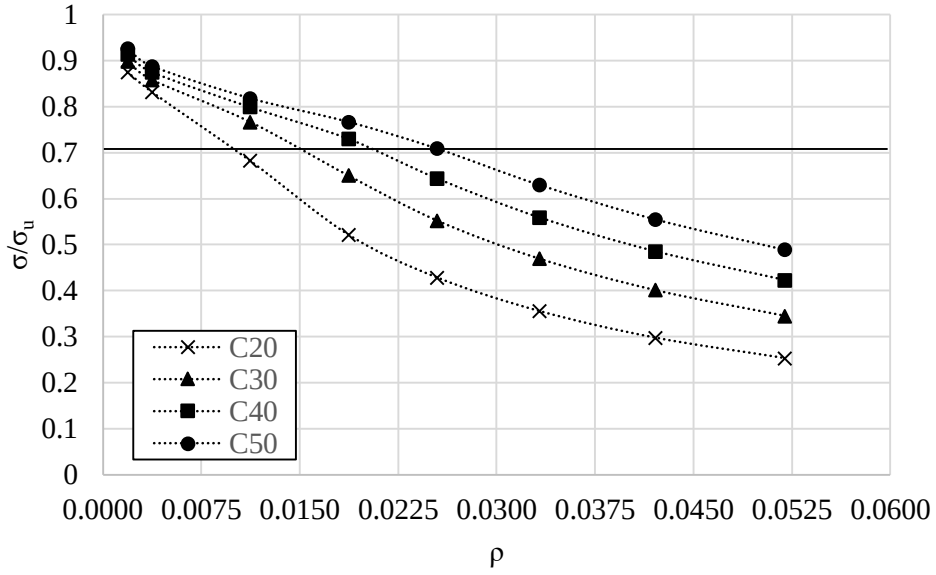

Fig. 5.17: Effect of reinforcement ratio on the exploitation of strain hardening for beams reinforced with grade 1.4307 austenitic stainless steel.

It is shown in the figures that further exploitation of the strain hardening capacity in the reinforcement is achieved when a relatively higher grade of concrete is employed. This is mainly because the higher strength concrete can carry greater compressive forces allowing the rebar to reach greater levels of stress. In all cases, it is observed that the level of stress in the stainless steel is relatively lower when a higher reinforcement ratio is employed. This is because an increase in the steel cross-sectional area generally reduces the levels of stress and strain in the reinforcement and increases the depth of the neutral axis, which causes a relative increase in the levels of applied stress and strain in the concrete

resulting in crushing of the concrete. Accordingly, lower exploitation of the tensile strength in the reinforcement is achieved.

A balanced reinforcement ratio (ρ_{bal}) is defined as the ratio where concrete crushing and reinforcement yielding occur simultaneously in the cross section. In order to utilize and exploit the positive strain hardening properties of stainless steel reinforcement in the design of reinforced concrete beams, it is necessary to design the section to be under-reinforced. An under-reinforced section is when the reinforcement ratio is lower than the balanced ratio (i.e. $\rho < \rho_{bal}$). This allows the reinforcement to yield first and then develop some strain hardening before the section fails due to crushing of concrete. It ensures enough ductility in the section to avoid sudden catastrophic failure of the reinforced concrete member. On the other hand, if the beam is designed to be over-reinforced (i.e. $\rho > \rho_{bal}$), failure will occur by crushing of the concrete before the rebar yields, and the strain hardening characteristics of the stainless steel will not be exploited. This design case is neither desirable nor efficient, but could still be employed if a higher partial safety factor is considered.

A balanced reinforcement ratio (ρ_{bal}) can be identified for stainless steel reinforced concrete sections as the reinforcement ratio at which when the tensile strain in the rebar reaches to 0.2% strain ($\varepsilon_{0.2}$) simultaneously with the concrete on the top surface reaching the ultimate crushing strain (ε_{cu}). This requires obtaining the depth of the neutral axis (y) from the strain distribution in Fig. 4.1, as presented in Eq. (5.1):

$$y = \frac{d}{1 + \varepsilon_{0.2}/\varepsilon_{cu}} \tag{5.1}$$

The equilibrium of internal forces can be applied, as presented in Eq. (5.2), by assuming the depth of the compressive stress block of the concrete is 0.8y and the concrete compressive stress in the concrete stress block is $0.85f_c$:

$$0.68f_c y\, b - A_s\sigma_s = 0 \tag{5.2}$$

In this expression, the tensile stress (σ_s) is the 0.2% proof stress of the reinforcement ($\sigma_{0.2}$).

By substituting Eq. (5.1) into Eq. (5.2), Eq. (5.3) is obtained:

$$0.68f_c\left(\frac{d}{1+\varepsilon_{0.2}/\varepsilon_{cu}}\right) b - A_s\sigma_{0.2} = 0 \tag{5.3}$$

The balanced reinforcement ratio (ρ_{bal}) is obtained by rearranging Eq. (5.3), as follows:

$$\rho_{bal} = \frac{A_s}{bd} = \frac{0.68}{\sigma_{0.2}}\left(\frac{f_c}{1 + \varepsilon_{0.2}/\varepsilon_{cu}}\right) \tag{5.4}$$

In the case of under-reinforced section, the reinforcement ratio must be greater than the minimum ratio required to prevent the rupture of the rebar which it can be obtained using Eq. (5.5).

$$\rho_{min} = \frac{0.68}{\sigma_u}\left(\frac{f_c}{1+\varepsilon_u/\varepsilon_{cu}}\right) \tag{5.5}$$

5.8 Deflections

A realistic estimation of the levels of deflection that develop in a structure is imperative to ensure acceptable serviceability and the comfort of end-users. Thus, global design standards typically provide limiting values for deflections which should not be exceeded. In Eurocode 2, for example, the allowable deflection is limited to span/250 for members subjected to quasi-permanent loads (EN 1992-1-1, 2004). Deflections are in important consideration for concrete members reinforced with stainless steel owing to the excellent ductility of the reinforcing material. In the deflection calculations for RC beams, using the elastic modulus of stainless steel may result in over-conservative predictions due to the non-linear behaviour of the stainless steel, even in the low-strain range. Therefore, this section aims to evaluate the deflection design approach in Eurocode 2 for stainless steels RC beams. The predicted results from Eurocode 2 are compared with the corresponding values from the numerical model. The influences of implementing the secant modulus and the tangent modulus of stainless steel in the deflection calculations for RC beams are also explored.

In Eurocode 2, the deflection of a member is obtained based on the assumption that the concrete member comprises cracked and un-cracked sections, at the service load. Accordingly, the maximum deflection (δ_{EC2}) for RC members is calculated as follows:

$$\delta_{EC2} = (1-\zeta)\delta_1 + \zeta\delta_2 \tag{5.6}$$

In this expression, ζ is a distribution coefficient representing the tension stiffening phenomenon in the section, and is taken as zero for the un-cracked portion of the section, otherwise it is calculated using Eq. (5.7):

$$\zeta = 1 - \beta\left(\frac{M_{cr}}{M_a}\right)^2 \tag{5.7}$$

where β is a coefficient that accounts for the effect of the duration of loading on the average strain, and is assumed to have a value of unity for a single short-term loading and 0.5 for sustained and cyclic loading. M_{cr} and M_a are the bending moment values calculated at the cracking and service loads, respectively. The cracking moment (M_{cr}) is determined as:

$$M_{cr} = \frac{f_t I_g}{y} \tag{5.8}$$

δ_1 and δ_2 are the deflection values obtained for the un-cracked section and cracked section, respectively, and are determined from Eqs. (5.9) and (5.10) for beams subjected to four point bending conditions:

$$\delta_1 = \frac{Pa}{24E_cI_g}(3L^2 - 4a^2) \tag{5.9}$$

$$\delta_2 = \frac{Pa}{24E_cI_{cr}}(3L^2 - 4a^2) \tag{5.10}$$

In these expressions, P is the applied load at each point, L is the clear span and a is the distance between the support and the nearest loading point. I_g and I_{cr} are the second moment of area calculated on the basis of the un-cracked and cracked sections, respectively, determined using the expressions in Eqs. (5.11) and (5.12):

$$I_g = \frac{bh^3}{12} \tag{5.11}$$

$$I_{cr} = \frac{bd^3k^3}{3} + nA_sd^2(1-k)^2 \tag{5.12}$$

where $k = \sqrt{2\rho n + (\rho n)^2} - \rho n$

In Eq. (5.12), the term n refers to the modular ratio between the reinforcement and the concrete, given as the ratio of E to E_c.

In the case of extreme load conditions, deflections corresponding to the ultimate bending moment would be an important point of consideration. However, for serviceability requirements, the deflection of the beam is calculated in this analysis at the mid-span of the member at the service moment, which is 30% of the ultimate bending moment (0.3Mu), as well as at 67% of the ultimate bending moment (0.67Mu). Table 5.3 presents a comparison between the measured deflections from the numerical model (δ_{FE}) and the predicted values obtained using Eurocode 2 (δ_{EC2}), using the expressions given in Eqs. (5.6)-(5.12). The results presented in the table are for beams made from C40 concrete which are 300 mm in width and 428 mm in depth, and employ the elastic modulus for the stainless steel (E) in the calculations. In order to study the influence of the stainless steel constitutive relationship on the deflection of RC beams, various reinforcement ratios (ρ) are considered to develop different levels of stress in the reinforcement. It is observed that the Eurocode 2 design deflections at $0.3M_u$ are in very good agreement with the corresponding numerical values (δ_{EC2}/δ_{FE}) with the maximum and average differences being around -38% and -2%, respectively. These same values at $0.67M_u$ are -28% and -15%, respectively.

Table 5.3: Results of the predicted deflection obtained from Eurocode 2 in comparison with the measured values from the FE model.

Reinforcement ratio (ρ)	Grades	Bending moment		Deflections at $0.3M_u$			Deflections at $0.67M_u$		
		$0.3M_u$ (kNm)	$0.67M_u$ (kNm)	δ_{EC2} (mm)	δ_{FE} (mm)	δ_{EC2}/δ_{FE}	δ_{EC2} (mm)	δ_{FE} (mm)	δ_{EC2}/δ_{FE}
0.0019	1.4311	22.7	50.6	0.38	0.36	1.05	6.05	6.47	0.94
	1.4162	25.6	57.1	0.43	0.70	0.62	7.80	8.19	0.95
	1.4307	23.6	52.6	0.40	0.42	0.95	6.36	6.70	0.95
0.0039	1.4311	40.9	91.3	2.16	2.07	1.04	9.10	9.31	0.98
	1.4162	46.0	102.7	3.04	3.05	1.00	10.64	11.22	0.95
	1.4307	42.2	94.2	2.32	2.38	0.98	9.17	9.51	0.96
0.0078	1.4311	75.0	167.5	4.05	3.79	1.07	10.15	11.34	0.90
	1.4162	86.6	193.3	4.91	4.76	1.03	11.96	13.82	0.87
	1.4307	79.6	177.8	4.24	4.02	1.06	10.49	12.02	0.87
0.0117	1.4311	103.4	231.0	4.39	4.27	1.03	10.30	12.30	0.84
	1.4162	118.7	265.1	5.18	5.20	1.00	12.02	14.83	0.81
	1.4307	109.7	244.9	4.56	4.47	1.02	10.63	12.84	0.83
0.0156	1.4311	122.9	274.4	4.30	4.26	1.01	9.89	12.27	0.81
	1.4162	143.1	319.6	5.12	5.27	0.97	11.69	15.37	0.76
	1.4307	133.9	299.1	4.59	4.62	0.99	10.50	13.36	0.79
0.0216	1.4311	152.6	340.9	4.29	4.51	0.95	9.73	13.27	0.73
	1.4162	158.6	354.2	4.52	4.78	0.94	10.23	14.15	0.72
	1.4307	157.2	351.0	4.31	4.53	0.95	9.76	13.28	0.74

Fig. 5.18(a) and (b) demonstrate the influence that the reinforcement ratio has on the beam deflections at $0.3M_u$ and $0.67M_u$, respectively. It is clear that Eurocode 2 predictions are in very good agreement with the corresponding measured values from the FE model in almost all cases for beams which are at the service load, corresponding to a bending moment of $0.3M_u$. On the other hand, the code results in over-conservative predictions for beams with relatively higher reinforcement ratios, when the beam is subjected to $0.67M_u$. It is also observed that the deflections rise with an increase of reinforcement ratio up to specific point (i.e. at a reinforcement ratio of around 1%) after which remains more or less constant. This indicates that the deflection is more influenced by the reinforcement ratio for relatively low values of ρ, where the stress level in the reinforcement is relatively greater.

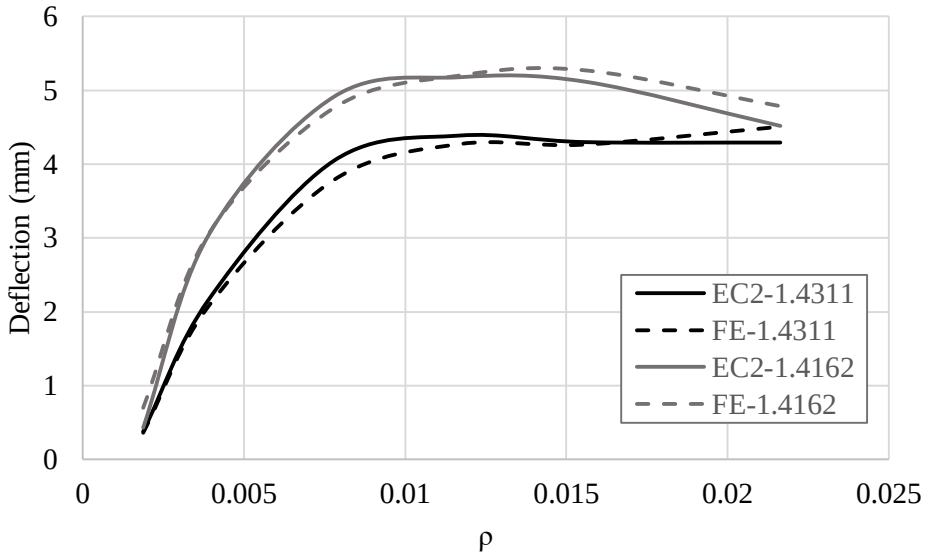

(a)

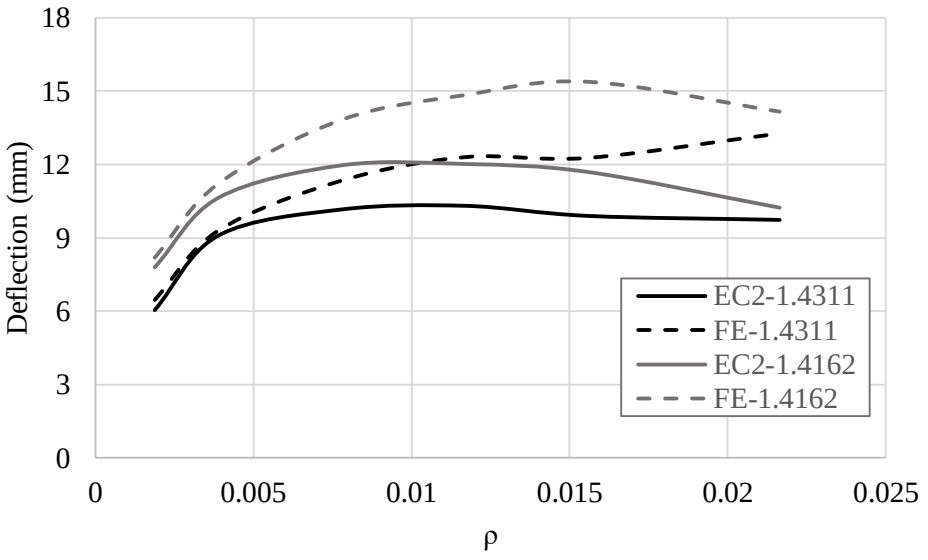

(b)

Fig. 5.18: Effect of reinforcement ratio on the deflection of a stainless steel reinforced concrete beam at (a) $0.3M_u$ and (b) $0.67M_u$.

As stated before, the current design approach in Eurocode 2 (EN 1992-1-1, 2004) calculates the deflection on the basis of the modulus of elasticity of the reinforcement. This assumption is acceptable in the case of carbon steel reinforcement, however it may result in an over-conservative prediction in the case of stainless steel reinforcement owing to its nonlinear behaviour. In the design of structural stainless steel sections, it is recommended to use the secant modulus in deflection calculations rather than the elastic modulus (SCI, 2017). In order to investigate this for reinforced concrete design, the predicted deflections calculated using secant modulus and also the tangent modulus of the stainless steel reinforcement are compared with their corresponding numerical values.

The secant modulus of elasticity (E_{sec}) for stainless steel is obtained from the modified Ramberg-Osgood material model presented earlier in Eqs. (4.1) and (4.2) according to:

$$E_{sec} = \frac{E}{1+0.002\frac{E}{\sigma}\left(\frac{\sigma}{\sigma_{0.2}}\right)^{n}} \qquad \text{for} \quad \sigma \leq \sigma_{0.2} \qquad (5.13)$$

$$E_{sec} = \frac{\sigma}{\varepsilon_{0.2} + \frac{\sigma-\sigma_{0.2}}{E_2} + \left(\varepsilon_u - \varepsilon_{0.2} - \frac{\sigma_u-\sigma_{0.2}}{E_2}\right)\left(\frac{\sigma-\sigma_{0.2}}{\sigma_u-\sigma_{0.2}}\right)^{m}} \qquad \text{for} \quad \sigma_{0.2} < \sigma \leq \sigma_u \qquad (5.14)$$

The tangent modulus of elasticity (E_{tan}) is the derivative of the secant modulus and is determined as follows:

$$E_{tan} = \frac{\sigma_{0.2}\,E}{\sigma_{0.2} + 0.002\,n\,E\left(\frac{\sigma}{\sigma_{0.2}}\right)^{n-1}} \qquad \text{for} \quad \sigma < \sigma_{0.2} \qquad (5.15)$$

$$E_{tan} = \frac{1}{\frac{1}{E_2} + \left(\varepsilon_u - \varepsilon_{0.2} - \frac{\sigma_u-\sigma_{0.2}}{E_2}\right)\left(\frac{m}{(\sigma_u-\sigma_{0.2})^{m}}\right)(\sigma-\sigma_{0.2})^{m-1}} \qquad \text{for} \quad \sigma_{0.2} < \sigma \leq \sigma_u \qquad (5.16)$$

In order to obtain the secant modulus and the tangent modulus of the reinforcement at $0.3M_u$ and $0.67M_u$, the stress in the reinforcement must first be determined. An elastic analysis of the section is conducted to obtain the depth of the neutral axis (y) and the stress in the reinforcement, according to the stress and strain distributions presented in Fig. 5.19.

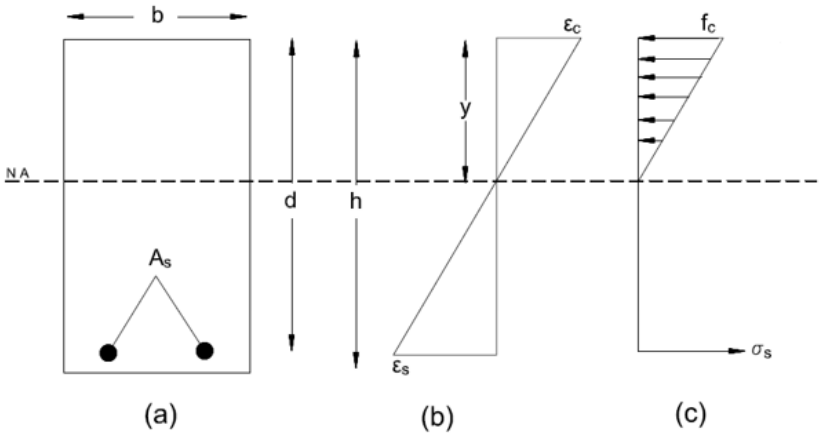

Fig. 5.19: Elastic analysis of a reinforced concrete beam including (a) the cross-section (b) the strain distribution, (c) the stress distribution in the section.

The location of the neutral axis can be obtained from Eq. (5.17):

$$y = d\left(\sqrt{2\rho n + \rho^2 n^2} - \rho n\right) \tag{5.17}$$

where n is the modular ratio between the reinforcement and concrete:

$$n = \frac{E_{sec}}{E_c} \quad \text{for secant modulus}$$

$$n = \frac{E_{tan}}{E_c} \quad \text{for tangent modulus} \tag{5.18}$$

Once the neutral axis depth is located, the stress in the reinforcement is calculated from the stress distribution in Fig. 5.19(c), as follows:

$$\sigma_s = \frac{M_a}{A_s(d - y/3)} \tag{5.19}$$

Since the secant and tangent moduli are functions of the stress in the reinforcement, an iterative technique is required to obtain the solution of Eq. (5.19). A flow chart describing the solution procedure for determining the secant modulus is given in Fig. 5.20. The same solution procedure can be followed to determine the tangent modulus. Then, the deflections of the beam for load levels corresponding to $0.3M_u$ and $0.67M_u$ are calculated using secant modulus and the tangent modulus.

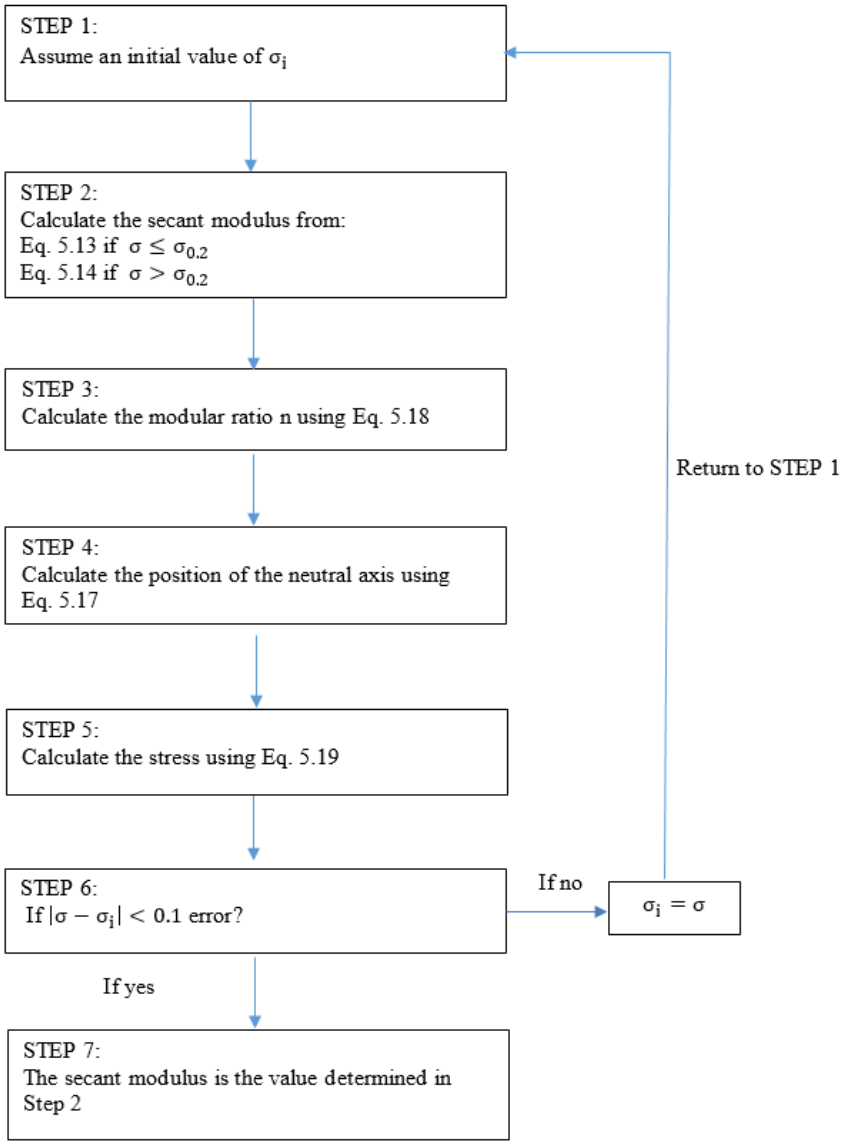

Fig. 5.20: Flow chart of the solution procedure.

The predicted deflections obtained using the elastic modulus (δ_{EC2}), secant modulus ($\delta_{EC2(Esec)}$) and tangent modulus ($\delta_{EC2(Etan)}$) for the stainless steel grades considered herein, are presented in Table 5.4 in comparison with the corresponding numerical values (δ_{FE}). The results show that implementing the secant modulus in the calculations of deflection provides quite accurate predictions at $0.3M_u$ with maximum and average $\delta_{EC2(Esec)}/\delta_{FE}$ values of -38% and 0%, respectively. However, these results are quite similar in terms of accuracy as the corresponding deflections obtained using the elastic modulus of stainless steel, as presented earlier, which gave maximum and average δ_{EC2}/δ_{FE} values of -38% and -2%, respectively. On the other hand, at $0.67M_u$, using the secant modulus in deflection calculations results in un-conservative predictions with maximum and average $\delta_{EC2(Esec)}/\delta_{FE}$ values of 55% and 18%, respectively. The corresponding values when the elastic modulus is used in the calculations are -28% and -15%, respectively, as previously presented.

Using the tangent modulus in deflection calculations at load levels corresponding to $0.3M_u$ results in maximum and average $\delta_{EC2(Etan)}/\delta_{FE}$ values of -38% and 6%, respectively, whilst at $0.67M_u$ the maximum and average $\delta_{EC2(Etan)}/\delta_{FE}$ values are 1130% and 205%, respectively. It is clear that the using the tangent modulus to calculate the deflections results in a significant overestimation of the deflections compared with the numerical model values, especially at higher load levels.

Table 5.4: Deflection results obtained using the initial modulus, secant modulus and the tangent modulus of stainless steel in comparison with the measured values from the FE model.

Reinforcement ratio	Grade	Bending moment (kNm)		Deflections at $0.3M_u$			Deflections at $0.67M_u$		
		0.3Mu	0.67Mu	δ_{EC2}/δ_{FE}	$\delta_{EC2(Esec)}/\delta_{FE}$	$\delta_{EC2(Etan)}/\delta_{FE}$	δ_{EC2}/δ_{FE}	$\delta_{EC2(Esec)}/\delta_{FE}$	$\delta_{EC2(Etan)}/\delta_{FE}$
0.00187	1.4311	22.7	50.6	1.05	1.05	1.05	0.94	1.36	12.30
	1.4162	25.6	57.1	0.62	0.62	0.62	0.95	1.35	2.89
	1.4307	23.6	52.6	0.95	0.95	0.95	0.95	1.46	4.02
0.00390	1.4311	40.9	91.3	1.04	1.09	1.29	0.98	1.48	5.91
	1.4162	46.0	102.7	1.00	1.01	1.05	0.95	1.26	2.45
	1.4307	42.2	94.2	0.98	1.01	1.11	0.96	1.55	3.60
0.00779	1.4311	75.0	167.5	1.07	1.12	1.29	0.90	1.41	3.60
	1.4162	86.6	193.3	1.03	1.04	1.08	0.87	1.09	1.94
	1.4307	79.6	177.8	1.06	1.08	1.19	0.87	1.33	2.79
0.01169	1.4311	103.4	231.0	1.03	1.06	1.19	0.84	1.35	2.94
	1.4162	118.7	265.1	1.00	1.00	1.03	0.81	0.96	1.52
	1.4307	109.7	244.9	1.02	1.04	1.12	0.83	1.15	2.17
0.01559	1.4311	122.9	274.4	1.01	1.03	1.11	0.81	1.14	2.16
	1.4162	143.1	319.6	0.97	0.98	0.99	0.76	0.85	1.21
	1.4307	133.9	299.1	0.99	1.01	1.06	0.79	1.01	1.72
0.02165	1.4311	152.6	340.9	0.95	0.97	1.02	0.73	0.94	1.57
	1.4162	158.6	354.2	0.94	0.95	0.95	0.72	0.76	0.90
	1.4307	157.2	351.0	0.95	0.96	0.99	0.74	0.85	1.23

In summary, the results presented in this analysis show that there is only a minor improvement in the deflection predictions by adopting the secant modulus rather than the elastic modulus in the calculations. The predictions obtained using the tangent modulus were significantly less accurate than when the elastic modulus or the secant modulus is employed. Therefore, it is recommended to use the elastic modulus in the calculation of deflections for stainless steel RC beams. It is noteworthy that the predicted deflections for beams with a reinforcement ratio 0.187% at loads corresponding to $0.3M_u$ are typically the same for each stainless steel grade considered herein. After a careful examination of these cases, it was found that applied load is lower than the cracking moment and therefore the deflection is calculated only on the basis of an un-cracked section. In this scenario, the second moment of area is calculated based on the gross area of the section which is the same irrespective of the reinforcement modulus of elasticity.

5.9 A summary of the recommendations for the codes of practice

A comprehensive parametric study has been carried out to investigate the effect of the most influential parameters on the performance of stainless steel concrete beams including various concrete strengths and reinforcement grades and different geometries. Consequently, the following recommendations for the codes of practice have been summarized as follows:

- It is shown that further exploitation of the strain hardening capacity in the rebar is achieved when a relatively higher grade of concrete is employed.
- It is also found that the geometry of the beam has a relatively small influence on the exploitation of strain hardening.
- It is observed that the levels of stress in the rebar are relatively lower when a higher reinforcement ratio is employed.
- It is recommended that the elastic modulus is employed in the calculation of deflections for stainless steel RC beams.

5.10 Concluding remarks

The full and simplified version of a deformation-based design method for the analysis of these elements has been further developed and examined herein. It has been compared with the current design rules in Eurocode 2 and shown to provide very favourable results, in terms of accuracy and efficiency. A comprehensive parametric study was conducted to study the influence that various geometric and material properties have on the capacity of the members. Moreover, this chapter provides guidance for selecting an appropriate reinforcement ratio in order to achieve maximum exploitation of the strain hardening properties of the stainless steel reinforcement. In the final section of the chapter, the serviceability limit state for stainless steel reinforced concrete beams has been explored through a detailed analysis of the deflection behaviour.

Chapter 6: Bond behaviour of stainless steel reinforced concrete

6.1 Introduction

The current chapter is focussed on the bond relationship that develops between stainless steel rebar and the surrounding concrete, which is critical to the load-carrying performance and serviceability and is therefore important information for designers. Bond is clearly a key property that needs to be considered when assessing the response of reinforced concrete and composite structures. It has a direct influence on the structural performance and inadequate bond can cause many different issues including ineffective anchorage, widespread cracking of the concrete and excessive deflections or rotations. Thus, having an accurate and realistic knowledge of the bond strength is imperative especially for the serviceability limit state.

However, bond is a relatively complex phenomenon owing to the many inter-related parameters which govern its development. Amongst the most influential parameters are the quality of the concrete and the surface geometry of the reinforcing bar. For example, voids that develop in the concrete during the casting and hardening process may result in a reduction in the local bond strength. Other factors which influence the development of bond strength include the cover distance, the clear space between adjacent bars, the number and size of bar layers and the direction of casting with respect to the orientation of the bars. The influence of bar stresses on the bond behaviour is relatively small as long as the bar does not yield. However, once it yields, the transverse forces between the bars and the concrete decrease resulting in a reduction in the bond stress-slip response.

Bond stress is developed by an adhesive action combined with frictional forces and the mechanical interlocking of the concrete against the bar-surface deformities. For plain, smooth bars, the development of bond relies primarily on adhesion and friction although there may be some interlocking if the bar surface is rough. Therefore, the use of ribbed reinforcement rather than plain bars significantly increases the bond strength that develops. The relative rib area (f_P), which is a dimensionless property, is used as indication of the quality of the rib geometry according to EN 15630-1 (2010). A typical value in the range of 0.05-0.10 for the relative rib area is appropriate for generating adequate bond strength and providing a good service-load performance. It has been shown that bond strength increases linearly with the increase of relative rib area (Darwin and Graham, 1993). The relative rib area is calculated as shown in Eq. (6.1).

$$f_P = \frac{1}{\pi . \phi .} \sum_{i=1}^{n} \frac{F_{p,i} \sin\beta_{i_i}^{\circ}}{c_i} \tag{6.1}$$

in which F_P is the area of the longitudinal section of a single rib, ϕ is the bar diameter, n is the number of indentation rows and c and β° are the rib spacing and rib inclination, respectively.

Current design standards such as Eurocode 2 (EN 1992-1-1, 2004) and MC2010 (Fédération Internationale du Béton, 2013) do not include specific rules for stainless steel reinforced concrete, and generally suggest using the same criteria as for traditional carbon steel reinforced concrete. There has been considerable research into stainless steel reinforcement, especially in recent years, but most has focussed on the corrosion behaviour (e.g. Bautista et al., 2007; Alvarez et al., 2011; Serdar et al., 2013), with limited research on the bond behaviour in a corrosive environment (e.g. Calderon-Uriszar-Aldaca et al., 2018 and Zhou et al., 2017). There have been very few studies in to the bond behaviour of stainless steel rebar, and these have even resulted in inconclusive results with one study showing that the bond developed by some austenitic and duplex stainless steel bars is lower than for similar carbon steel reinforcement (e.g. Aal Hassan, 2003) whilst other publications have shown the opposite finding (e.g. Ahlborn and DenHartigh, 2003; Johnson, 2010). Accordingly, the work presented in this chapter aims to investigate the bond behaviour of stainless steel rebar encased in concrete with reference to that of traditional carbon steel, and suggest suitable values which can be used in design. In addition, the applicability of current bond design rules in Eurocode 2 and MC2010 in terms of bond strength, anchorage length and lap length, is examined. Accordingly, this chapter proceeds with a background of the information currently available in design standards, following by a detailed description and analysis of a pull-out test experimental programme involving both stainless steel and carbon steel rebars. Finally, a suitable bond-slip model for stainless steel reinforcement is proposed.

6.2 Current standards of practice

The bond strength that develops between steel reinforcement and the surrounding concrete is an influential property in the behaviour of reinforced concrete, as it governs the composite action and hence cracks development, anchorage of the bars in the concrete and also the transfer of stresses at laps. Accordingly, international design standards such as Eurocode 2 (EN 1992-1-1, 2004) and the Model Code 2010 (Fédération Internationale du Béton, 2013) include design predictions for the bond strength, and also these other important performance criteria. Of course, as stated before, bond is a complex and multi-faceted phenomena, so different design codes adopt various simplifications in order to aid designers. In this section, the provisions provided in Eurocode 2 and MC2010 are summarized, as well as their key differences.

6.2.1 Eurocode 2 (2004)

In Eurocode 2, to obtain the design anchorage length and lap length, the design bond strength (f_{bd}) must first be calculated, followed by the basic anchorage length ($I_{b,rqd}$). The design bond strength is determined as follows:

$$f_{bd} = 2.25\eta_1\eta_2 f_{ctd} \quad (6.2)$$

In this expression, η_1 is a coefficient related to the bond condition and the bars position during concreting, and a value of unity represents good bond condition and 0.7 represents all other conditions. η_2 is a coefficient related the bar diameter (ϕ) and is taken as unity when the diameter is less than 32 mm and is otherwise determined using Eq. (6.3):

$$\eta_2 = \frac{132-\phi}{100} \text{ for } \phi > 32 \text{ mm} \quad (6.3)$$

The tensile concrete strength (f_{ctd}) is obtained as a function of the characteristic concrete compressive strength (f_c) as given in Eq. (6.4):

$$f_{ctd} = 0.21(f_c)^{2/3} \quad \text{for concrete strength} \leq C60/75. \quad (6.4)$$

Eurocode 2 states that the tensile concrete strength is limited for concrete class C60/75, unless it can be verified that the bond strength can be increased above this limit.

The basic anchorage length is determined as:

$$I_{b,rqd} = \frac{\phi\, \sigma_{sd}}{4\, f_{bd}} \quad (6.5)$$

where σ_{sd} is the design stress in the reinforcing bar.

The design anchorage length (I_{bd}) is calculated using Eq. (6.6):

$$I_{bd} = \alpha_1\alpha_2\alpha_3\alpha_4\alpha_5 I_{b,rqd} \geq I_{b,min} \quad (6.6)$$

In this expression, $I_{bd,min}$ is the minimum accepted value for the design anchorage length, determined as:

$$I_{b,min} \geq \max\{0.3I_{b,rqd}; 10\phi; 100 \text{ mm}\} \quad \text{for anchorage in tension} \quad (6.7)$$

α_1 and α_2 are coefficients related to the form of bar and the minimum cover distance, respectively, and α_3, α_4 and α_5 are coefficients related to the condition of confinement. These parameters are obtained as follows for reinforcement that is in tension:

$\alpha_1 = 1$ for straight bars.

$\alpha_2 = 1 - 0.15(c_d - \phi)/\phi \geq 0.7$ and ≤ 1.0

$\alpha_3, \alpha_4,$ and α_5 are taken as unity if there is no confinement provided by transverse reinforcement, welded transverse reinforcement and transverse pressure, respectively.

The design lap length (I_0) is calculated using Eq. (6.8):

$$I_0 = \alpha_1\alpha_2\alpha_3\alpha_5\alpha_6 I_{b,rqd} \geq I_{0,min} \quad (6.8)$$

In this expression, ($I_{0,min}$) is the minimum accepted value for the design lap length, determined as:

$$I_{0,min} \geq \max\{0.3\alpha_6 I_{b,rqd}; 15\phi; 200\ mm\} \quad (6.9)$$

where α_6 is coefficient related to the percentage of the lapped bars relative to the total cross-section area which is taken as 1 for percentage lower than 25%.

6.2.2 Model Code 2010 (2013)

The Model Code 2010 as it will be referred to, hereafter, provides guidance for the design of reinforced and prestressed concrete by the International Federation for Structural Concrete (known as the fib, or Fédération Internationale du Béton). Similar to Eurocode 2, MC2010 requires calculation of the design bond strength (f_{bd}) in order to establish the required anchorage and lap lengths. It is noteworthy that the symbols used in this section may vary from those employed in the MC2010, but are changed herein to be consistent with the earlier discussions.

The bond strength is determined as:

$$f_{bd} = (\alpha_2 + \alpha_3) f_{bd,0} \quad (6.10)$$

where α_2 and α_3 represent the influence of passive confinement from the concrete cover and from transverse reinforcement. These values are found from:

$\alpha_2 = (c_{min}/\phi)^{0.5} . (c_{max}/c_{min})^{0.15}$ for ribbed bars;

$\alpha_2 = (c_{min}/\phi)^{0.8} . (c_{max}/c_{min})^{0.15}$ for epoxy-coated or plain bars; and

$\alpha_3 = K_d . (K_{tr} - \alpha_t/50)$

c_{max} and c_{min} are cover parameters, α_t is 0.5 for bars with size up to 25 mm and K_d and K_{tr} are the effectiveness factor dependent on the reinforcement details and the density of the transverse reinforcement relative to the anchored or lapped bars, respectively. K_d and K_{tr} are taken as zero in the case where no transverse reinforcement is provided.

$f_{bd,0}$ is the basic bond strength which is a function of the characteristic concrete compressive strength (f_c) and is calculated using Eq. (6.11):

$$f_{bd,0} = \eta_1 \eta_2 \eta_3 \eta_4 (f_c/25)^{0.5} \quad (6.11)$$

In this expression, the following values are employed for the various constants:

η_1= 1.75 for ribbed bars;

η_2 = 1 for good bond conditions;

$\eta_3 = 1$ for $\phi < 25$; and

η_4 represents the characteristic strength of the reinforcement (f_{yk}) which is being anchored or lapped and is obtained from the values given in Table 6.1.

Table 6.1: Determining η_4 coefficient.

Characteristic strength of the reinforcement f_{yk} (MPa)	η_4
400	1.2
500	1.0
600	0.85
700	0.75
800	0.68

The design anchorage length (I_b) is calculated as presented in Eq. (6.12):

$$I_b = \frac{\phi \sigma_{sd}}{4 f_{bd}} \geq I_{b,min} \tag{6.12}$$

In this expression, $I_{b,min}$ is the minimum accepted value for the design anchorage length, determined as:

$$I_{b,min} > \max\{\frac{0.3 \phi f_{yd}}{4 f_{bd}}; 10\phi, 100 \text{ mm}\}$$

where σ_{sd} is the stress in the bar to be anchored by bond over the anchorage length and is obtained as follows:

$$\sigma_{sd} = \alpha_1 f_{yd} \tag{6.13}$$

$$\alpha_1 = A_{s,cal}/A_{s,ef}$$

In these expressions, f_{yd} is the design yield strength of the reinforcement, and $A_{s,cal}$ and $A_{s,ef}$ are the required area of reinforcement determined in design and the actual area of reinforcement as provided, respectively.

The design lap length (I_0) is calculated as given in Eq. (6.14):

$$I_0 = \alpha_4 \frac{\phi f_{yd}}{4 f_{bd}} \geq I_{0,min} \tag{6.14}$$

In this expression, $I_{0,min}$ is the minimum accepted value for the design lap length, determined as:

$$I_{0,min} > \max\{\frac{0.7 \phi f_{yd}}{4 f_{bd}}; 15\phi, 200 \text{ mm}\}$$

where α_4 is typically taken as unity but it can be reduced to 0.7 when the calculated stress in the bar at the ultimate limit state throughout the lap length does not exceed 50% of the reinforcement characteristic strength.

6.2.2.1 Bond stress-slip model

In addition to the design bond strength and anchorage length values, MC2010 also provides two different design bond stress-slip relationships. The designer selects the appropriate relationship to employ based on the failure mode, either failure through bond or confinement. The general bond stress-slip model is shown in Fig. 6.1, and has four main stages for pullout failure. Firstly, and with reference to Fig. 6.1, while the slip (s) is less than s_1, the bond stress is developing as the ribs on the rebars penetrate into the concrete. This stage is characterized by local crushing and micro-cracking of the concrete. Then, in the second stage when $s_1 < s < s_2$, the bond strength plateaus at the maximum value of τ_{bmax}. This represents the bond capacity which is influenced mainly by the degree of confinement. This is followed by the third stage ($s_2 < s < s_3$) in which the bond stress decreases as the interlocking mechanical bonds between the ribs and concrete reduce. Finally, when $s > s_3$, the constant residual bond level (τ_{bf}) is reached, which is mainly comprised of frictional resistance.

The bond-slip relationship provided in MC2010 describes the bond stress (τ_b) as a function of the relative displacement (s), as presented in Eqs. (6.15), (6.16), (6.17) and (6.18) for the four stages, respectively:

$$\tau_b = \tau_{bmax}\,(s/s_1)^{\alpha} \qquad \text{for } 0 \le s \le s_1 \tag{6.15}$$

$$\tau_b = \tau_{bmax} \qquad \text{for } s_1 \le s \le s_2 \tag{6.16}$$

$$\tau_b = \tau_{bmax} - (\tau_{bmax} - \tau_{bf})(s - s_2)/(s_3 - s_2) \qquad \text{for } s_2 \le s \le s_3 \tag{6.17}$$

$$\tau_b = \tau_{bf} \qquad \text{for } s_3 \le s \tag{6.18}$$

The parameters required in these equations are given in Table 6.2, where τ_{bf} is the residual bond stress, c_{clear} is the clear distance between adjacent ribs and f_{cm} is the mean cylinder concrete compressive strength and is calculated using Eq. (6.19):

$$f_{cm} = f_c + 8 \tag{6.19}$$

Table 6.2: Parameters defining the bond stress-slip relationship.

	Pull-out failure	Splitting failure (unconfined)
τ_{bmax}	$2.5(f_{cm})^{0.5}$	$2.5(f_{cm})^{0.5}$
$\tau_{bu\ split}$	-	Eq. (6.20)
s_1	1.0 mm	$s(\tau_{bu\ split})$
s_2	2.0 mm	s_1
s_3	c_{clear}	$1.2s_1$
α	0.4	0.4
τ_{bf}	$0.4\tau_{bmax}$	0

It is noteworthy that the values given in Table 6.2 are for a "good" bond conditions and are only valid for ribbed rebars in which the tensile strain in the rebar is lower than its yield limit.

The other bond stress-slip model given in MC2010 is for splitting failure, and in this, the bond strength ($\tau_{bu,split}$) is determined as follows:

$$\tau_{bu,split} = 6.5\eta_2 \left(\frac{f_{cm}}{25}\right)^{0.25} \left(\frac{25}{\phi}\right)^{0.2} \left[\left(\frac{C_{min}}{\phi}\right)^{0.33} \left(\frac{C_{max}}{C_{min}}\right)^{0.1} + k_m K_{tr}\right] \quad (6.20)$$

In this expression, k_m represents the efficiency of the confinement from the transverse reinforcement and is taken as zero when no transverse reinforcement is provided.

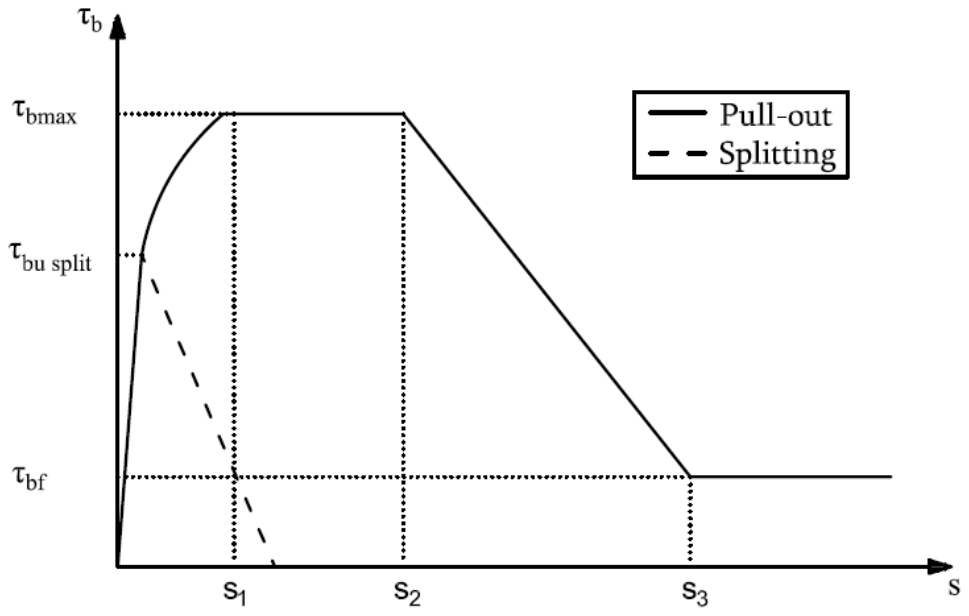

Fig. 6.1: Bond stress-slip model in MC2010 (Fédération Internationale du Béton, 2013).

It is clear from the above discussion that Eurocode 2 provides relatively more simplistic design procedures for predicting the design bond strength compared with the MC2010. However, Eurocode 2 does not provide design guidelines for predicting the bond stress-slip relationship. On the other hand, MC2010 includes the influence of important parameters in the design expression such as the confinement effect, presence of transverse reinforcement, form of the indentations, bar size and the characteristic yield strength of the rebar. Neither Eurocode 2 nor MC2010 account for the influence that the reinforcement material type has on the bond response.

6.3 Experimental programme

In order to assess the bond strength between stainless steel reinforcing bars and the surrounding concrete, and to compare the behaviour to carbon steel reinforcement, a series of pull-out tests has been conducted. A further aim of this study is to investigate if the existing design criteria which have been produced on the basis of test results on carbon steel rebar, can be used for stainless steel reinforced concrete. Different concrete strengths and reinforcement grades are included in the test programme. Concrete compression tests and reinforcement tensile tests have also been carried out to determine the characteristic material properties.

6.3.1 Type of bond test

There are a number of different methods for bond testing available in the literature. As is clear from earlier discussions, there are many factors which influence bond strength, which makes quantifying this property quite challenging. In addition to the material and geometric properties, bond behaviour is influenced by the details of the test setup which affect the stress conditions in both the concrete and the reinforcement, as well as at the interface. The most widely-used experimental set-ups for evaluating bond strength are the pull-out and beam tests. The beam test requires large specimens and comprises two half-beams which are connected at the bottom by the reinforcing bar and at the top by a hinge. This arrangement closely replicates a real structural arrangement where both the rebar and the surrounding concrete are in tension. On the other hand, the pull-out test is a more straight-forward and simple arrangement in which the reinforcement is embedded at the centre of a cubic or cylindrical concrete specimen, over a controlled bonded length. In this case, the concrete is subjected to compressive stress whilst the reinforcement is in tension. Although this may not represent the actual scenario in reinforced concrete structures, the pull-out test is widely adopted in research because of its capability to provide a reasonable bond response, the relatively low cost and the ease of fabrication. They are generally accepted as providing excellent basis for comparison at least, and for understanding the relative influence that different properties, such as reinforcement type, may have on the bond. Therefore, the pull-out test has been selected in the current programme.

6.3.2 Material properties

6.3.2.1 Concrete

There were three different concrete mixes designed for the tests to produce C20, C40 and C60 concrete. The concrete was made using high strength Portland cement (CEM I 52.5 N) and the mix proportions are summarized in Table 6.3. As stated in the table, a super plasticizer was used to enhance the workability of the C60 concrete because it had a relatively low water to cement ratio. In addition to the pull-out samples, a number of additional cylindrical specimens were casted in order to conduct compression tests. These were carried out in accordance with the guidance given in EN 12390-3 (2009), as shown in Fig. 6.2. A total of 18 cylindrical specimens with a diameter of 100 mm and depth of 200 mm were casted and then cured in a water tank for 28 days. Sulphur capping was applied at both ends of the specimens, as shown in Fig. 6.3, to avoid any reduction of the measured strength owing to stress concentrations caused by irregularity of the surface. The mean compressive strength from each of the design mixes was determined as the average of six samples, and is presented in Table 6.3. It is noteworthy that the mean measured compressive strengths of concrete are quite less than the targeted values in some cases. This may be linked to the fact that cylindrical concrete sample provides lower compression strength compared with that of a cube.

Fig. 6.2: Concrete compression testing machine.

Fig. 6.3: Cylindrical concrete samples capped with sulphur.

Table 6.3: Concrete mix proportions.

Target concrete grade	w/c ratio	Mix proportions (kg/m^3)						Mean measured compressive strength (MPa)	Standard deviation (MPa)
		Cement (kg/m^3)	Water (kg/m^3)	Sand (kg/m^3)	Coarse aggregate (kg/m^3)	Aggregate size (mm)	Super Plasticizer (kg/m^3)		
C20	0.75	304	229	990	862	4-14	-	24.5	2.59
C40	0.53	365	195	736	1117	4-14	-	33.7	2.71
C60	0.36	450	164	751	1088	5-16	5.9	51.2	1.93

6.3.2.2 Reinforcement

Austenitic stainless steel is the most common type of stainless steel material that is used for reinforcement and therefore grade 1.4301 is selected in this study. Pull-out tests on carbon steel grade B500 rebar are also conducted. In both cases, for the stainless and carbon steel tests, bars with a diameter of 10 mm and 12 mm are included. The geometrical details of all of the bars included in this study have been closely examined and measured, and the data is presented in Table 6.4.

The 12 mm stainless steel rebars are a new version of grade 1.4301 reinforcement known as ‘‘grib-rib’’ which is available as high strength material (Stainless UK, 2016). This was not deliberately ordered as part of this study but is now the default form of 12 mm stainless steel rebar that is available in the UK. The manufacturers claim that the grib-rib bars provide better bond behaviour compared with regular stainless steel rebar because they comprise three series of transverse ribs around the bar cross-section rather than the typical two series. On the other hand, all of the carbon steel rebars included in this study consist of two series of transverse ribs at the cross-section and also two longitudinal ribs. The relative rib areas (f_p) presented in Table 6.4 are calculated using Eq. (6.1). It is noteworthy that the stainless steel and carbon steel reinforcements comply with the requirements given in BS 6744 (2016) and BS 4449+A3 (2005), respectively, which are presented in Table 6.5,

apart from the relative rib area for the 10 mm diameter stainless steel rebar which is found to be lower than the minimum required value.

Table 6.4: Geometrical properties of the reinforcing bars.

Material	Bar diameter (mm)	Maximum Rib height (mm)	Rib spacing (mm)	Rib inclination (β°)	F_P area of a single rib (mm^2)	Relative rib area (f_P)
Stainless steel	10	0.67	9.34	50°	5.74	0.030
Stainless steel (grib-rib)	12	0.75	7.58	55°	7.19	0.062
Carbon steel	10	1.03	6.85	55°	7.74	0.059
Carbon steel	12	1.16	7.04	60°	10.13	0.066

Table 6.5: Ranges for rib parameters for stainless steel BS 6744 (2016) and carbon steel BS 4449+A3 (2005).

Rib height (mm)	Rib spacing (mm)	Rib inclination (β°)	Min relative rib area for 10 and 12 mm bar diameter (f_P)
0.03d – 0.15d	0.4d – 1.2d	35° - 75°	0.04

Tensile tests have been conducted in order to obtain the characteristic stress-strain curves and the mechanical properties of both the carbon and stainless steel rebars, in accordance with EN 6892-1 (2016), and the results are presented in Fig. 6.4 and Table 6.6, respectively. Three repeat tests were carried out on each type of bar, and the average response is taken for the value presented. In Fig. 6.4, both the overall response is presented as well as a closer view of the elastic portion of the behaviour. It is clear from the graph that the stainless steel and carbon steel rebars exhibit quite different stress-strain responses. The stainless steel specimens are much more ductile, with high ultimate strains and significant strain hardening, and also have a continuous curve without a clearly defined yield point. On the other hand, the carbon steel bars show a clear yield plateau followed by a moderate degree of strain hardening and limited ductility.

With reference to the data presented in Table 6.6, the yield stress (f_y) for the stainless steels are 515 and 715 N/mm^2 for the 10 mm and 12 mm bars, respectively, where the equivalent values for the carbon steel rebars are 589 and 554 N/mm^2, respectively. The ultimate stress (f_u) for stainless steels are 19.6% and 36.8% higher than that of carbon steel for 10 mm and the 12 mm bars, respectively. As expected, the grib-rib stainless steel rebars exhibit the highest strength value among the others.

Additionally, the stainless steels provide greater ductility than the carbon steel by around 159% and 129% for 10 mm and the 12 mm bars, respectively. It is also observed that the bars with diameter of 12 mm have lower ductility than those with diameter of 10 mm by around 35.0% and 26.3% for stainless steel and carbon steel, respectively. Moreover, the modulus of elasticity for stainless steel and carbon steel are quite similar, apart from the grib-rib stainless steel rebar which shows relatively lower modulus of elasticity compared to the equivalent carbon steel rebar.

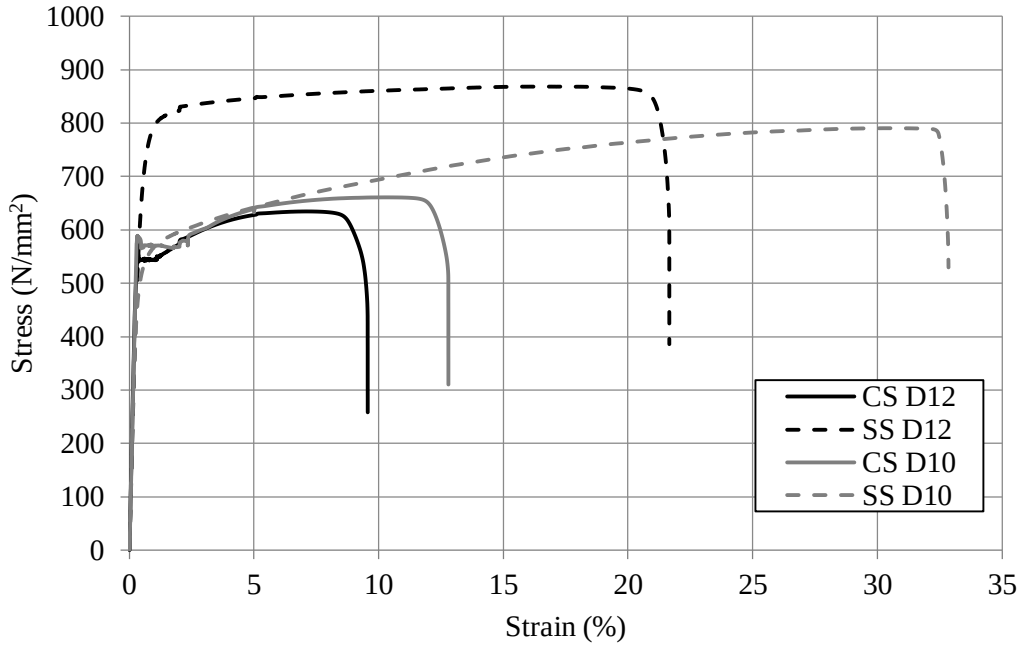

(a)

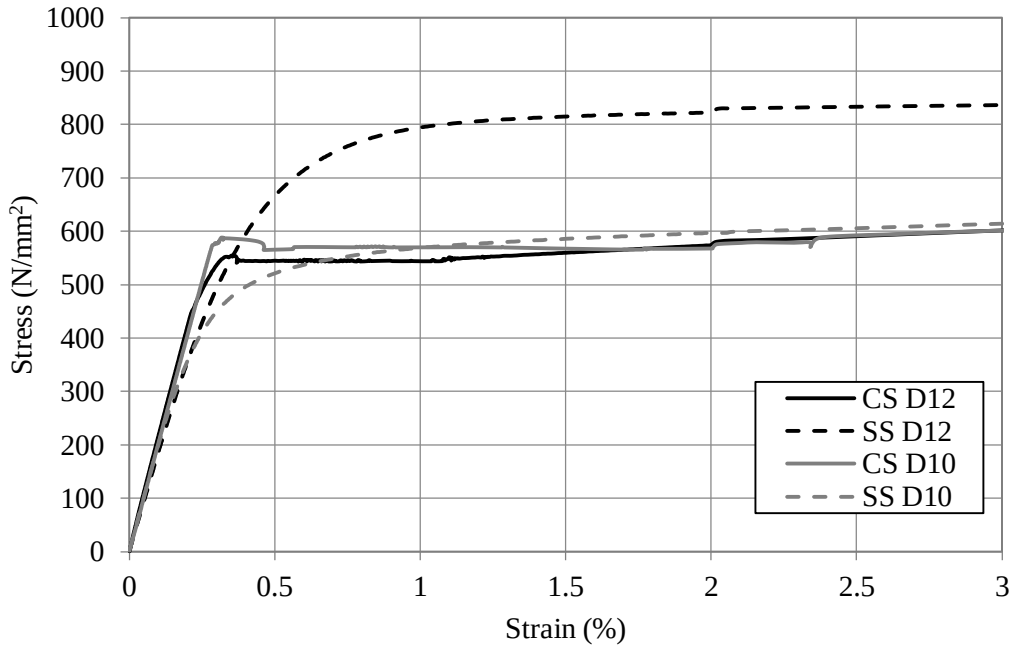

(b)

Fig. 6.4: Stress-strain curves of stainless steels and carbon steels (a) full curve and (b) more detailed view of the elastic region.

Table 6.6: Mechanical properties of the reinforcements.

Material	Diameter (mm)	Yield stress f_y (N/mm^2)	Ultimate strength f_u (N/mm^2)	Modulus of elasticity E (N/mm^2)	Ductility % (mm/mm)
Stainless steel	10	515	790	200899	32.39
Stainless steel (grib-rib)	12	715	868	184000	21.05
Carbon steel	10	589	661	201368	12.49
Carbon steel	12	554	635	211766	9.21

6.3.3 Bond test arrangement

A total of 72 pull-out test samples were prepared, in accordance with the guidance in EN 10080 (2005), in two phases. The first phase comprised 60 tests with 12 more cast for Phase 2. The moulds were fabricated from PVC material, as shown in Fig. 6.5. In the first phase of testing, each specimen was 110 mm in diameter and 120 mm in height. A single piece of rebar which was 500 mm in length was positioned at the centre of the specimen. The bond length was set at 60 mm for all specimens, so either 5 or 6 times the bar diameter, to reduce the effect of the longitudinal compressive stresses caused by bearing of the concrete against the plate that restrains the pull-out specimen (Carvalho et al., 2018). The concrete was then cast in a vertical direction, and was compacted using manual procedures. All specimens were demoulded the day after casting and then cured in a water tank for 28 days, at a temperature of 21˚C. Fig. 6.6 presents an image of a specimen in the testing machine as well as a schematic of the pull-out test arrangement. Two transducers were used to measure the slip and then the average value was taken. These were located on the bottom of the specimen, as shown in the figure.

The second stage of testing was planned based on the results of the first phase, where splitting failure was prevalent (this will be discussed in more detail later). Accordingly, 12 more samples were prepared, each of which was 200 mm in length in order to avoid splitting failure. Cubic moulds were used in this phase due to unavailability of cylindrical moulds with a large enough diameter to avoid splitting of the concrete. In these samples, the bond length was set at 5 times the bar diameter and the overall bar length was 500 mm. As before, the stainless steel reinforcing bar was positioned in the centre of the specimen. The target concrete strength was 40 MPa and these specimens were cast in a horizontal direction and compacted using an electrical vibrator.

Fig. 6.5: Photo of the rig used for casting pull-out specimens.

(a)

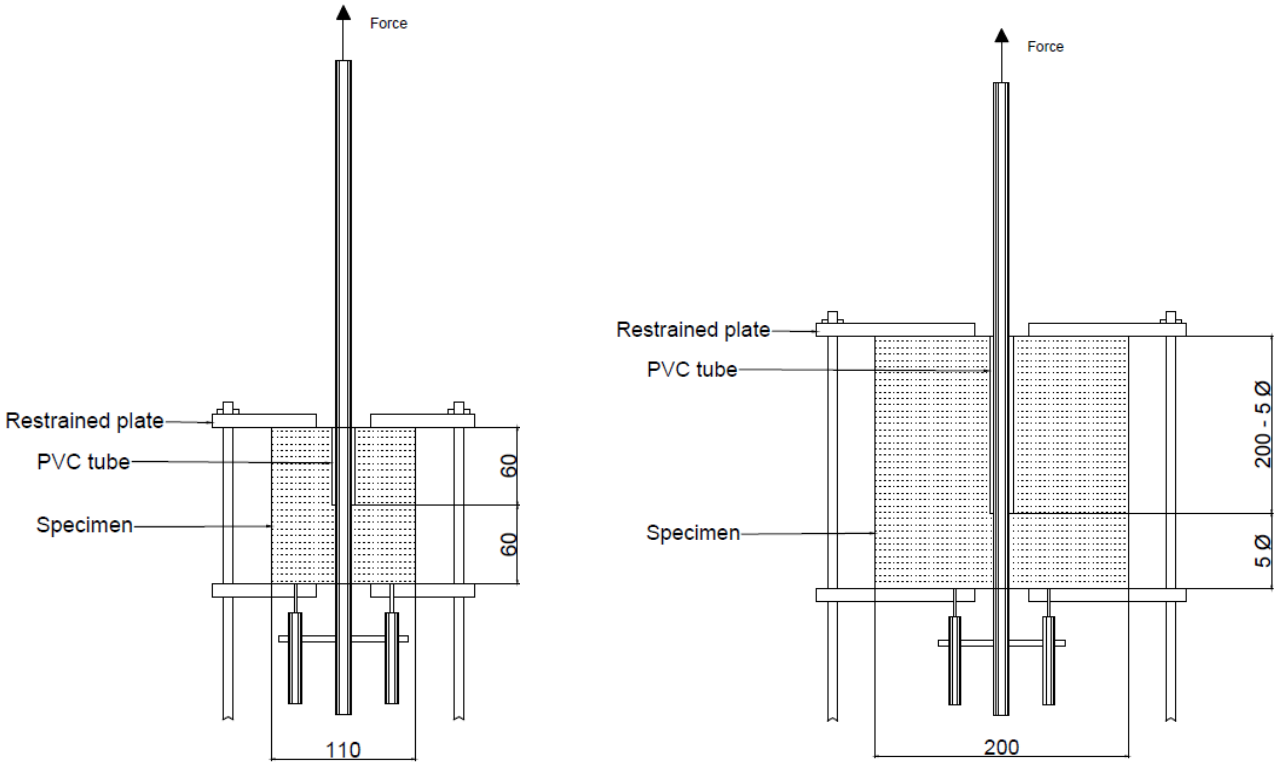

(b) (c)

Fig. 6.6: Pull-out test arrangement including (a) an image of the testing machine, (b) a schematic of the pull-out set-up for phase 1 and (c) a schematic of the pull-out set-up for phase 2. All dimensions are given in mm with a scale 1:7.

6.4 Test results

The pull-out test results are presented in Table 6.7. The programme included 5 repetitions of each specimen and the results presented in the table reflect the average behaviour. The results obtained from these repetitions are reported in Appendix C. A reference-system was adopted to label each specimen, where the first portion of the name denotes the type of rebar used (i.e. stainless steel (SS) or carbon steel (CS), the next term between the two hyphens defines the bar diameter (D10 or D12 for 10 mm and 12 mm reinforcement, respectively), the third portion is the target concrete strength, whilst the last number refers to the phase of testing. In Table 6.7, the ultimate experimental bond strength (τ) is calculated using Eq. (6. 21), where F is the ultimate applied load, l is the bonded length and ϕ is the diameter of the rebar:

$$\tau = \frac{F}{\pi \phi l} \tag{6. 21}$$

Fig. 6.7(a) presents an image from a specimen in the first phase of testing. All of the cylindrical specimens in this group failed by splitting, irrespective of the type or size of the reinforcement. This is mainly attributed to the insufficient confinement provided by the concrete as well, perhaps, as the relatively long bonded length compared to the total length of the specimen. On the other hand, pull-out failure was observed for all cubic specimens in Phase 2, as shown in Fig. 6.7(b), which were designed to provide more confinement.

Fig. 6.8 presents the bond-slip response for the bond tests conducted in Phase 1 of the test programme, for samples with (a) C20, (b) C40 and (c) C60 concrete, respectively. All of these specimens failed by splitting of the concrete. Generally, with reference to the graphs, it is observed that the stainless steel rebars exhibit lower ultimate bond strength compared with that of carbon steels by around 28% on average. Using a higher bar diameter resulted in a slight improvement in the ultimate bond strength, relative to carbon steel. It is also shown that the samples with stainless steel rebars had a relatively lower softening response compared to that of carbon steels in all cases except the specimen with 12 mm stainless steel and C60 concrete strength. Additionally, it is noted that the ultimate bond strength is highly influenced by the strength of concrete as the samples with C60 concrete strength achieved greater bond strengths by around 87% and 64% compared with the specimens made from C20 concrete, for stainless steel and carbon steel, respectively.

Fig. 6.9 presents the bond-slip response for the samples from Phase 2 of the bond test programme, all of which failed by pull-out failure. Similar to the earlier observations, it is again shown that stainless steels achieve lower ultimate bond strength values compared with carbon steel reinforcement, by around 40% on average. By comparing specimens with the same concrete strength and bar diameter from Phase 1 and 2, it is clear that the difference in ultimate bond strength between the samples with stainless steel and carbon steel rebars is even greater when pull-out failure occurs rather than splitting.

Additionally, it is noteworthy that stainless steels exhibit lower ultimate bond strength in phase 2 compared to that of phase 1. The reason for this could be attributed to the influence that the geometry of specimens has on the bond strength of stainless steels. In general, the samples with stainless steel exhibit a more rapid reduction of bond strength also in the softening range compared to those with carbon steel, as well as lower residual bond values. It is also interesting to observe in Fig. 6.9 that the bond response for samples with stainless steel rebar fluctuates in the post-peak range, which did not occur for either the carbon steel reinforced samples or those in Phase 1 which failed by splitting. This could be linked to the rib spacing in the reinforcement since it is observed that the distance between the two plateaus is quite coinciding to the rib spacing. In the following sub-sections, the tests results are further analysed and the impact of particular properties such as concrete strength, bar diameter and reinforcement material type are discussed.

(a) (b)

Fig. 6.7: Failure mode for specimens with stainless steel reinforcement from (a) phase 1- splitting failure and (b) phase 2- pull-out failure.

Table 6.7: Ultimate bond strength results of the pull-out tests.

Specimen	Mean measured compressive strength, f_c (MPa)	Bar diameter, ϕ (mm)	Failure mode	Ultimate bond strength, τ (MPa)	Standard deviation (MPa)	Difference in the ultimate bond strength, SS/CS (%)
SS-D10-C20-1	24.5	10	Splitting	12.1	0.75	-24.4
CS-D10-C20-1			Splitting	16.1	0.77	
SS-D12-C20-1		12	Splitting	12.0	0.49	-35.2
CS-D12-C20-1			Splitting	18.5	0.51	
SS-D10-C40-1	33.7	10	Splitting	21.3	1.56	-15.6
CS-D10-C40-1			Splitting	25.2	1.36	
SS-D12-C40-1		12	Splitting	18.9	1.19	-27.8
CS-D12-C40-1			Splitting	26.1	0.82	
SS-D10-C40-2	34.5	10	Pull-out	14.2	2.00	-46.1
CS-D10-C40-2			Pull-out	26.3	1.09	
SS-D12-C40-2		12	Pull-out	17.5	1.83	-34.3
CS-D12-C40-2			Pull-out	26.6	0.60	
SS-D10-C60-1	51.2	10	Splitting	22.4	1.28	-15.0
CS-D10-C60-1			Splitting	26.4	1.30	
SS-D12-C60-1		12	Splitting	22.7	0.59	-25.1
CS-D12-C60-1			Splitting	30.26	0.64	

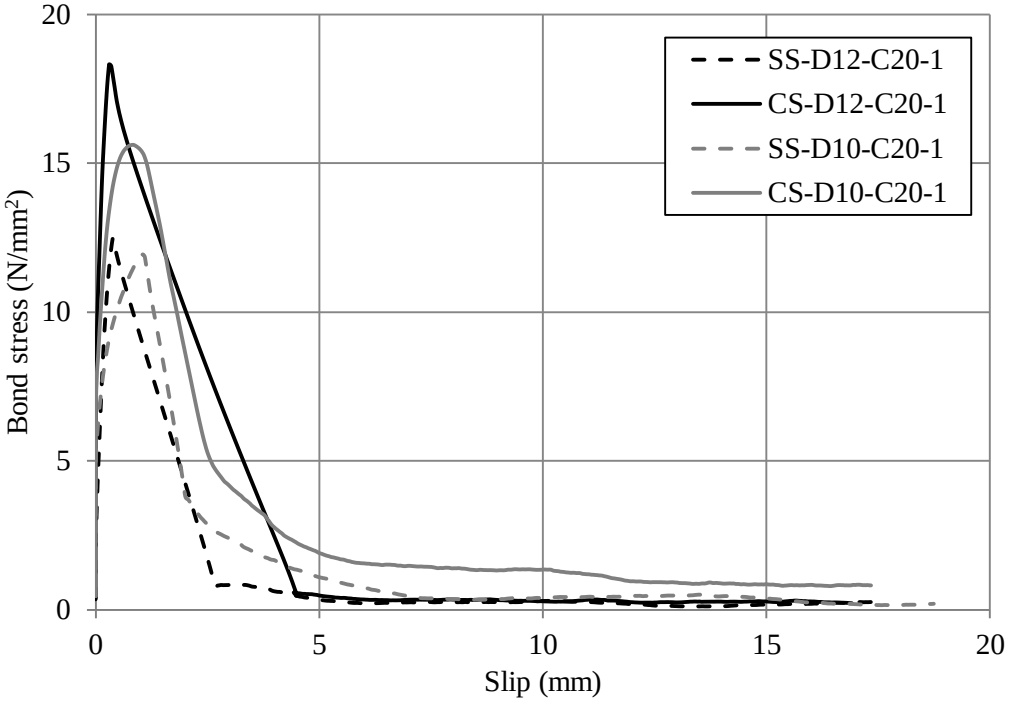
SS-D12-C20-1
CS-D12-C20-1
SS-D10-C20-1
CS-D10-C20-1
Bond stress (N/mm2)
Slip (mm)
0
5
10
15
20

(a)

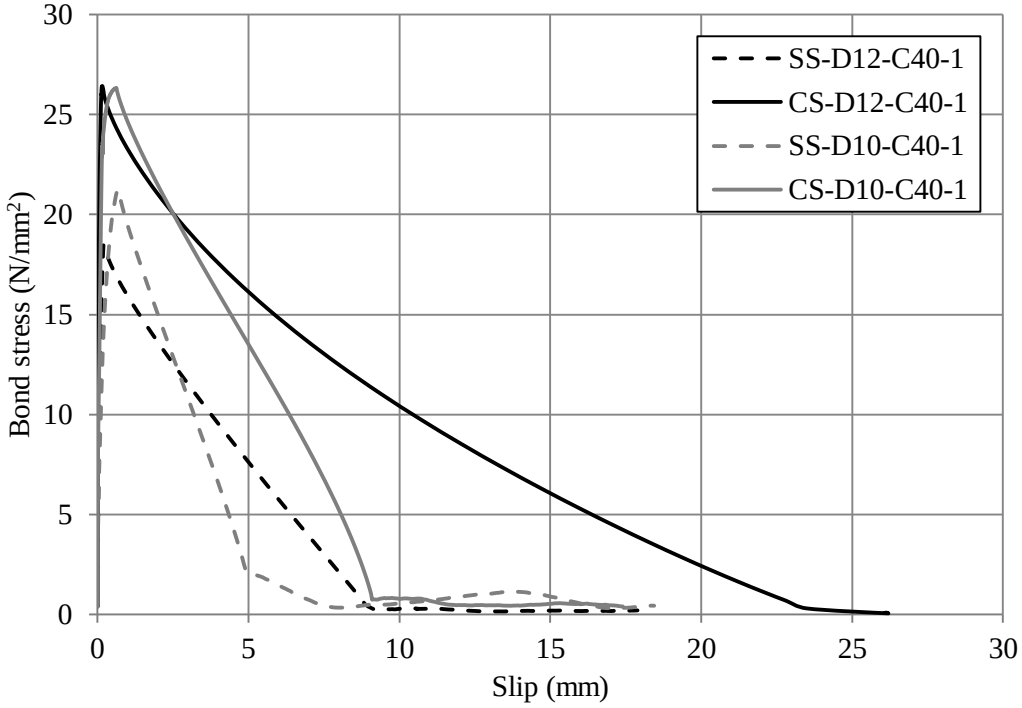
SS-D12-C40-1
CS-D12-C40-1
SS-D10-C40-1
CS-D10-C40-1
Bond stress (N/mm2)
Slip (mm)
0
5
10
15
20
25
30

(b)

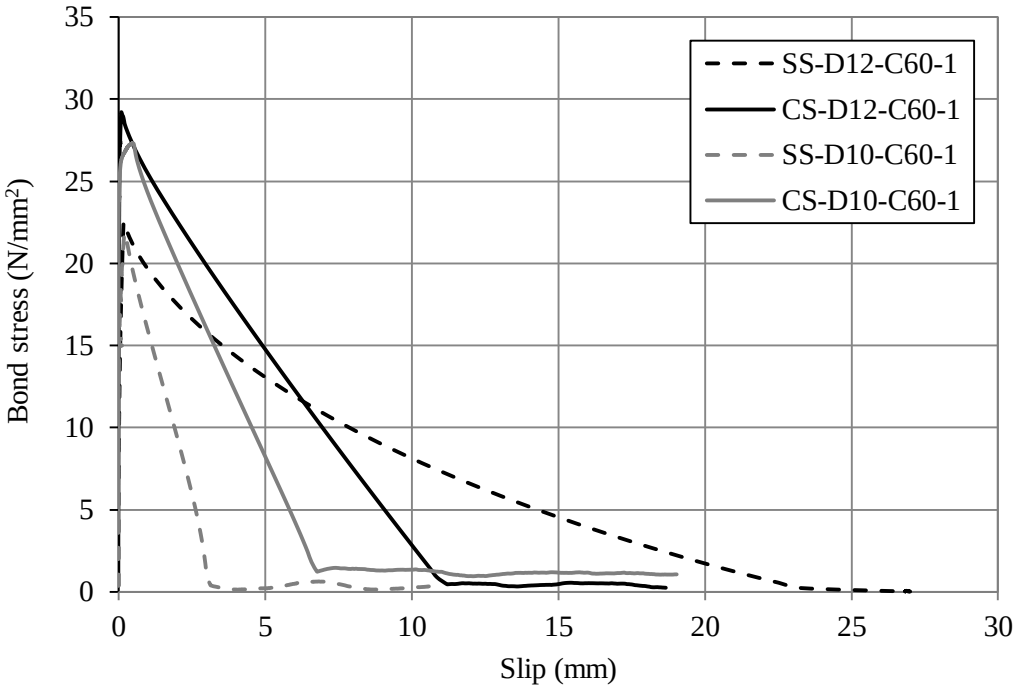

(c)

Fig. 6.8: Splitting bond stress-slip curves for carbon and stainless steel reinforcements with concrete strength (a) 20 MPa (b) 40 MPa and (c) 60 MPa.

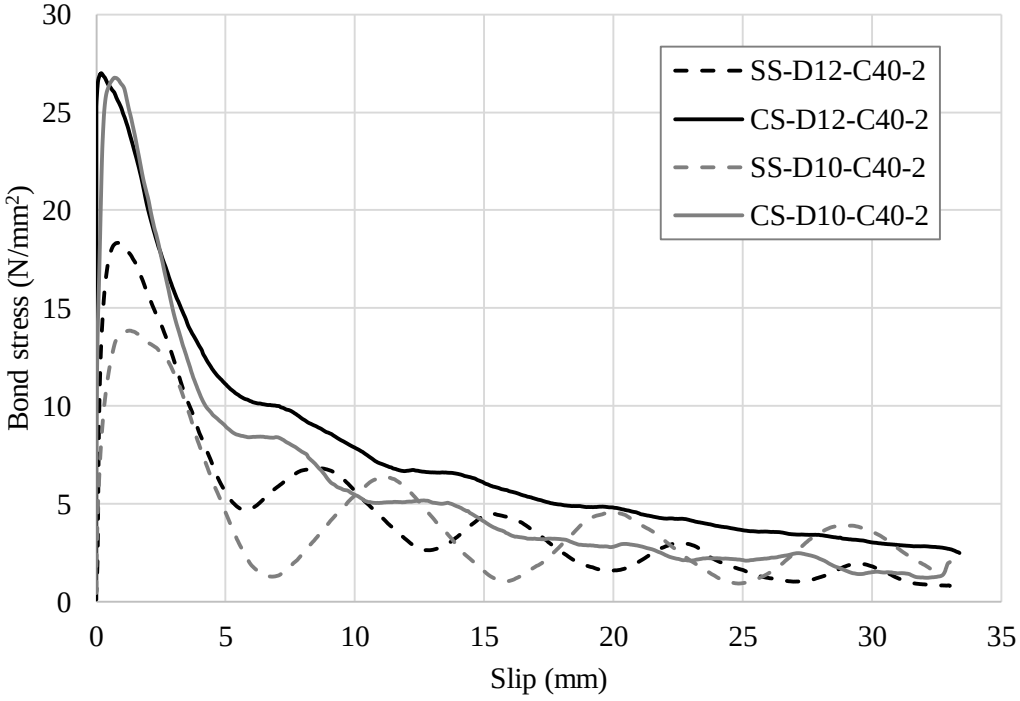

Fig. 6.9: Pull-out bond stress-slip curves for carbon and stainless steel reinforcements with concrete strength 40 MPa.

6.4.1 Reinforcement material and diameter

It was observed in the previous section that stainless steel rebars achieve lower ultimate bond strength values compared with carbon steels, in all cases examined in the current programme. For the samples that experienced splitting failure, the bond that develops for the 12 mm stainless steel rebar is 35.2%, 27.8% and 25.1% lower than for carbon steel rebar for C20, C40 and C60, respectively. These same values for the 10 mm bars are 24.4%, 15.6% and 15%, respectively. It is shown that for both bar diameters examined, the difference between stainless steel and carbon steel is greatest when the concrete strength is relatively low, i.e. for the samples with C20 concrete. This is most likely owing to the fact the stainless steels have lower relative rib areas than the carbon steel bars, and this influence is greater when the concrete strength is relatively low.

It is also observed that using bars with a greater diameter increases the difference in the ultimate bond strength between stainless steel and carbon steel, in all cases in Phase 1. This is attributed to the fact that increasing the bar diameter from 10 mm to 12 mm enhances the ultimate bond strength for carbon steel by around 11% on average whereas in contrast there is no considerable improvement for stainless steels or even results in lower bond strength in some particular cases. In contrast, for the samples that experienced pull-out failure in Phase 2, it is found that using bars with a greater diameter decreases the difference in the ultimate bond strength between stainless steel and carbon steel. It is observed that the bond strength for stainless steel increases by around 23% when the bar diameter changes from 10 mm to 12 mm. The equivalent value for carbon steel is just 1%. It is likely that the reason for this disparity is owing to the difference in the geometry of the samples used in Phase 1 and 2, including bonded length. Therefore, conducting further tests on the influence of the bar diameter would be recommended.

6.4.2 Concrete strength

Fig. 6.10 (a) and (b) represent the influence that concrete strength has on the bond stress-slip behaviour for 10 mm stainless steel and carbon steel samples, respectively. The figures show that the samples with relatively higher concrete strength exhibit greater bond strength, in all cases. For example, the ultimate bond strength that develops for 10 mm diameter samples with C60 concrete strength is improved by around 85% and 65% for stainless steel and carbon steel rebars, respectively, compared to those with C20 concrete strength. These same values for 12 mm bars are 89% and 63%. This conclusion is in line with the research findings reported by the International federation for structural concrete (Balazs et al., 2014; Gambarova et al., 2000).

It is noteworthy to observe that the samples with concrete strength C40 and C60 generate relatively similar ultimate bond strength values with difference being around 5.4% and 4.6% for stainless steel and carbon steel rebars, respectively, as shown in Fig. 6.10. This indicates that the influence of concrete strength becomes less significant after a certain strength level. This observation is in line

with the guidance given in Eurocode 2, where the design rules limit the bond strength to the value for C60/75 concrete strength class, unless it is verified that the average bond strength increases above this limit (EN 1992-1-1, 2004).

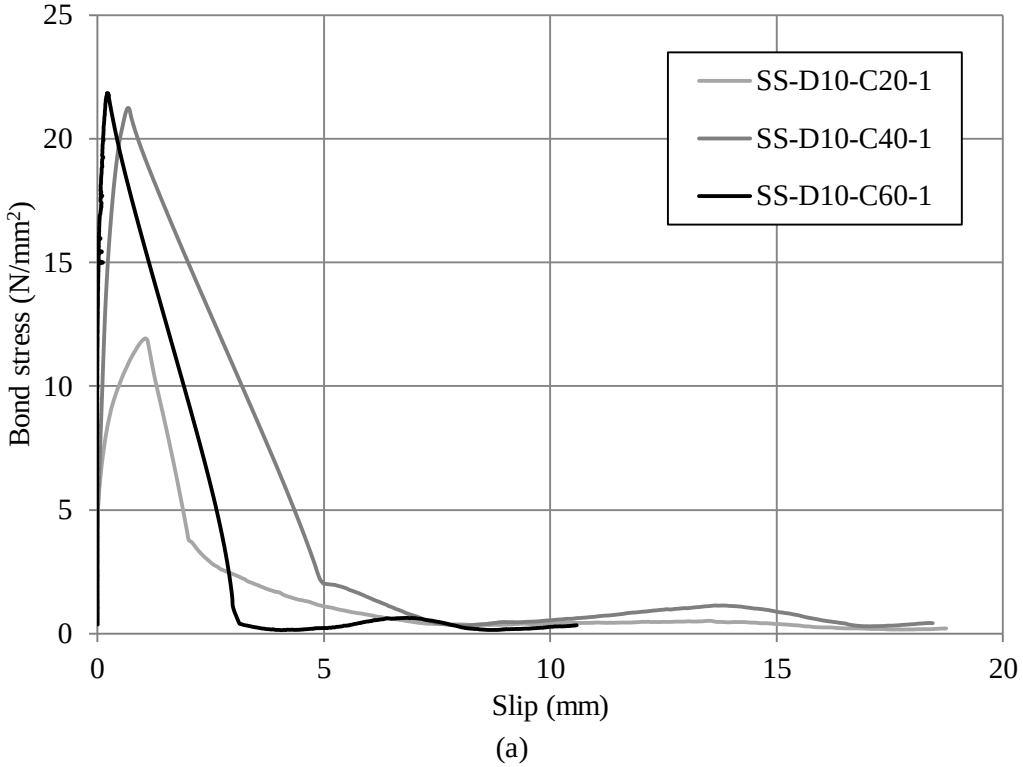

(a)

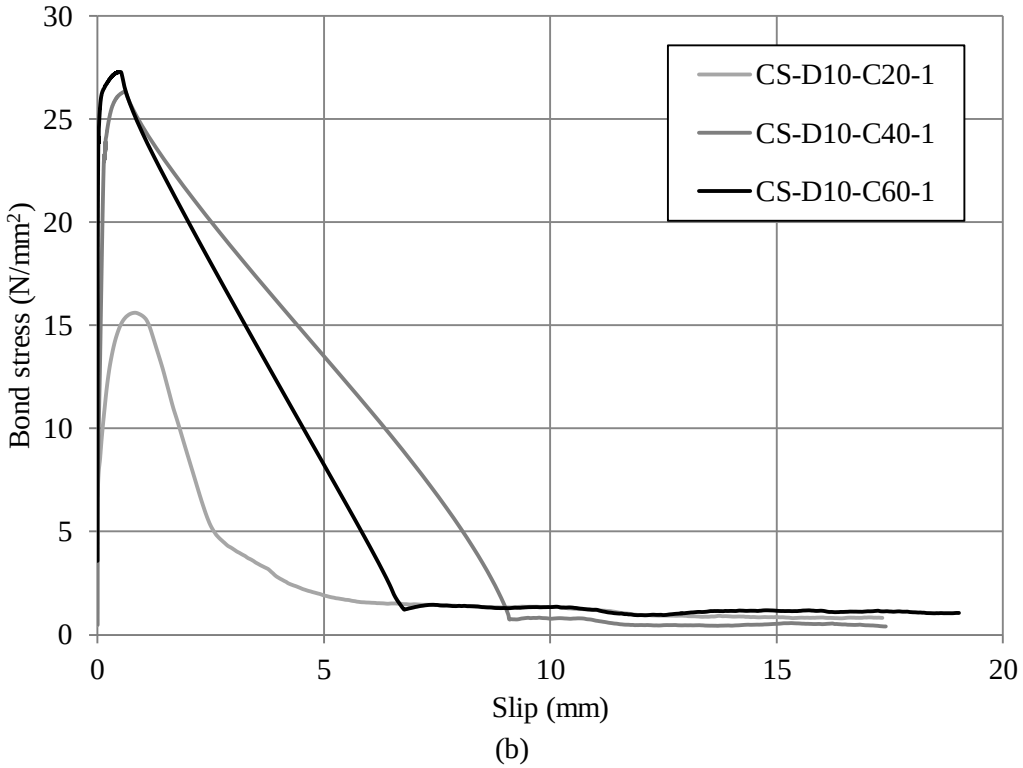

(b)

Fig. 6.10: Bond stress-slip curves for samples with 10 mm bar diameter and concrete strengths C20, C40 and C60 for (a) stainless steel and (b) carbon steel rebar.

6.5 Comparison with design codes

6.5.1 Design bond strength, anchorage and lap lengths

Understanding the bond behaviour that develops between reinforcement and the surrounding concrete is imperative in the design of reinforced concrete structures, as it underpins the composite performance of the member. However, bond is a highly complex phenomenon that is influenced by many inter-related parameters which are difficult to measure and predict and therefore most global design standards provide quite conservative estimates for the bond strength that develops. In this context, the aim of this section is to evaluate the current design rules in Eurocode 2 and MC2010 for reinforced concrete through comparison with the experimental results discussed previously, in terms of bond strength, anchorage length and lap length, as shown in Table 6.8. Both stainless steel and carbon steel are included in the analysis.

The experimental anchorage and lap lengths are obtained by substituting the experimental bond strength values into the appropriate Eurocode 2 design expressions without considering the minimum design values. It is noteworthy that the characteristic values for concrete and the reinforcement obtained experimentally and described in Section 6.3.2 are employed in this section in order to provide more realistic comparison. Since both codes predict bond strength on the basis of the characteristic values, the experimental bond results are presented here as the characteristic values which obtained using Eq. (6.19).

It is observed from the data presented in Table 6.8 that the design bond strength values predicted by both Eurocode 2 and MC2010 are very conservative when compared with the experimental ultimate bond strength values obtained in the current analysis. The Eurocode 2 bond strength predictions are around 49% and 73% less than the test values for stainless steel and carbon steel reinforcement, respectively, whereas the equivalent values for MC2010 are 59% and 78%, respectively. In all cases included in the current study, MC2010 is more conservative in its predictions of the design bond strength compared with Eurocode 2 with the average difference being around 19%.

With reference to the data in Table 6.8, it is observed that bond strength values obtained from Eurocode 2 for samples with stainless steel are identical to those with carbon steel for each concrete category irrespective of the bar size. On the other hand, in MC2010, it is observed that the difference in bond strength predictions between stainless steels and carbon steels are 13% and -19.6% on average for 10 mm and 12 mm bar diameter, respectively. As discussed in Section 6.2, the bond design rules in both codes are not influenced by the reinforcement type. Hence, this disparity in the prediction of bond is mainly because MC2010 takes into account the characteristic yield strength of the reinforcement and a higher reduction factor is applied for the rebar with greater characteristic yield strength. Since the 12 mm stainless steel rebar (grib-rib) has relatively higher strength property compared with the other bars, a lower bond strength is predicted.

Similar conclusions are found for the design anchorage and lap lengths, as both Eurocode 2 and MC2010 provide extremely conservative anchorage and lap lengths compared with those calculated based on the experimental results. For instance, the anchorage lengths predicted using Eurocode 2 and MC2010 are higher than the experimental values by around 116% and 310% on average for stainless steel rebars and by around 281% and 570% for carbon steels, respectively. The equivalent values for the lap lengths are higher than the experimental results by around 134% and 310% on average for stainless steel rebars and by around 300% and 570% for carbon steel, respectively. It is clear that MC2010 is significantly more conservative than Eurocode 2, although it does take more of the influential material and geometrical properties in to account.

For 10 mm stainless steel, the anchorage lengths obtained using Eurocode 2 and MC2010 are lower than those for carbon steels by around 13% and 22% on average, respectively. On the other hand, the equivalent values for the 12 mm stainless steel are higher than those for carbon steels by 29% and 61%, respectively. Similar results are found for the lap lengths, as both Eurocode 2 and MC2010 require shorter lap lengths for the 10 mm stainless steel rebars compared with those for carbon steels by 7% and 22% on average. However, the codes require greater lap lengths for the 12 mm stainless steel rebars compared with those for carbon steels by 25% and 60% on average. As discussed earlier, the differences in the anchorage and lap lengths between stainless and carbon steel rebars are mainly attributed to the variations of the characteristic yield strength of the reinforcements.

In conclusion, the design bond values given in both Eurocode 2 and MC2010 are shown to be very conservative compared with the experimental results, even for the stainless steel reinforced concrete which was shown to have lower bond strength compared with regular carbon steel reinforced concrete. Therefore, it is concluded that the current design rules can be safely applied for stainless steel reinforced concrete structures, for the parameter range considered herein. However, the design codes provide inaccurate and inefficient predictions, mainly owing to the fact that they are not based wholly on fundamental principles with all key parameters considered. In the following sub-section, the design bond-slip model provided in the MC2010 is evaluated for the case of splitting and pull-out failure modes. Consequently, new bond-slip models are proposed for both stainless steel and carbon steel reinforced concrete.

Table 6.8: Results comparison with codes predictions

Specimens	Mean measured compressive strength, f_c (MPa)	Design bond strength, f_{bd} (MPa)			Design anchorage length, l_{bd} (mm)			Design lap length, l_0 (mm)		
		Exp	EC2	MC2010	Exp	EC2	MC2010	Exp	EC2	MC2010
SS-D10-C20-1	24.5	4.1	3.1	3.1	190	256	360	190	256	360
CS-D10-C20-1		8.1	3.1	2.8	111	293	464	111	293	464
SS-D12-C20-1		4.0	3.1	2.1	325	427	878	325	427	878
CS-D12-C20-1		10.5	3.1	2.6	96	331	547	96	331	547
SS-D10-C40-1	33.7	13.3	4.1	3.9	59	192	290	59	200	290
CS-D10-C40-1		17.2	4.1	3.4	52	219	373	52	219	373
SS-D12-C40-1		10.9	4.1	2.6	120	320	707	120	320	707
CS-D12-C40-1		18.1	4.1	3.3	56	248	441	56	248	441
SS-D10-C40-2	34.5	6.2	4.2	3.9	127	187	284	127	200	284
CS-D10-C40-2		18.3	4.2	3.5	49	213	365	49	213	365
SS-D12-C40-2		9.5	4.2	2.7	138	311	692	138	311	692
CS-D12-C40-2		18.6	4.2	3.3	54	241	431	54	241	431
SS-D10-C60-1	51.2	14.4	5.8	5.0	54	135	222	54	200	222
CS-D10-C60-1		18.4	5.8	4.5	49	154	286	49	200	286
SS-D12-C60-1		14.7	5.8	3.4	89	225	542	89	225	542
CS-D12-C60-1		22.3	5.8	4.3	45	174	338	45	200	338

6.5.2 Proposed bond stress-slip curve

The local bond stress-slip relationship is a key issue in design of reinforced concrete structures and has a significant influence on the crack propagation, stiffness and also integrity and resilience of members and frames. Owing to the previously-discussed complexity in analysing bond, and the variety of test conditions and structural applications, a large number of analytical models have been proposed in the literature to simulate the bond-slip response in reinforced concrete (e.g. Nilson, 1968; Somayaji and Shah, 1981; Harajli et al., 1995 and Oh and Kim, 2007). The model which was presented by Eligehausen et al. (1982) and then further developed for inclusion in MC2010 (Fédération Internationale du Béton, 2013) incorporates a more simplistic solution and corresponds to the experimental behaviour. Therefore, this model has been selected herein to evaluate the bond-slip response.

As discussed in the experimental analysis earlier in this chapter, stainless steel rebars exhibit relatively lower bond strengths compared with carbon steel reinforcement. Hence, it is very imperative to examine the applicability of using the bond-slip model given in MC2010 for concrete members with stainless steel reinforcement. Since both pull-out failure and splitting failure were experienced in the tests, the bond-slip response is evaluated in terms of both failure modes. The results presented in this section are obtained for samples with C40 concrete strength. The details of the bond-slip model given in MC2010 are described previously in Fig. 6.1 using Eqs. (6.15)-(6.18) together with the parameters defined in Table 6.2.

Fig. 6.11 presents the bond-slip curves predicted using MC2010 for the splitting failure mode together with the corresponding experimental results, for samples with bar diameter of 10 mm and 12 mm. It is generally shown that the bond-slip response obtained using MC2010 underestimates the experimental response, in all cases, by quite some margin. It is clear that the current bond-slip model provided in the MC2010 for splitting failure mode does not reflect the actual behaviour for both stainless steel and carbon steel, for the test parameters studied herein.

It has been shown in this chapter that the bond behaviour for stainless steel reinforced concrete is different to that of carbon steel reinforced concrete and therefore different bond-slip models are developed for each. The proposed curves for stainless steel and carbon steel are presented in Fig. 6.11 using Eqs. (6.15)-(6.18) together with the parameters defined in Table 6.9. The clear space between ribs (c_{clear}) is taken as 6 mm in all cases. It is evident from the data presented in Fig. 6.11 that the proposed curves provide a more accurate and representative depiction of the experimental behaviour in terms of the ascending branch, the ultimate bond strength and also softening range, in all cases. It is observed that implementing the proposed curves improves the ultimate bond strength by around 22% on average for stainless steel rebars and 38% for carbon steels.

Table 6.9: Parameters details for the proposed splitting bond-slip model.

	Splitting failure (unconfined)		
	Current model in MC2010	Proposed model for stainless steel	Proposed model for carbon steel
τ_{bmax}	$2.5(f_{cm})^{0.5}$	$3(f_{cm})^{0.5}$	$4(f_{cm})^{0.5}$
$\tau_{bu\ split}$	Eq. (6.20)	Eq. (6.22)	Eq. (6.23)
s_1	$s(\tau_{bu\ split})$	$0.5s(\tau_{bu\ split})$	$0.5s(\tau_{bu\ split})$
s_2	s_1	s_1	s_1
s_3	$1.2s_1$	c_{clear}	$1.5c_{clear}$
A	0.4	0.4	0.4
τ_{bf}	0	0	0

In addition to the bond stress-slip relationship, the expression given in Eq. (6.20) previously for the ultimate bond strength for the splitting failure mode has been updated based on the analysis presented herein for stainless steel and carbon steel, as presented in Eqs. (6.22) and (6.23), respectively. It is indicated that Eqs. (6.22) and (6.23) have been updated by only calibrating the first parameter in Eq. (6.20).

$$\tau_{bu,split} = 8.5\eta_2 \left(\frac{f_{cm}}{25}\right)^{0.25} \left(\frac{25}{\phi}\right)^{0.2} \left[\left(\frac{C_{min}}{\phi}\right)^{0.33} \left(\frac{C_{max}}{C_{min}}\right)^{0.1} + k_m K_{tr}\right] \quad (6.22)$$

$$\tau_{bu,split} = 11\eta_2 \left(\frac{f_{cm}}{25}\right)^{0.25} \left(\frac{25}{\phi}\right)^{0.2} \left[\left(\frac{C_{min}}{\phi}\right)^{0.33} \left(\frac{C_{max}}{C_{min}}\right)^{0.1} + k_m K_{tr}\right] \quad (6.23)$$

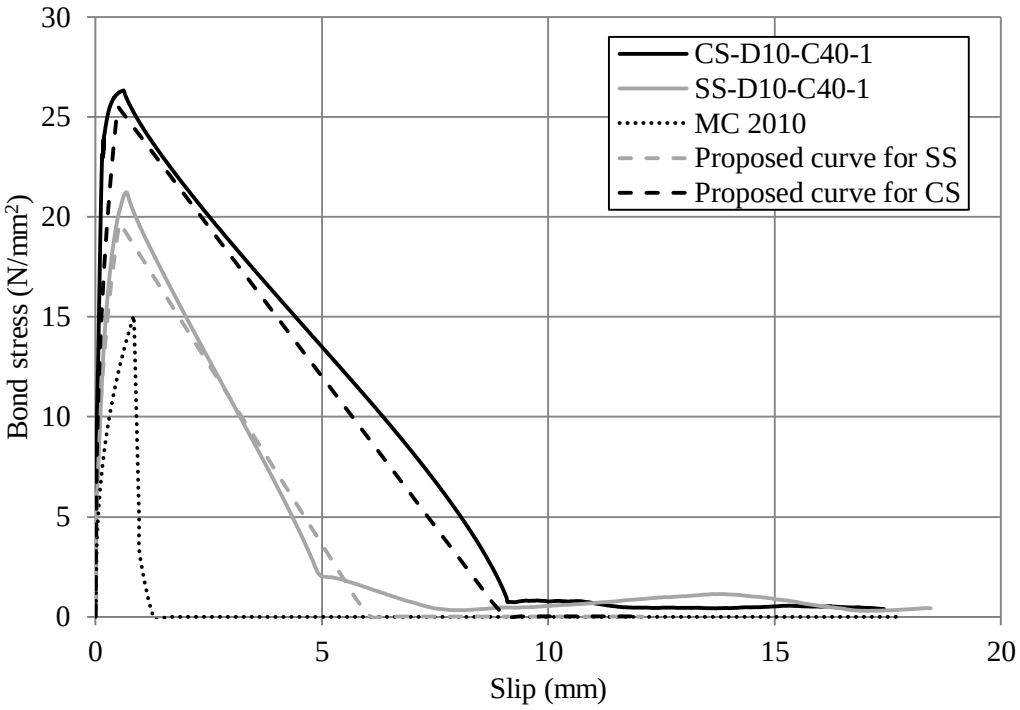

(a)

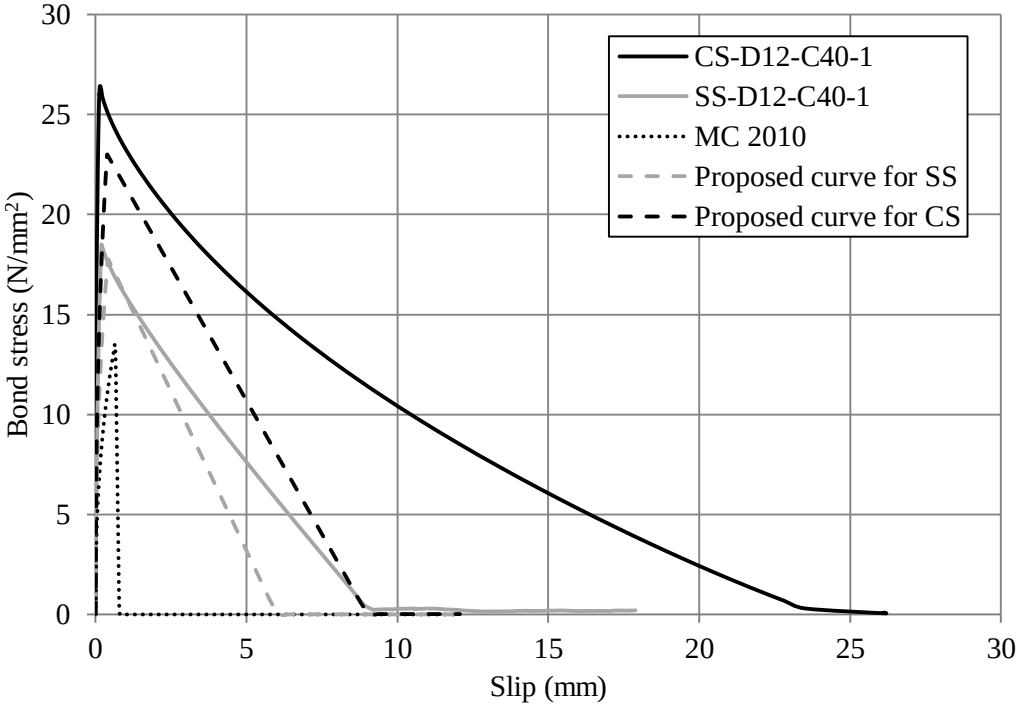

(b)

Fig. 6.11: Bond stress-slip curves for samples with reinforcement which is (a) 10 mm in diameter and (b) 12 mm in diameter.

Fig. 6.12 presents the bond-slip curves predicted using the MC2010 for pull-out failure, together with the corresponding values from the experimental programme, for both stainless and carbon steel reinforcement. Generally, it is clear that the MC2010 bond model does not reflect the actual bond-slip behaviour for either stainless steel or carbon steel reinforced concrete. For example, the MC2010 bond model results in a softer response in the ascending and descending branches and lower ultimate bond strength as well as an overestimation of the residual bond strength, compared with the experimental data. Moreover, the de-bonding part of the response is simulated in MC2010 as a linearly descending branch followed by constant level of the residual bond stress. It is very clear that this is quite different from the behaviour observed during the tests where the bond stress decreased gradually in an exponential manner.

The shape of the proposed bond model for the pull-out failure mode is presented in Fig. 6.13, together with the current model provided in MC2010. Since the post-peak region of the response has already been shown to be inaccurately represented by the MC2010, an exponential curve is implemented in order to reflect the experimental behaviour. The bond stress for the proposed model is calculated as a function of the relative displacement as given in Eqs. (6.24)-(6.26) and shown in Fig. 6.13. By comparing the proposed models with experimental responses, as presented in Fig. 6.12, it can be seen that the proposed models are in excellent agreement with experimental responses especially in the post-peak range, for both stainless steel and carbon steel reinforced concrete. It is believed that implementing these changes in the codes of practice will ensure providing more accurate and efficient design rules, which is extremely important for all structures, but particular those containing stainless steel reinforcement owing to its high initial cost.

$$\tau_b = \tau_{bmax}\,(s/s_1)^{\alpha} \qquad \text{for } 0 \le s \le s_1 \tag{6.24}$$

$$\tau_b = \tau_{bmax} \qquad \text{for } s_1 \le s \le s_2 \tag{6.25}$$

$$\tau_b = \tau_{bmax}\,(s_2/s)^{\alpha_1} \qquad \text{for } s_2 \le s \tag{6.26}$$

where these parameters are defined in Table 6.10.

Table 6.10: Parameters details for the proposed pull-out bond-slip model.

	Pull-out failure		
	Current model in MC2010	Proposed model for stainless steel	Proposed model for carbon steel
τ_{bmax}	$2.5(f_{cm})^{0.5}$	$2.4(f_{cm})^{0.5}$	$4(f_{cm})^{0.5}$
s_1	1.0 mm	0.5	0.2
s_2	2.0 mm	2	1
s_3	c_{clear}	-	-
α	0.4	0.4	0.4
α_1	-	0.9	0.6
τ_{bf}	$0.4\tau_{bmax}$	-	-

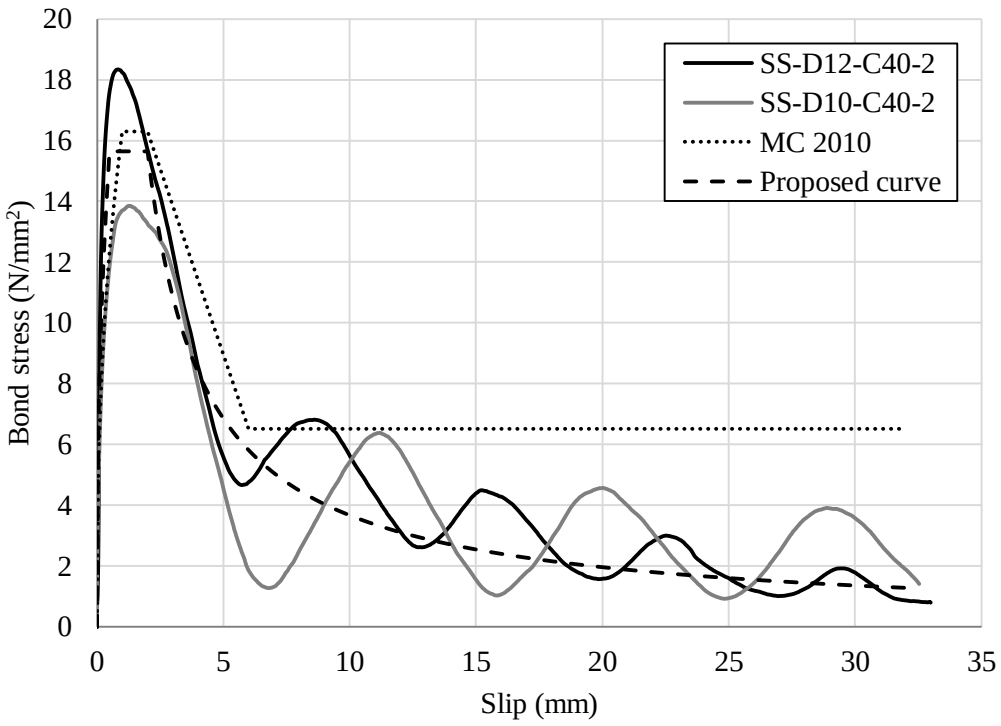

(a)

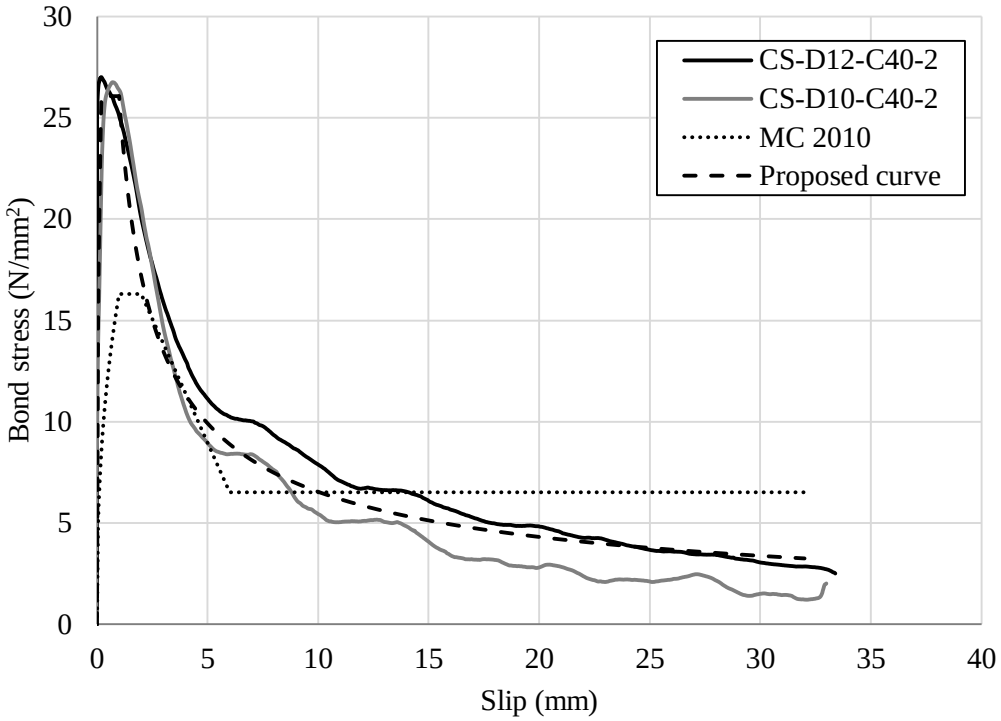

(b)

Fig. 6.12: Bond stress-slip curves for samples with (a) stainless steel and (b) carbon steel.

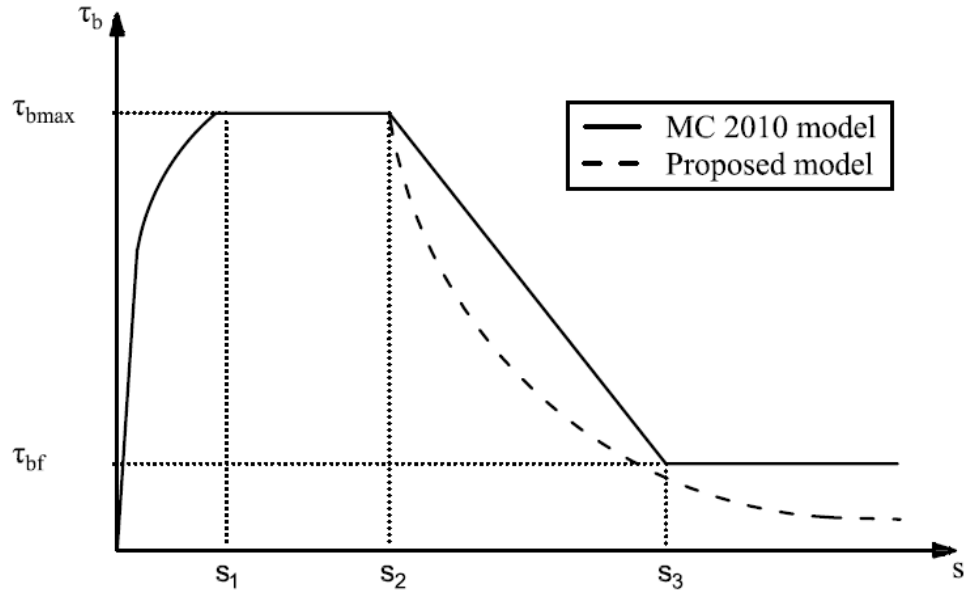

Fig. 6.13: Bond stress-slip models for pull-out failure mode.

6.6 A summary of the recommendations for the codes of practice

Following a detailed experimental and analytical analysis on the bond behaviour of stainless steel and carbon steel reinforcements, recommendations for the code of practice have been summarized as follows:

- For the range of data examined here, it is observed that the stainless steel rebars exhibit lower ultimate bond strength compared with that of carbon steels by around 28% on average.
- In general, the samples with stainless steel exhibit a more rapid reduction of bond strength also in the softening range compared to those with carbon steel, as well as lower residual bond values in the case of pull-out failure.
- It is shown that the samples with relatively higher concrete strength exhibit greater bond strength. However, the influence of concrete strength becomes less significant after a certain strength level.
- The design bond values given in both Eurocode 2 and MC2010 are shown to be very conservative compared with the experimental results, even for the stainless steel reinforced concrete.
- It is concluded that the current design rules can be safely applied for stainless steel reinforced concrete structures, for the parameter range considered herein. However, the design codes provide inaccurate and inefficient predictions, mainly owing to the fact that they are not based wholly on fundamental principles with all key parameters considered.
- It is generally shown that the bond-slip response obtained using MC2010 underestimates the experimental response, in all cases, by quite some margin, which does not reflect the actual behaviour for both stainless steel and carbon steel, for the test parameters studied herein.
- The post-peak region of the response has already been shown to be inaccurately represented by the MC2010, therefore it is suggested to implement an exponential curve in order to reflect the experimental behaviour.
- Consequently, new bond-slip models are proposed for both stainless steel and carbon steel reinforced concrete, as discussed in Section 6.5.2.

6.7 Concluding remarks

This chapter has presented a detailed analysis of the bond behaviour between stainless steel reinforcement and the surrounding concrete, including both experimental and design analysis. It is shown that stainless steel rebar generally develops lower bond strength with the surrounding concrete compared with equivalent carbon steel reinforcement. Moreover, it is shown that existing design codes are extremely conservative and generally underestimate the actual bond strength by a significant margin. Therefore, following detailed analysis, it is concluded that current design rules can be safely applied for stainless steel rebar, although more accurate and efficient methods can be

achieved. Hence, new design parameters are proposed reflecting the bond behaviour of stainless steel rebar, so that more efficient designs can be achieved.

Chapter 7: Conclusions and suggestions for future research

7.1 Introduction

There are currently huge demands to improve the durability and the resilience of reinforced concrete structures, mainly because of corrosion of the reinforcement and as a result of deterioration and carbonation of concrete. In aggressive environments, corrosion is difficult to avoid especially for those structures reinforced with traditional carbon steels. In this context, the use of stainless steel reinforcement is an ideal solution to treat the corrosion problem owing to its exceptional corrosion resistance. This chapter presents a summary of the main research findings and primary conclusions drawn from this thesis. Additionally, this chapter provides recommendations for further research building on the current work.

7.2 Conclusions

This thesis has presented a detailed study into the behaviour of stainless steel reinforcement in reinforced concrete. The current design approach for stainless steel reinforced concrete members has been evaluated. Accordingly, a new deformation-based design method that harnesses the advantages of material strain hardening in the design has been developed to predict the bending moment capacity for stainless steel reinforced concrete beams. The design method is developed in two forms, first as a full model in which the whole material response is considered and then as a simplified model incorporating a more simplistic elastic-linear hardening stainless steel constitutive response. Finally, the proposed method is validated by utilising the numerical model.

A comprehensive parametric study has been carried out to investigate the effect of the most influential parameters on the performance of stainless steel concrete beams including various concrete strengths and reinforcement grades and different geometries. Moreover, the serviceability limit state of stainless steel reinforced concrete beams has been assessed through analysing the deflection behaviour compared to the predicted response from Eurocode 2.

The bond behaviour of stainless steel reinforced concrete has been explored in comparison with the traditional reinforced concrete, through experimental testing and analysis. The results are also compared with existing design rules in terms of bond strength, anchorage length and lap length. Finally, suitable bond-slip models for stainless steel and also carbon steel reinforcements are proposed.

Overall, the results and analysis presented in this thesis have provided an excellent basis for engineers to specify stainless steel reinforcement in reinforced concrete beams in an efficient and sustainable manner, with minimal wastage of materials. The main conclusions from the work presented in this thesis are as follows:

- Stainless steel is a very ductile material that has distinctive characteristics such as corrosion and fire resistance, durability and excellent sustainability credentials. A strong case was presented for why stainless steel can provide a legitimate solution for some of the most common and expensive challenges associated with concrete infrastructure, i.e. premature failure or loss of the structural capacity through degradation of the steel reinforcement.

- There are two main barriers to more widespread use of stainless steel rebar in construction. Firstly, there is a perception amongst engineers that it is prohibitively expensive. Although stainless steel is undoubtedly more expensive than carbon steel in terms of initial costs, over the life time of a structure if maintenance and rehabilitation works can be avoided through the use of more durable materials, then stainless steel provides a very competitive and efficient design option. This is certainly an area that warrants a more detailed analysis, once efficient design rules have been established. Secondly, there is a huge dearth of useful design data and guidance to assist engineers in the specification of stainless steel reinforced concrete, which is the focus of the current thesis.

- Current design codes such as Eurocode 2 do not include specific guidance for stainless steel and therefore ignore the significant strain hardening characteristics and high levels of ductility that it offers. This design approach provides inaccurate strength capacity predictions. It is concluded that ignoring strain hardening of stainless steel results in overly-conservative and inaccurate capacity predictions and underestimates the load-bearing capacity of stainless steel concrete beams.

- The current study implements the Continuous Strength Method for the design of reinforced concrete beams including full and simplified approaches which incorporate the distinctive mechanical characteristics of stainless steel. It is shown that the full and simplified analytical solutions provide a reliable means for predicting the capacity of beam. These approaches can be used by engineers wishing to include stainless steel reinforced concrete in their designs, without the inefficiencies of existing methods.

- A comprehensive parametric study has been conducted to study the influence that various geometric and material properties have on the capacity of stainless steel reinforced concrete members and on the exploitation of strain hardening in the rebar. It is shown that further exploitation of the strain hardening capacity in the rebar is achieved when a relatively higher grade of concrete is employed. It is also found that the geometry of the beam has a relatively small influence on the exploitation of strain hardening. Moreover, it is observed that the

levels of stress in the rebar are relatively lower when a higher reinforcement ratio is employed.

- In the design of structural stainless steel sections, it is recommended to use the secant modulus in deflection calculations rather than the elastic modulus. In order to investigate this for reinforced concrete design, the predicted deflections calculated using secant modulus and also the tangent modulus of the stainless steel reinforcement are compared with their corresponding numerical values. The results presented in Chapter 5 show that there is only a minor improvement in the deflection predictions by adopting the secant modulus rather than the elastic modulus in the calculations. The predictions obtained using the tangent modulus were significantly less accurate than when the elastic modulus or the secant modulus is employed. Therefore, it is recommended that the elastic modulus is employed in the calculation of deflections for stainless steel RC beams.

- From the data and analysis presented in Chapter 6, it is clear that stainless steel reinforcement exhibits lower bond strength compared with carbon steel reinforcement. The current bond design rules in global design standards such as Eurocode 2 and MC2010 do not reflect this fact, but are shown to be very conservative nonetheless. The code predictions are compared with the experimental findings, in terms of bond strength, anchorage length and lap length and it is shown that the standards are overly conservative for both stainless and carbon steel reinforcements. Although the current design rules in Eurocode 2 and MC2010 can be safely applied for stainless steel reinforced concrete, they provide neither an accurate nor efficient solution. Moreover, the bond stress-slip model presented in the MC2010 has been examined in terms of pull-out and splitting failure modes and has been found to not reflect the experimental response. Therefore, new design parameters have been proposed which more accurately depict the true behaviour.

7.3 Recommendations for further research

This thesis has filled significant knowledge gaps in the design of stainless steel reinforced concrete and enables stainless steel rebars to be specified in design with more confidence. However, there are still other aspects which should be explored to thoroughly understand the behaviour of stainless steel reinforced concrete owing to this being relatively new and novel topic. Therefore, the following suggestions are proposed for future research:

- Stainless steel reinforcement is exploited widely in the construction industry and can be found in a wide range of applications owing to its favourable characteristics in terms of corrosion resistance, long life cycle, formability, durability and recyclability. These distinctive

properties depend on the constituent elements of the stainless steel alloy. However, there is currently a lack of useful guidance in global design standards to assist engineers in the selection of the appropriate stainless steel grade. Therefore, it is recommended to establish a new classification system considering the key parameters including the metallurgical composition, exposure conditions, type of the application and design lifetime.

- It is now clear that the different grades may demonstrate different behaviour owing to the variations in the chemical composition. Therefore, it is recommend to study the metallurgical behaviour of various grades of stainless steel reinforcement.

- There is a huge dearth of the experimental data in the literature into the structural behaviour of stainless steel reinforced concrete members, and therefore it is highly encouraged to conduct experimental tests on this topic to build robust understanding of the behaviour and to provide a sufficient data which can be used for numerical validation purposes.

- A new deformation-based design method has been proposed in this thesis including full and simplified approach in order to exploit the significant strain hardening and ductility of stainless steel reinforcement in the flexural design of reinforced concrete beams. This approach has been successfully implemented and shown to improve the load bearing capacity of the section. Hence, it is suggested to extend this approach for different applications including columns, slabs and retaining walls. Moreover, a detailed analysis of the behaviour of building frames and systems, rather than individual elements, is required.

- Although, this thesis has demonstrated a comprehensive analysis to study the behaviour of stainless steel reinforced concrete and the most influential parameters, the behaviour was only assessed under normal conditions and therefore it is recommended to study the behaviour under excessive load conditions including fire and earthquake conditions.

References

Aal Hassan, A. (2003) 'Bond of reinforcement in concrete with different types of corroded bars', Master Thesis, Reyerson University, Toronto, pp. 106.

Aalco. (2013) 'Specifications for Stainless Steel Products'. Available at: http://www.aalco.co.uk/literature/files/aalco-stainless-steel.pdf (Accessed: 26/3/2017).

Abdella, K. (2006) 'Inversion of a full-range stress–strain relation for stainless steel alloys', International Journal of Non-Linear Mechanics, 41(3), pp. 456-463.

Afshan, S. and Gardner, L. (2013) 'The continuous strength method for structural stainless steel design', Thin-Walled Structures, 68, pp. 42-49.

Ahlborn, T. and DenHartigh, T. (2003) 'Comparative bond study of stainless and high-chromium reinforcing bars in concrete', Transportation Research Record: Journal of the Transportation Research Board, (1845), pp. 88-95.

Alfano, G., De Cicco, Ph. D, Fiorenzo & Prota, A. (2011) 'Intermediate debonding failure of RC beams retrofitted in flexure with FRP: Experimental results versus prediction of codes of practice', Journal of Composites for Construction, 16(2), pp. 185-195.

Alih, S. and Khelil, A. (2012) 'Behavior of inoxydable steel and their performance as reinforcement bars in concrete beam: Experimental and nonlinear finite element analysis', Construction and Building Materials, 37, pp. 481-492.

Alvarez, S.M., Bautista, A. and Velasco, F. (2011) 'Corrosion behaviour of corrugated lean duplex stainless steels in simulated concrete pore solutions', Corrosion Science, 53(5), pp. 1748-1755.

Ashraf, M., Gardner, L. and Nethercot, D.A. (2008) 'Structural stainless steel design: resistance based on deformation capacity', Journal of Structural Engineering, 134(3), pp. 402-411.

BA 84/02 (2003) 'Design manual for roads and bridges part 15: use of stainless steel reinforcement in highway structures'. Highways Agency UK.

Baddoo, N.R. (2008) 'Stainless steel in construction: A review of research, applications, challenges and opportunities', Journal of Constructional Steel Research, 64(11), pp. 1199-1206.

Baddoo, R. and Burgan, A. (2012) 'Structural Design of Stainless Steel', SCI Publication No. P291. The Steel Construction Institute.

Balazs, G., Cairns, J., Eligehausen, R., Lettow, S., Metelli, G., Pantazopoulou, S. and Plizzari, G. (2014) 'Bond and anchorage of embedded reinforcement: background to the fib model code for concrete structures 2010', Bulletin 72, pp. 7.

Bautista, A., Blanco, G., Velasco, F., Gutiérrez, A., Palacín, S., Soriano, L. & Takenouti, H. (2007) 'Passivation of duplex stainless steel in solutions simulating chloride-contaminated concrete', Materiales de Construcción, 57(288), pp. 17-32.

Bautista, A., Blanco, G., Velasco, F., Gutiérrez, A., Palacín, S., Soriano, L. and Takenouti, H. (2007) 'Passivation of duplex stainless steel in solutions simulating chloride-contaminated concrete', Materiales de Construcción, 57(288), pp. 17-32.

Bertolini, L., Gastaldi, M., Pedeferri, P. and Redaelli, E. (2002) 'Factors influencing the corrosion resistance of austenitic and duplex stainless steel bars in chloride bearing concrete', 15th International Corrosion Congress-ICC, pp. 1-9.

British Highways Authority (2003) 'Advice note: Design manual for roads and bridges BA84/02:" The use of stainless steel reinforcement in highway structures'. Available at: https://www.bssa.org.uk/cms/File/REBar%20report.pdf (Accessed: 5 March 2019).

British Stainless Steel Association. (2000) 'Classification of stainless steel types'. Available at: https://www.bssa.org.uk/cms/File/SSAS1.2-Classification%20of%20Stainless%20Steels.pdf (Accessed: 25/3/2017).

British Stainless Steel Association. (2003) 'The use of stainless steel reinforcement on bridges'. Available at: http://www.bssa.org.uk/cms/File/REBar%20report.pdf (Accessed: 11 April 2017).

British Stainless Steel Association. (2016) 'Recycling of stainless steel'. Available at: http://www.bssa.org.uk/topics.php?article=92 (Accessed: 9/4/2017).

Briz, E., Biezma, M. and Bastidas, D. (2018) 'Stress corrosion cracking of new 2001 lean–duplex stainless steel reinforcements in chloride contained concrete pore solution: An electrochemical study', Construction and Building Materials, 192, pp. 1-8.

BS 4449+A3 (2005) 'Steel for the reinforcement of concrete. Weldable reinforcing steel. Bar, coil and decoiled product. Specifications', British Standards Institution.

BS 6744 (2016) 'Stainless steel bars for the reinforcement of concrete. Requirements and test methods', British Standards Institution.

Bypour, M., Gholhaki, M., Kioumarsi, M. and Kioumarsi, B. (2019) 'Nonlinear analysis to investigate effect of connection type on behavior of steel plate shear wall in RC frame', Engineering Structures, 179, pp. 611-624.

Calderon-Uriszar-Aldaca, I., Briz, E., Larrinaga, P. and Garcia, H. (2018) 'Bonding strength of stainless steel rebars in concretes exposed to marine environments', Construction and Building Materials, 172, pp. 125-133.

Carvalho, E.P., Miranda, M.P., Fernandes, D.S. and Alves, G.V. (2018) 'Comparison of test methodologies to evaluate steel-concrete bond strength of thin reinforcing bar', Construction and Building Materials, 183, pp. 243-252.

Castro, H., Rodriguez, C., Belzunce, F. and Canteli, A. (2003) 'Mechanical properties and corrosion behaviour of stainless steel reinforcing bars', Journal of Materials Processing Technology, 143, pp. 134-137.

Chen, W., Hao, H. and Chen, S. (2015) 'Numerical analysis of prestressed reinforced concrete beam subjected to blast loading', Materials & Design (1980-2015), 65, pp. 662-674.

Cotsovos, D.M. (2013) 'Cracking of RC beam/column joints: Implications for the analysis of frame-type structures', Engineering Structures, 52, pp. 131-139.

Cramer, S., Covino, B., Bullard, S., Holcomb, G., Russell, J., Nelson, F., Laylor, H. and Soltesz, S. (2002) 'Corrosion prevention and remediation strategies for reinforced concrete coastal bridges', Cement and Concrete Composites, 24(1), pp. 101-117.

Darwin, D. and Graham, E.K. (1993) Effect of deformation height and spacing on bond strength of reinforcing bars, ACI Structural Journal, 90 (6), pp. 646-657.

Dassault Systèmes. (2016) Abaqus user's Guide Manual [Computer program]. http://dixon:2080/texis/search/?query=concrete+materialandgroup=bkandCDB=v2016and submit.x=0andsubmit.y=0.

Dede, T. and Ayvaz, Y. (2009) 'Nonlinear analysis of reinforced concrete beam with/without tension stiffening effect', Materials & Design, 30(9), pp. 3846-3851.

Dong, J., Wang, Q. and Guan, Z. (2013) 'Structural behaviour of RC beams with external flexural and flexural–shear strengthening by FRP sheets', Composites Part B: Engineering, 44(1), pp. 604-612.

Earij, A., Alfano, G., Cashell, K. and Zhou, X. (2017) 'Nonlinear three–dimensional finite–element modelling of reinforced–concrete beams: Computational challenges and experimental validation', Engineering Failure Analysis, 82, pp. 92-115..

Edvardsen, C. (2008) 'Tailor-made concrete structures–Case studies from projects worldwide'. Available at: http://www.abece.com.br/web/restrito/restrito/pdf/ch011.pdf (Accessed: 5 March 2017).

Eladly, M.M. (2020) 'Behaviour of stainless steel beam-to-column bolted connections–Part 1: Simplified FE model', Journal of Constructional Steel Research, 164, pp. 105784.

Eligehausen, R., Popov, E.P. and Bertero, V.V. (1982) 'local bond stress-slip relationships of deformed bars under generalized excitations', (4) pp. 69-80

EN 10080 (2005) 'Steel for the reinforcement of concrete– Weldable reinforcing steel–General', European Committee for Standardization (CEN).

EN 10088-1 (2014) 'Stainless steels– Part 1: List of stainless steels', European Committee for Standardization (CEN).

EN 10088-2 (2014) 'Stainless steels– Part 2: Technical delivery conditions for sheet/plate and strip of corrosion resisting steels for general purposes', European Committee for Standardization (CEN).

EN 12390-3 (2009) 'Testing hardened concrete Part 3: Compressive strength of test specimens', European Committee for Standardization (CEN).

EN 15630-1 (2010) 'Steel for the reinforcement and prestressing of concrete. Test methods Part 1: Reinforcing bars, wire rod and wire', European Committee for Standardization (CEN).

EN 1992-1-1. (2004) 'Eurocode 2: Design of concrete structures part 1-1: General rules and rules for buildings', European Committee for Standardization (CEN).

EN 6892-1 (2016) 'Metallic materials- Tensile testing part 1: Method of test at room temperature', European Committee for Standardization (CEN).

Evans, K. (2002) 'RB Rebak in Corrosion Science–A Retrospective and Current Status in Honor of Robert P', Frankenthal, PV, 13, pp. 344-354.

Fan, S., Ding, X., Sun, W., Zhang, L. and Liu, M. (2016) 'Experimental investigation on fire resistance of stainless steel columns with square hollow section', Thin-Walled Structures, 98, pp. 196-211.

Fan, S., Tan, K.H. and Nguyen, M.P. (2018) 'Numerical Model to Determine Shear Capacity of Reinforced Concrete Deep Beams Exposed to Fire', in High Tech Concrete: Where Technology and Engineering Meet. Springer, pp. 1410-1419.

Fan, S., Tan, K.H. and Nguyen, M.P. (2018) 'Numerical Model to Determine Shear Capacity of Reinforced Concrete Deep Beams Exposed to Fire', in High Tech Concrete: Where Technology and Engineering Meet. Springer, pp. 1410-1419.

Farzad, M., Shafieifar, M. and Azizinamini, A. (2019) 'Experimental and numerical study on bond strength between conventional concrete and Ultra High-Performance Concrete (UHPC)', Engineering Structures, 186, pp. 297-305.

Fédération Internationale du Béton (2013) Fib Model Code for Concrete Structures 2010. Berlin: Wilhelm Ernst & Sohn Verlag fur Architektur und Technische.

Gambarova, P, Balazs, G, Vliet, AB, Cairns, J, Eligehausen, R, Engstrom, B, Giuriani, E, Leon, R, Mayer, U, McCabe, S, Noghabai, K, Plizzari, G, Rosati, GP, Russo, G, Shima, H, Ueda, T and Vandewalle, L (2000) 'Bond mechanics including pull-out and splitting failures', Bulletin - Fédération internationale du béton, pp. 1-97.

García-Alonso, M., Escudero, M., Miranda, J., Vega, M.I., Capilla, F., Correia, M., Salta, M., Bennani, A. and González, J. (2007) 'Corrosion behaviour of new stainless steels reinforcing bars embedded in concrete', Cement and Concrete Research, 37(10), pp. 1463-1471.

Gardner L., Nethercot D.A. (2004) 'Structural stainless steel design: a new approach'. Journal of Structural Engineering, 82(21),pp. 21-30.

Gardner, L. (2005) 'The use of stainless steel in structures', Progress in Structural Engineering and Materials, 7(2), pp. 45-55.

Gardner, L. (2008) 'The continuous strength method', Proceedings of the Institution of Civil Engineers - Structures and Buildings, 161(3), pp. 127-133.

Gardner, L. and Theofanous, M. (2008) 'Discrete and continuous treatment of local buckling in stainless steel elements', Journal of Constructional Steel Research, 64(11), pp. 1207-1216.

Gardner, L., Bu, Y., Francis, P., Baddoo, N.R., Cashell, K.A. and McCann, F. (2016) 'Elevated temperature material properties of stainless steel reinforcing bar', Construction and Building Materials, 114, pp. 977-997.

Gardner, L., Wang, F. and Liew, A. (2011) 'Influence of strain hardening on the behavior and design of steel structures', International Journal of Structural Stability and Dynamics, 11(05), pp. 855-875.

Gardner, L., Yun, X., Macorini, L. and Kucukler, M. (2017) 'Hot-rolled steel and steel-concrete composite design incorporating strain hardening', Structures, 9, pp. 21-28.

Gedge, G. (2003) 'Rationale for using stainless steel reinforcement in the UK construction industry', Arup Materials Consulting, UK.

George, J., Rama, J.K., Kumar, M.S. and Vasan, A. (2017) 'Behavior of Plain Concrete Beam subjected to Three Point Bending using Concrete Damaged Plasticity (CDP) Model', Materials Today: Proceedings, 4(9), pp. 9742-9746

Harajli, M., Hout, M. and Jalkh, W. (1995) 'Local bond stress-slip behavior of reinforcing bars embedded in plain and fiber concrete', Materials Journal, 92(4), pp. 343-353.

Hassanein, M. and Silvestre, N. (2013) 'Flexural behavior of lean duplex stainless steel girders with slender unstiffened webs', Journal of Constructional Steel Research, 85, pp. 12-23.

Helland, S. (2013) 'Design for service life: implementation of fib Model Code 2010 rules in the operational code ISO 16204', Structural Concrete, 14(1), pp. 10-18.

Huang, Y. and Young, B. (2014) 'Design of cold-formed lean duplex stainless steel members in combined compression and bending', Journal of Structural Engineering, 141(5), pp. 04014138.

Huang, Y. and Young, B. (2014) 'Stress–strain relationship of cold-formed lean duplex stainless steel at elevated temperatures', Journal of Constructional Steel Research, 92, pp. 103-113.

Jamali, A., Angst, U., Adey, B. and Elsener, B. (2013) 'Modeling of corrosion-induced concrete cover cracking: A critical analysis', Construction and Building Materials, 42, pp. 225-237.

Johnson, J.B. (2010) 'Bond strength of corrosion resistant steel reinforcement in concrete', Master of Science in Civil Engineering, Faculty of the Virginia Polytechnic Institute and State University.

Kalina R. D., Mac Lean S., and Breen J. E. (2011) 'Comparative Study of Mechanical and Corrosion Resistance Properties of Bridge Post-Tensioning Strands', The Center for Transportation Research at The University of Texas. Austin.

Kmiecik, P. and Kamiński, M. (2011) 'Modelling of reinforced concrete structures and composite structures with concrete strength degradation taken into consideration', Archives of civil and mechanical engineering, 11(3), pp. 623-636.

Lan, X., Chen, J., Chan, T. and Young, B. (2018) 'The continuous strength method for the design of high strength steel tubular sections in compression', Engineering Structures, 162, pp. 177-187.

Lee, J. and Fenves, G.L. (1998) 'Plastic-damage model for cyclic loading of concrete structures', Journal of Engineering Mechanics, 124(8), pp. 892.

Liew, A. and Gardner, L. (2015) 'Ultimate capacity of structural steel cross-sections under compression, bending and combined loading', Structures, 1, pp. 2-11.

Lopes, N., Real, P.V., da Silva, L.S. and Franssen, J. (2012) 'Numerical analysis of stainless steel beam-columns in case of fire', Fire Safety Journal, 50, pp. 35-50.

Lubliner, J., Oliver, J., Oller, S. and Onate, E. (1989) 'A plastic-damage model for concrete', International Journal of Solids and Structures, 25(3), pp. 299-326.

Markeset, G., Rostam, S. and Klinghoffer, O. (2006) ‘Guide for the use of stainless steel reinforcement in concrete structures’, Norwegian Building Research Institute, Norway.

McGurn, J. (1998) 'Stainless steel reinforcing bars in concrete', Proceedings of the International Conference of Corrosion and Rehabilitation of Reinforced Concrete Structures, Orlando, FL, FHWA.

Medina, E., Medina, J.M., Cobo, A. and Bastidas, D.M. (2015) 'Evaluation of mechanical and structural behavior of austenitic and duplex stainless steel reinforcements', Construction and Building Materials, 78, pp. 1-7.

Metals4U. (2019) 'Stainless steel reinforcing bar'. Available at: https://www.metals4u.co.uk/stainless-steel/c8/reinforcing-bar/c1875 (Accessed: 19/11 2019).

Mirambell, E. and Real, E. (2000) 'On the calculation of deflections in structural stainless steel beams: an experimental and numerical investigation', Journal of Constructional Steel Research, 54(1), pp. 109-133.

Nationwide Stainless. (2019) 'Stainless Steel Rebar'. Available at: https://www.nationwidestainless.co.uk/products/stainless_steel_rebar/ (Accessed: 19/11/2019).

Nickel Institute (2018) 'Progreso pier built with nickel-containing stainless steel'. Available at: https://www.nickelinstitute.org/media/2541/progresopierrepackagefb.pdf (Accessed: 11/04 2019).

Nilson, A.H. (1968) 'Nonlinear analysis of reinforced concrete by the finite element method', Journal Proceedings. , pp. 757-766.

Nurnberger, U. (1996) Stainless Steel in Concrete: State of the Art Report. European Federation of Corrosion.

Obaidat, Y.T., Heyden, S., Dahlblom, O., Abu-Farsakh, G. and Abdel-Jawad, Y. (2011) 'Retrofitting of reinforced concrete beams using composite laminates', Construction and Building Materials, 25(2), pp. 591-597.

Oh, B.H. and Kim, S.H. (2007) 'Realistic models for local bond stress-slip of reinforced concrete under repeated loading', Journal of Structural Engineering, 133(2), pp. 216-224.

Otieno, M.B., Beushausen, H.D. and Alexander, M.G. (2011) 'Modelling corrosion propagation in reinforced concrete structures–A critical review', Cement and Concrete Composites, 33(2), pp. 240-245.

Pérez-Quiroz, J., Terán, J., Herrera, M., Martínez, M. and Genescá, J. (2008) 'Assessment of stainless steel reinforcement for concrete structures rehabilitation', Journal of Constructional Steel Research, 64(11), pp. 1317-1324.

Pietro, P., Luca, B., Fabio, B., Tommaso, P. (1998) 'Behavior of Stainless Steels in Concrete', Repair and Rehabilitation of Reinforced Concrete Structures: The State of the Art, pp. 192.

Rabi, M., Cashell, K. and Shamass, R. (2019) 'Flexural analysis and design of stainless steel reinforced concrete beams', Engineering Structures, 198, pp. 109432.

Ramberg, W. & Osgood, W.R. (1943) 'Description of stress-strain curves by three parameters'.

Rasmussen, K.J.R. (2003) 'Full-range stress–strain curves for stainless steel alloys', Journal of Constructional Steel Research, 59(1), pp. 47-61.

RILEM. (1994) Technical recommendations for the testing and use of construction materials. Taylor & Francis, London.

SCI. (2017) 'Design Manual for Structural Stainless Steel', fourth edition, SCI Publication No. P413. The Steel Construction Institute.

Serdar, M., Žulj, L.V. & Bjegović, D. (2013) 'Long-term corrosion behaviour of stainless reinforcing steel in mortar exposed to chloride environment', Corrosion Science, 69, pp. 149-157.

Serdar, M., Žulj, L.V. and Bjegović, D. (2013) 'Long-term corrosion behaviour of stainless reinforcing steel in mortar exposed to chloride environment', Corrosion Science, 69, pp. 149-157.

Shamass, R. and Cashell, K. (2017) 'Behaviour of Composite Beams Made Using High Strength Steel', Structures, 12, pp. 88-101.

Shamass, R. and Cashell, K.A., (2018) 'Analysis of Stainless Steel-Concrete Composite Beams', Journal of Constructional Steel Research, 152, pp. 132-142.

Shamass, R., Zhou, X. and Alfano, G. (2014) 'Finite-element analysis of shear-off failure of keyed dry joints in precast concrete segmental bridges', Journal of Bridge Engineering, 20(6), pp. 04014084

Sharif, A.M., Al-Mekhlafi, G.M. and Al-Osta, M.A. (2019) 'Behavior of circular stainless steel stub columns internally strengthened by longitudinal carbon steel bars', Engineering Structures, 199, pp. 109617.

Sharif, A.M., Al-Mekhlafi, G.M. and Al-Osta, M.A. (2019) 'Behavior of circular stainless steel stub columns internally strengthened by longitudinal carbon steel bars', Engineering Structures, 199, pp. 109617.

Smale, K. (2018) 'From the scene | Collapsed Italy bridge laid bare'. Available at: https://www.newcivilengineer.com/latest/from-the-scene-collapsed-italy-bridge-laid-bare-17-08-2018/ (Accessed: 18 September 2019).

Solhmirzaei, R. and Kodur, V. (2017) 'Modeling the response of ultra high performance fiber reinforced concrete beams', Procedia Engineering, 210, pp. 211-219.

Somayaji, S. and Shah, S.P. (1981) 'bond stress versus slip relationship and cracking response of tension members.', Journal of the American Concrete Institute, 78(3), pp. 217-225.

Stainless UK (2016) 'Stainless steel reinforcing bar'. Available at: https://www.stainless-uk.co.uk/products/rebar/ (Accessed: 07/30 2019).

Su, M., Young, B. and Gardner, L. (2016) 'The continuous strength method for the design of aluminium alloy structural elements', Engineering Structures, 122, pp. 338-348.

Sunayana, S. and Barai, S.V. (2019) 'Performance of fly ash incorporated recycled aggregates concrete column under axial compression: Experimental and numerical study', Engineering Structures, 196, pp. 109258.

Technical Research Centre of Finland (2011) 'Design with stainless steel rebars applying Eurocode 2', Research Report Nº VTT-S-06464-11. VTT Expert Services Ltd.

Theofanous, M., Propsert, T., Knobloch, M. and Gardner, L. (2016) 'The continuous strength method for steel cross-section design at elevated temperatures', Thin-Walled Structures, 98, pp. 94-102.

Thousandswonder. (2015) Stonecutters Bridge. Available at: http://www.thousandwonders.net/Stonecutters+Bridge (Accessed: 10 April 2017).

Tondini, N., Rossi, B. and Franssen, J. (2013) 'Experimental investigation on ferritic stainless steel columns in fire', Fire Safety Journal, 62, pp. 238-248.

Truman, J. (1985) 'The Initiation and Growth of High Alloy (Stainless) Steel Production in Alloys 1900-1950.', Historical Metallurgy.Journal of the Historical Metallurgy Society Oxford, 19(1), pp. 116-125.

Wang, T. and Hsu, T.T. (2001) 'Nonlinear finite element analysis of concrete structures using new constitutive models', Computers and Structures, 79(32), pp. 2781-2791.

Wang, Y., Yang, L., Gao, B., Shi, Y. and Yuan, H. (2014) 'Experimental study of lateral-torsional buckling behavior of stainless steel welded I-section beams', International Journal of Steel Structures, 14(2), pp. 411-420.

Yang, L., Zhao, M., Xu, D., Shang, F., Yuan, H., Wang, Y. and Zhang, Y. (2016) 'Flexural buckling behaviour of welded stainless steel box-section columns', Thin-Walled Structures, 104, pp. 185-197.00

Zhou, Y., Ou, Y. and Lee, G.C. (2017) 'Bond-slip responses of stainless reinforcing bars in grouted ducts', Engineering Structures, 141, pp. 651-665.

Appendix A

Examples of the analytical calculations are included herein.

Section details:

Austenitic stainless steel grade 1.4311.

$A_s = 226.2$ mm2.

Section dimensions are 300 mm in width and 428 mm in height.

Concrete cover is 25 mm.

Eurocode 2

Assuming that $\kappa_y \leq \kappa_{cu}$, which means that the reinforcements yield before concrete crushes.

The position of the neutral axis (y) is determined from the equilibrium of the internal forces as follows:

$0.68 f_c y\, b - A_s \sigma_s = 0$

y =10.64 mm.

Now check the assumption ($\kappa_y \leq \kappa_{cu}$).

$$\kappa_y = \frac{\varepsilon_y}{d - y} = \frac{0.0024}{403.6 - 10.64} = 6 * 10^{-6}$$

$$\kappa_{cu} = \frac{\varepsilon_{cu}}{y} = \frac{0.0035}{10.64} = 3.3 * 10^{-4}$$

κy ≤ κcu OK

The bending moment capacity is calculated as follows:

$M_{pl} = A_s \sigma_s (d - 0.4y)$

$M_{pl} = 43.3$ kNm

Full analytical model

In order to obtain the bending moment capacity of the section using the actual stress-strain behaviour of stainless steel, an iterative method is required to locate the position of the neutral axis (y).

Firstly, assume an initial value of the neutral axis (e.g. yi = 50 mm).

Calculate the curvature $\kappa = \min(\kappa_{su}, \kappa_{cu})$.

where

$\kappa_{su} = \frac{\varepsilon_u}{d-y}$ and $\kappa_{cu} = \frac{\varepsilon_{cu}}{y}$.

$\kappa = 0.00007$.

Calculate the strain in the rebar; $\varepsilon_s = \kappa(d - y) = 0.02475$.

Calculate the proof strain; $\varepsilon_{0.2} = \frac{\sigma_{0.2}}{E} + 0.002 = 0.00437$.

$\varepsilon_s \geq \varepsilon_{0.2}$, this means the rebar yields and therfore Eq. (4.16) is used to obtain the stress in the rebar (σ_s).

$\sigma_s = 617 \text{N/mm}^2$.

The position of the neutral axis (y) is determined from the equilibrium of the internal forces as follows:

$0.68 f_c y\, b - A_s \sigma_s = 0$.

y =13.68 mm.

Since the difference between the obtained value of the neutral axis and the initial one is greater than 0.1 error, the process must be repeated using the obtained value until the condition $|y - y_i| < 0.1$ is acheived.

The position of the neutral axis is 15.18 mm.

The bending moment capacity is calculated as follows:

$M_{pl} = A_s \sigma_s (d - 0.4y)$.

$M_{pl} = 61.4$ kNm.

<u>Simplified model</u>

Assuming that the section always fails due to concrete crushing (i.e. κsu > κcu) and the tensile strain of the reinforcement is higher than the yield strain (i.e. $\varepsilon_s > \varepsilon_y$), the position of the neutral axis is calculated as follows:

$0.68 f_c b\, y^2 + \left(E_{sh}\varepsilon_{cu} + E_{sh}\varepsilon_y - \sigma_{0.2}\right) A_s\, y - A_s E_{sh} \varepsilon_{cu} d = 0$.

where $E_{sh} = \frac{\sigma_u - \sigma_{0.2}}{C_2 \varepsilon_u - \varepsilon_y}$ and C2 is 0.25 for grade 1.4311.

The position of the neutral axis (y) is 16.12 mm.

The bending moment capacity is calculated as follows:

$M_{pl} = A_s \sigma_s (d - 0.4y)$

$M_{pl} = 65.1$ kNm

Check $\kappa_{su} > \kappa_{cu}$; 0.000996 > 0.000217 OK

$\varepsilon_s > \varepsilon_y$; 0.0842 > 0.0024 OK

Appendix B

In this section, an example of the numerical data obtained from Abaqus software for beam U2 have been reported in Table B1. Details of the reinforcement and geometry for beam U2 can be found in Fig. 3.5 (d).

Table B. 1: Numerical data for beam U2.

Time step	Displacement (mm)	Load (kN)
0	0	0
0.01	0.254156	7.224386
0.0125	0.317989	9.12364
0.013438	0.341851	9.81751
0.014844	0.37761	10.83993
0.015371	0.391057	11.2172
0.015404	0.391898	11.24076
0.015437	0.392739	11.26428
0.015449	0.393054	11.2731
0.015468	0.393527	11.28632
0.015496	0.394237	11.30613
0.015537	0.395302	11.3358
0.015553	0.395701	11.34692
0.015577	0.396301	11.36359
0.015612	0.397201	11.38856
0.015665	0.398553	11.42595
0.015678	0.398891	11.4353
0.015691	0.399229	11.44464
0.015711	0.399735	11.45865
0.01574	0.400495	11.47967
0.015785	0.401663	11.51128
0.015852	0.403503	11.5601
0.015952	0.406315	11.63851
0.016102	0.410449	11.73126
0.016328	0.416433	11.75553
0.016412	0.418648	11.74913
0.016444	0.419475	11.74468
0.016492	0.420707	11.73436
0.016563	0.422536	11.7166
0.01667	0.425252	11.7081
0.01671	0.426266	11.70867
0.01677	0.427784	11.72133
0.016793	0.428353	11.7279
0.016827	0.429205	11.74222
0.01684	0.429524	11.74824
0.016859	0.430003	11.75876
0.016887	0.430721	11.77798

0.016898	0.43099	11.78567
0.016914	0.431393	11.79829
0.016938	0.431996	11.81959
0.016974	0.432879	11.85639
0.017028	0.434153	11.91998
0.01711	0.436088	12.02112
0.017232	0.439132	12.13455
0.017415	0.443834	12.19934
0.017484	0.445626	12.21177
0.017587	0.448403	12.22679
0.017741	0.452636	12.289
0.017973	0.458918	12.41883
0.01832	0.468081	12.56998
0.018842	0.481635	12.7976
0.019624	0.502117	13.14099
0.020797	0.532987	13.56241
0.021237	0.544578	13.71233
0.021402	0.548915	13.76759
0.021649	0.555378	13.84756
0.021742	0.557796	13.87709
0.021881	0.561424	13.92065
0.02209	0.566897	13.98669
0.022403	0.574867	14.00644
0.022716	0.582951	14.05251
0.023029	0.591193	14.17991
0.023499	0.603619	14.37799
0.024203	0.622089	14.55886
0.02526	0.649874	14.81765
0.026846	0.691539	15.2059
0.029224	0.753839	15.76866
0.030115	0.777202	15.97924
0.031453	0.812335	16.29021
0.03346	0.864686	16.72568
0.034212	0.884431	16.90122
0.034494	0.891844	16.96813
0.0346	0.894624	16.99326
0.034759	0.898792	17.03057
0.034997	0.905024	17.0836
0.035086	0.907358	17.10292
0.03522	0.910849	17.1306
0.035232	0.911176	17.13318
0.035237	0.911299	17.13415
0.035244	0.911483	17.1356
0.035255	0.911759	17.13777
0.035271	0.912173	17.141
0.035287	0.912586	17.14422

0.035302	0.913	17.14742
0.035326	0.913614	17.15218
0.03535	0.914217	17.1569
0.035374	0.914802	17.16155
0.03541	0.91565	17.16746
0.035463	0.916951	17.16577
0.035544	0.919007	17.11816
0.035664	0.92214	16.98112
0.035845	0.92686	16.84428
0.036117	0.933929	16.90538
0.036524	0.944439	17.09272
0.037135	0.96016	17.28159
0.038051	0.983991	17.5415
0.039426	1.01987	17.85815
0.041487	1.073522	18.26904
0.044579	1.153724	18.88919
0.049218	1.274146	19.8397
0.050378	1.304194	20.07638
0.050396	1.304663	20.08007
0.050403	1.304839	20.08145
0.050413	1.305103	20.08353
0.050428	1.3055	20.08664
0.050434	1.305648	20.08781
0.050442	1.305871	20.08956
0.050455	1.306205	20.09219
0.050475	1.306706	20.09614
0.050504	1.307458	20.1018
0.050547	1.308584	20.10356
0.050612	1.310262	20.06137
0.05071	1.312721	19.91969
0.050857	1.316323	19.78261
0.051078	1.321764	19.9093
0.051408	1.330184	20.25172
0.051904	1.343085	20.48635
0.051951	1.344297	20.50566
0.05202	1.346118	20.52798
0.052047	1.346801	20.53537
0.052086	1.347827	20.54424
0.052101	1.348212	20.54725
0.052123	1.348789	20.55109
0.052131	1.349006	20.55244
0.052143	1.349331	20.55424
0.052162	1.349819	20.55647
0.052169	1.350001	20.55724
0.052179	1.350276	20.55825
0.052195	1.350688	20.55943

0.052219	1.351308	20.56052
0.052254	1.35225	20.56075
0.052307	1.353708	20.55856
0.052387	1.355951	20.55438
0.052506	1.359347	20.56147
0.052685	1.364397	20.58192
0.052752	1.366279	20.58879
0.052852	1.369074	20.58585
0.053003	1.373198	20.53485
0.05323	1.379194	20.43505
0.05357	1.387878	20.40485
0.054079	1.400786	20.55254
0.054843	1.420415	20.82297
0.05599	1.450022	21.08816
0.057709	1.494463	21.41825
0.058354	1.511124	21.54071
0.058596	1.517371	21.58726
0.058687	1.519713	21.60489
0.058823	1.523226	21.63174
0.058874	1.524544	21.64186
0.05895	1.52652	21.65713
0.058979	1.52726	21.66288
0.059022	1.528371	21.67152
0.059038	1.528788	21.67477
0.059062	1.529413	21.67965
0.059071	1.529647	21.68148
0.059085	1.529999	21.68423
0.059106	1.530526	21.68838
0.059136	1.531313	21.69463
0.059182	1.532475	21.7043
0.059251	1.534175	21.72054
0.059354	1.536719	21.7465
0.05951	1.540583	21.7678
0.059742	1.546471	21.77459
0.060091	1.555472	21.82033
0.060615	1.569118	21.92871
0.0614	1.589304	22.07559
0.062185	1.60949	22.21493
0.062382	1.61454	22.25136
0.062676	1.622122	22.31256
0.063118	1.633499	22.40683
0.06378	1.650557	22.53939
0.064774	1.676127	22.71694
0.066265	1.714511	22.99589
0.068501	1.772077	23.42668
0.071856	1.85846	24.08551

0.073113	1.890794	24.32031
0.075	1.939217	24.65523
0.075118	1.942243	24.67465
0.075236	1.945268	24.68361
0.075354	1.94829	24.68551
0.075531	1.952815	24.71228
0.075796	1.959606	24.80162
0.076194	1.969838	24.92146
0.076791	1.985212	25.02565
0.077687	2.008243	25.16949
0.07903	2.042809	25.41857
0.080037	2.06874	25.60793
0.080415	2.078463	25.68064
0.08045	2.079375	25.68747
0.080504	2.080742	25.69777
0.080583	2.082792	25.71331
0.080598	2.083177	25.71623
0.080621	2.083754	25.72061
0.080654	2.084619	25.7272
0.080667	2.084943	25.72967
0.080686	2.085429	25.73337
0.080714	2.086159	25.73893
0.080757	2.087252	25.74721
0.080821	2.088881	25.75968
0.080916	2.09128	25.77589
0.08106	2.094842	25.78145
0.081275	2.100244	25.7695
0.081598	2.108514	25.82159
0.082083	2.121065	25.96361
0.08281	2.139871	26.11877
0.0839	2.167977	26.31197
0.084309	2.178514	26.38545
0.084923	2.19432	26.49532
0.085153	2.200213	26.53368
0.085383	2.20608	26.56476
0.085613	2.211956	26.59373
0.085958	2.220817	26.65415
0.086475	2.23415	26.75991
0.087252	2.254114	26.90013
0.088416	2.284003	27.11122
0.089581	2.313879	27.32323
0.090745	2.343774	27.53405
0.092492	2.388615	27.84897
0.095112	2.455904	28.33487
0.099042	2.556771	29.05046
0.102972	2.657625	29.76602

0.106902	2.758358	30.47865
0.108376	2.796134	30.74547
0.108514	2.799675	30.76993
0.108566	2.801003	30.77888
0.108586	2.801501	30.7822
0.108615	2.802248	30.78704
0.108626	2.802528	30.78883
0.108642	2.802949	30.79145
0.108648	2.803106	30.79242
0.108657	2.803343	30.79385
0.108671	2.803697	30.79592
0.108692	2.804229	30.79879
0.108723	2.805027	30.80007
0.10877	2.806224	30.76167
0.10884	2.808019	30.59597
0.108945	2.810693	30.36278
0.109102	2.814621	30.36549
0.109339	2.820463	30.70709
0.109693	2.829402	31.00856
0.110048	2.838489	31.14685
0.110402	2.847633	31.21736
0.110934	2.861345	31.27215
0.111732	2.881853	31.33039
0.112928	2.912608	31.49082
0.114723	2.95865	31.8164
0.115396	2.975907	31.94042
0.116406	3.001794	32.12566
0.11792	3.040648	32.39631
0.118488	3.05522	32.49571
0.119339	3.077081	32.64082
0.119659	3.085286	32.69534
0.120138	3.097626	32.77389
0.120857	3.116131	32.88726
0.121935	3.143803	33.076
0.123552	3.185315	33.36297
0.125977	3.247616	33.78148
0.129616	3.341208	34.39877
0.133254	3.434639	35.02255
0.136893	3.528037	35.6447
0.14235	3.66813	36.56087
0.147808	3.808088	37.47883
0.153265	3.947834	38.38343
0.153777	3.960939	38.46946
0.154545	3.980601	38.59991
0.155696	4.010076	38.7866
0.155714	4.010537	38.78952

0.155732	4.010997	38.79246
0.155759	4.011688	38.79693
0.155799	4.012724	38.79452
0.15586	4.014278	38.72209
0.155951	4.016608	38.54975
0.156088	4.020072	38.44197
0.156292	4.025193	38.6069
0.1566	4.032891	38.88906
0.157061	4.04463	39.07262
0.157752	4.062393	39.19581
0.15879	4.088988	39.31092
0.160345	4.128807	39.52091
0.162679	4.188447	39.89482
0.16618	4.277933	40.47295
0.171431	4.412153	41.32139
0.176682	4.546408	42.16901
0.181933	4.680695	43.01554
0.18981	4.882203	44.28761
0.19981	5.138195	45.92273
0.20231	5.202193	46.33319
0.202935	5.218194	46.43549
0.203873	5.242195	46.5871
0.204224	5.251183	46.6089
0.204576	5.260148	46.64443
0.204927	5.269105	46.71213
0.205455	5.282546	46.80857
0.205982	5.296004	46.92358
0.206509	5.309486	47.03172
0.2073	5.329734	47.15902
0.208487	5.360113	47.32874
0.210267	5.405657	47.60585
0.212936	5.473901	48.04064
0.216941	5.57063	48.66387
0.222948	5.69779	49.4706
0.228954	5.803457	50.13497
0.234961	5.887615	50.65834
0.240968	5.950338	51.05178
0.246975	5.991594	51.31123
0.252981	6.011373	51.43553
0.258988	6.009678	51.3999
0.264995	5.986555	50.91431
0.271002	5.941994	49.97842
0.273254	5.919805	49.52701
0.276633	5.880724	48.69774
0.281701	5.809559	47.16217
0.289304	5.67553	43.99673

0.296906	5.531624	40.40545
0.304508	5.387756	36.74247
0.312111	5.243907	33.04638
0.319713	5.09994	29.34078
0.327315	4.955885	25.65054
0.334918	4.811725	21.98413
0.34252	4.667553	18.34886
0.34502	4.620163	17.16051
0.34877	4.549124	15.3909
0.354395	4.442575	12.76895
0.362832	4.282777	8.930913
0.364942	4.24433	8.008048
0.367051	4.208247	7.151063
0.370215	4.158569	5.994974
0.374961	4.093923	4.512539
0.382081	4.019293	2.867477
0.384581	3.999377	2.423683
0.388331	3.975893	1.939932
0.393956	3.954528	1.49328
0.402393	3.95385	1.478869
0.404893	3.90079	0.20148
0.408643	3.97757	2.126975
0.414268	4.01655	3.195178
0.422706	4.106338	5.650017
0.432706	4.261438	9.879378
0.435206	4.308376	11.13868
0.438956	4.384608	13.25317
0.444581	4.500947	16.473
0.453018	4.67539	21.30402
0.463018	4.882139	27.01499
0.473018	5.088894	32.64784
0.475518	5.140573	34.0334
0.479268	5.218088	36.09566
0.484893	5.334327	39.13229
0.493331	5.508726	43.46296
0.498331	5.612243	45.71353
0.505831	5.769449	48.18479
0.511456	5.888176	49.38625
0.517081	6.006204	50.39302
0.522705	6.123803	51.31886
0.528331	6.241259	52.20314
0.533956	6.358702	53.06746
0.536065	6.402734	53.38816
0.539229	6.468744	53.86318
0.543975	6.567638	54.56443
0.548721	6.666416	55.25754

0.553467	6.765271	55.9383
0.558213	6.864155	56.60157
0.558232	6.864541	56.60415
0.55825	6.864927	56.6067
0.558278	6.865507	56.61055
0.558289	6.865724	56.61201
0.558304	6.86605	56.61426
0.558328	6.866539	56.61777
0.558363	6.867271	56.6187
0.558398	6.868005	56.60204
0.558433	6.868738	56.56832
0.558486	6.869838	56.50988
0.558565	6.871488	56.45425
0.558684	6.873959	56.465
0.558862	6.877644	56.59455
0.55913	6.88315	56.71608
0.55953	6.891458	56.82022
0.560132	6.904009	56.90922
0.561034	6.922848	57.01034
0.562387	6.951079	57.16916
0.564416	6.993412	57.44023
0.567461	7.056931	57.84949
0.572027	7.152794	58.40097
0.576594	7.252395	58.65641
0.58116	7.352482	58.85068
0.585727	7.452927	59.02802
0.590294	7.554026	59.16339
0.597143	7.706355	59.33821
0.603993	7.859699	59.4873
0.610843	8.013341	59.60923
0.617693	8.167129	59.70725
0.624543	8.321035	59.79407
0.631392	8.475047	59.87663
0.638242	8.629282	59.95153
0.645092	8.783493	60.01538
0.651942	8.937436	60.06843
0.658792	9.091246	60.11502
0.665642	9.24501	60.15732
0.672491	9.398611	60.18957
0.679341	9.551981	60.21589
0.686191	9.705567	60.24329
0.688691	9.761649	60.25399
0.692441	9.845789	60.27063
0.698066	9.972054	60.29293
0.706504	10.16153	60.32217
0.714941	10.3512	60.34532

0.721269	10.49345	60.36011
0.727597	10.6357	60.3746
0.733925	10.77807	60.38643
0.740254	10.92057	60.39502
0.746582	11.06312	60.40341
0.75291	11.20569	60.41052
0.759238	11.34826	60.41735
0.765566	11.49082	60.42364
0.771894	11.63338	60.42934
0.778222	11.77592	60.43611
0.78455	11.91847	60.44133
0.790879	12.06098	60.44753
0.797207	12.20348	60.45329
0.79958	12.25692	60.45516
0.803139	12.33707	60.45843
0.808479	12.4573	60.46274
0.816488	12.63764	60.46877
0.824497	12.81797	60.47438
0.832506	12.99833	60.47837
0.835006	13.05464	60.4793
0.838756	13.1391	60.48061
0.844381	13.26581	60.48139
0.852818	13.45589	60.48218
0.859146	13.59849	60.48185
0.865474	13.74112	60.48028
0.871803	13.88377	60.47744
0.873385	13.91944	60.47667
0.874967	13.9551	60.47602
0.87734	14.0086	60.47494
0.880899	14.08885	60.47241
0.881233	14.09637	60.47202
0.881734	14.10766	60.47155
0.882484	14.12458	60.47097
0.883611	14.14998	60.46994
0.8853	14.18807	60.46831
0.887834	14.24521	60.46592
0.888784	14.26664	60.465
0.888874	14.26865	60.46491
0.889007	14.27166	60.46476
0.889208	14.27618	60.46446
0.889508	14.28296	60.46411
0.889959	14.29313	60.4638
0.890636	14.30839	60.46327
0.891651	14.33127	60.46218
0.893173	14.3656	60.46032
0.895456	14.41709	60.45759

0.898881	14.49434	60.4536
0.904018	14.61023	60.44649
0.909156	14.72613	60.43823
0.914293	14.84204	60.42913
0.915577	14.87102	60.42666
0.916862	14.9	60.42413
0.918788	14.94347	60.42029
0.921678	15.00868	60.4145
0.926013	15.10652	60.40509
0.930347	15.20437	60.39474
0.934682	15.30222	60.38316
0.941184	15.44902	60.36473
0.943622	15.50408	60.35741
0.94728	15.58667	60.34588
0.952766	15.71058	60.32713
0.954823	15.75705	60.31982
0.957909	15.82677	60.30864
0.962538	15.93135	60.29074
0.969481	16.08822	60.26242
0.974688	16.20587	60.2423
0.979896	16.32352	60.22276
0.987707	16.50001	60.19107
0.995518	16.67651	60.15627
1.003329	16.85301	60.11795
1.011141	17.02943	60.08077
1.018952	17.20583	60.04388
1.026763	17.38227	60.00793
1.034574	17.55863	59.97395
1.040432	17.69086	59.94801
1.046291	17.82308	59.92163
1.052149	17.95532	59.89691
1.058008	18.08758	59.87155
1.063866	18.21981	59.8468
1.069724	18.35205	59.82333
1.075583	18.48427	59.80015
1.08437	18.68251	59.76594
1.090961	18.83116	59.74326
1.097552	18.97983	59.72235
1.100023	19.03558	59.71446
1.103731	19.11919	59.70264
1.109291	19.24458	59.68645
1.113462	19.33862	59.67523
1.119718	19.47966	59.65967
1.125974	19.6207	59.6433
1.13223	19.76176	59.62733
1.134576	19.81466	59.62114

1.138095	19.894	59.6115
1.143374	20.01301	59.59688
1.151291	20.19164	59.57594
1.159209	20.3704	59.55454
1.167127	20.5491	59.53424
1.175045	20.72777	59.51573
1.179003	20.8171	59.50653
1.184942	20.9511	59.49333
1.187169	21.00134	59.48861
1.190509	21.07672	59.48225
1.195519	21.18978	59.47309
1.203035	21.35937	59.46027
1.210551	21.52893	59.44762
1.218066	21.69845	59.43502
1.220566	21.75483	59.43081
1.224316	21.8394	59.42443
1.229941	21.96625	59.41479
1.238379	22.15652	59.40055
1.246816	22.3468	59.3856
1.255254	22.53709	59.36988
1.265254	22.76263	59.35032
1.267754	22.81902	59.34509
1.271504	22.90359	59.33778
1.277129	23.03046	59.3262
1.285566	23.22079	59.30778
1.288066	23.27718	59.30198
1.291816	23.36179	59.29412
1.297441	23.48869	59.2832
1.305879	23.67903	59.26577
1.314316	23.8694	59.24734
1.316426	23.917	59.24243
1.31959	23.98839	59.23513
1.324336	24.09545	59.22425
1.331455	24.256	59.20782
1.333955	24.31238	59.2024
1.337705	24.39695	59.19462
1.34333	24.52381	59.18257
1.351768	24.7141	59.16516
1.354268	24.77049	59.1597
1.358018	24.85506	59.15158
1.363643	24.9819	59.13955
1.37208	25.1722	59.12289
1.380518	25.36253	59.10835
1.382627	25.41012	59.10477
1.385791	25.4815	59.09944
1.390537	25.5886	59.09131

1.397656	25.74925	59.07938
1.407656	25.975	59.06183
1.410156	26.03145	59.05722
1.413906	26.11615	59.05035
1.419531	26.24322	59.04026
1.421641	26.29087	59.03648
1.424805	26.36236	59.03081
1.429551	26.46959	59.02205
1.43667	26.63045	59.00845
1.43917	26.68692	59.00382
1.44292	26.77163	58.99721
1.448545	26.89869	58.98817
1.456982	27.0893	58.97565
1.459482	27.14577	58.97193
1.463232	27.23049	58.96612
1.468857	27.35757	58.9571
1.477295	27.5482	58.94346
1.479795	27.60468	58.93933
1.483545	27.68941	58.93355
1.48917	27.81647	58.92544
1.497607	28.00708	58.9131
1.5	28.06113	58.9097

Appendix C

Figures C.1- C.16 present the bond-slip response for the tests which are repeated for each category of parameters.

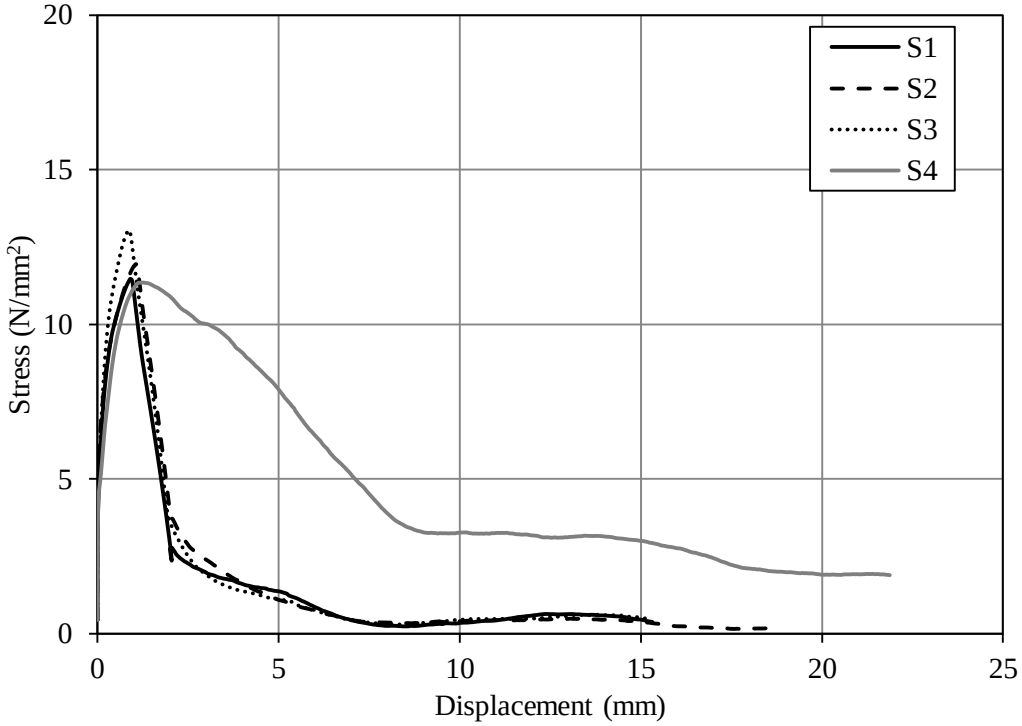

Fig. C. 1: Splitting bond stress-slip curves for stainless steel reinforcements with 10 mm diameter and 20 MPa concrete strength.

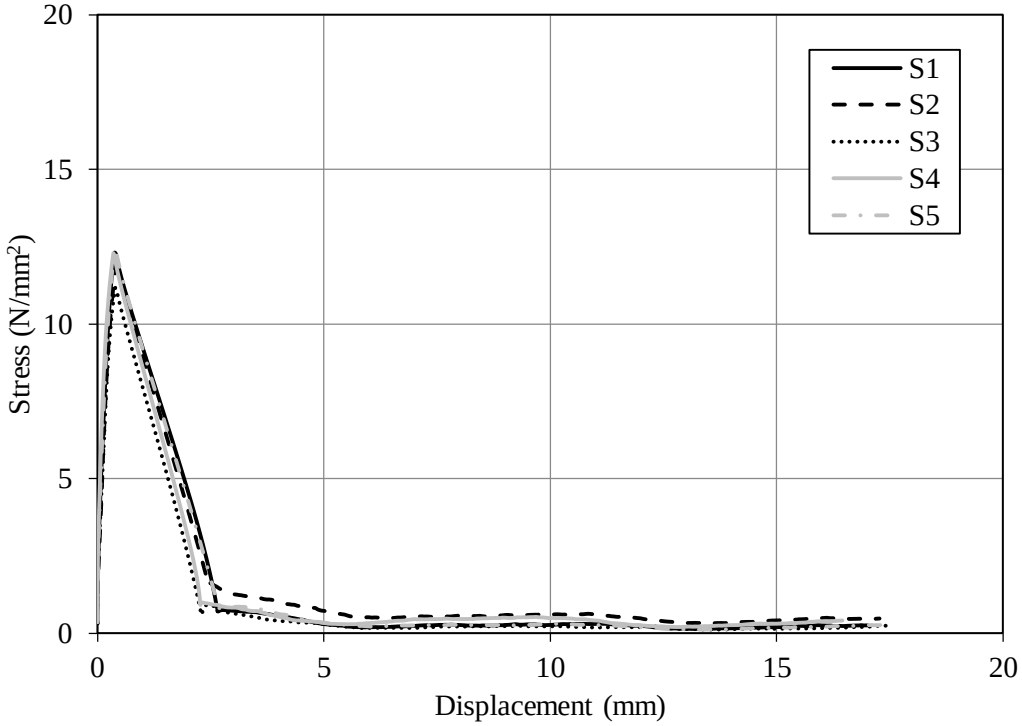

Fig. C. 2: Splitting bond stress-slip curves for stainless steel reinforcements with 12 mm diameter and 20 MPa concrete strength.

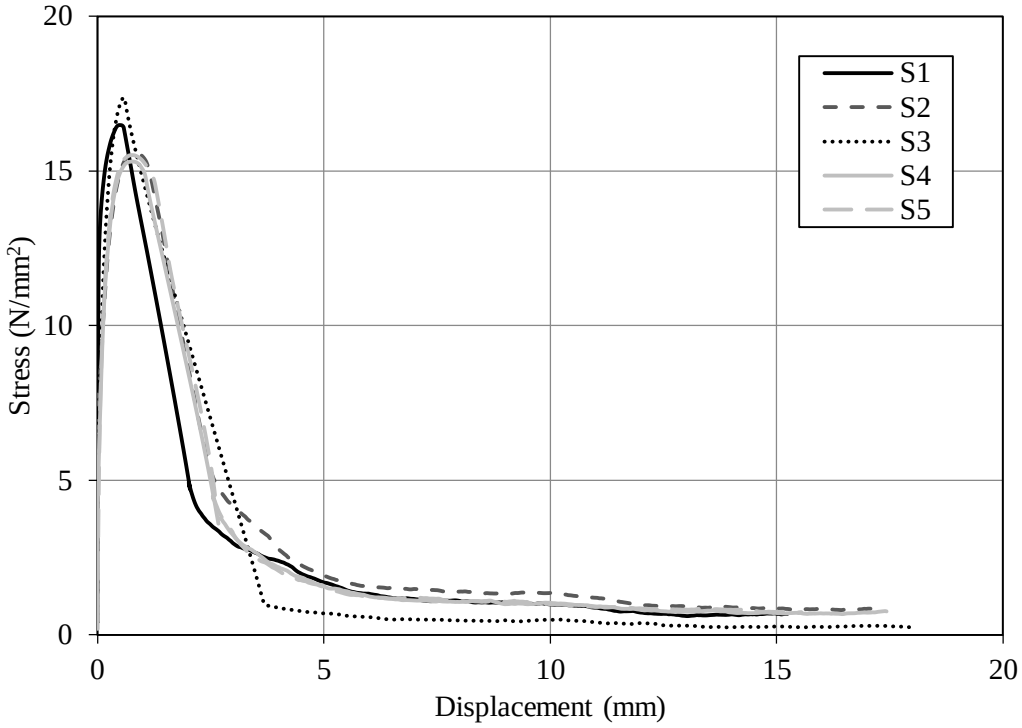

Fig. C. 3: Splitting bond stress-slip curves for carbon steel reinforcements with 10 mm diameter and 20 MPa concrete strength.

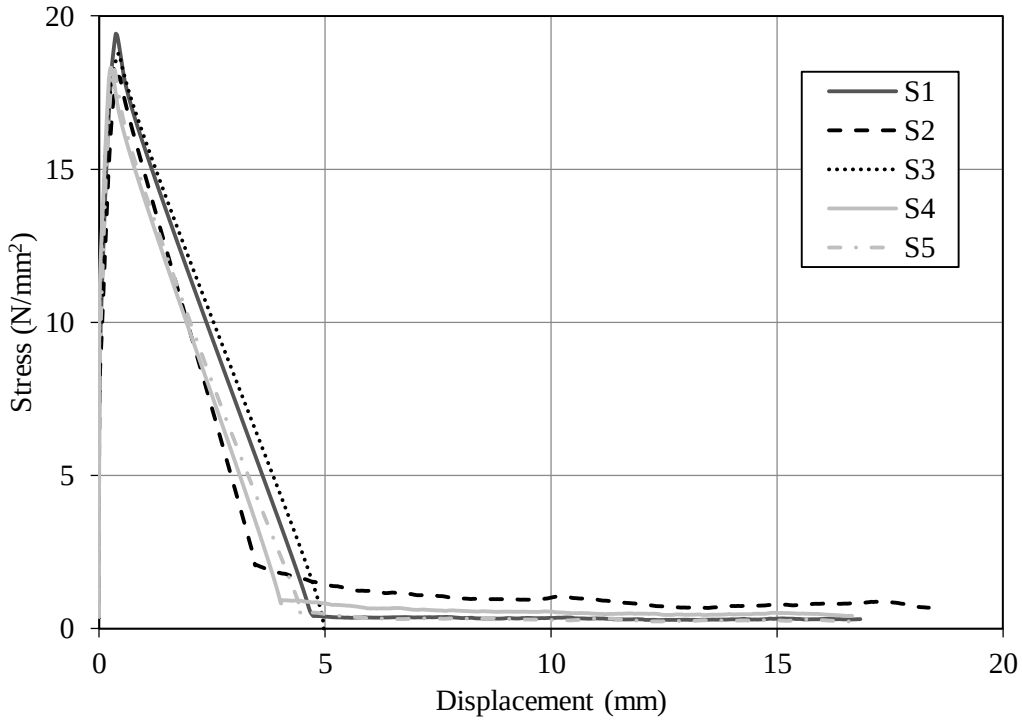

Fig. C. 4: Splitting bond stress-slip curves for carbon steel reinforcements with 12 mm diameter and 20 MPa concrete strength.

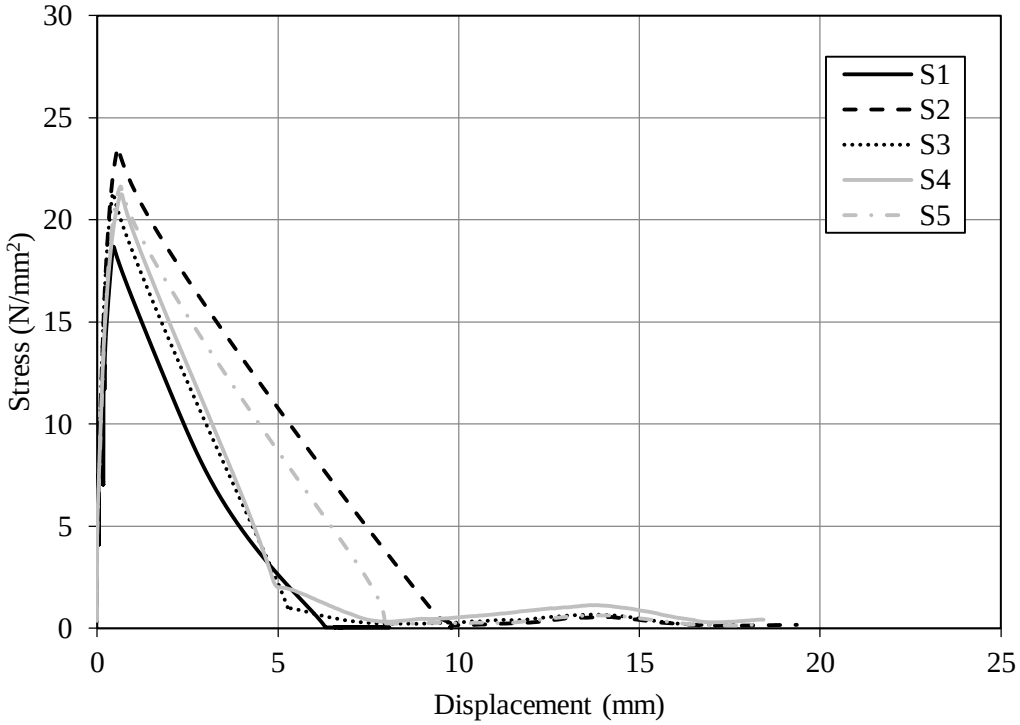

Fig. C. 5: Splitting bond stress-slip curves for stainless steel reinforcements with 10 mm diameter and 40 MPa concrete strength.

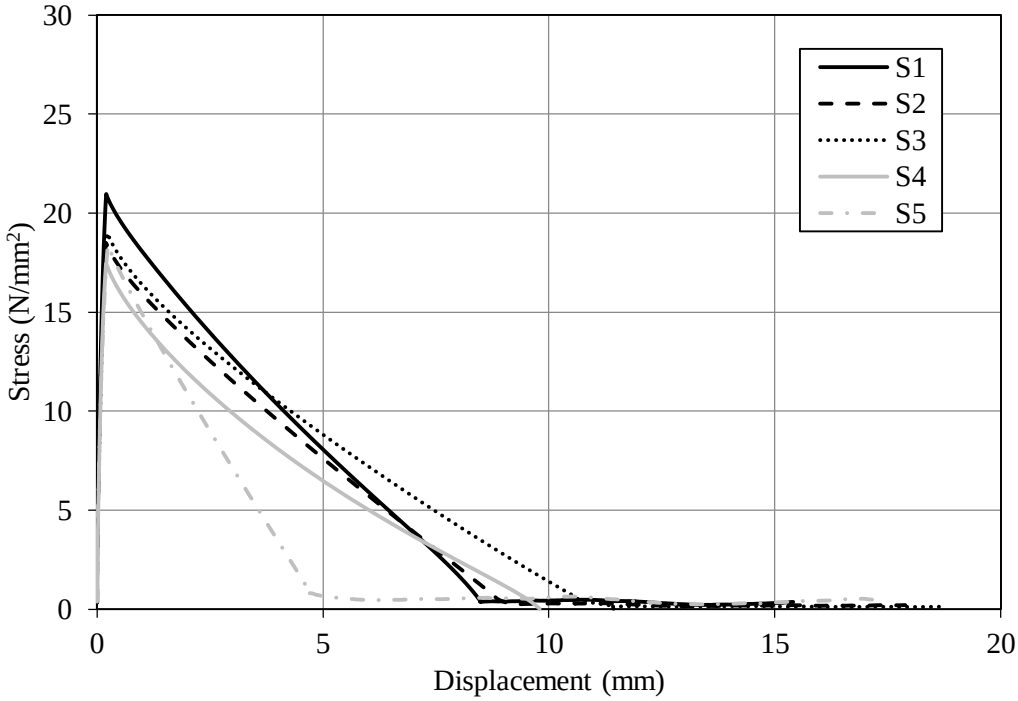

Fig. C. 6: Splitting bond stress-slip curves for stainless steel reinforcements with 12 mm diameter and 40 MPa concrete strength.

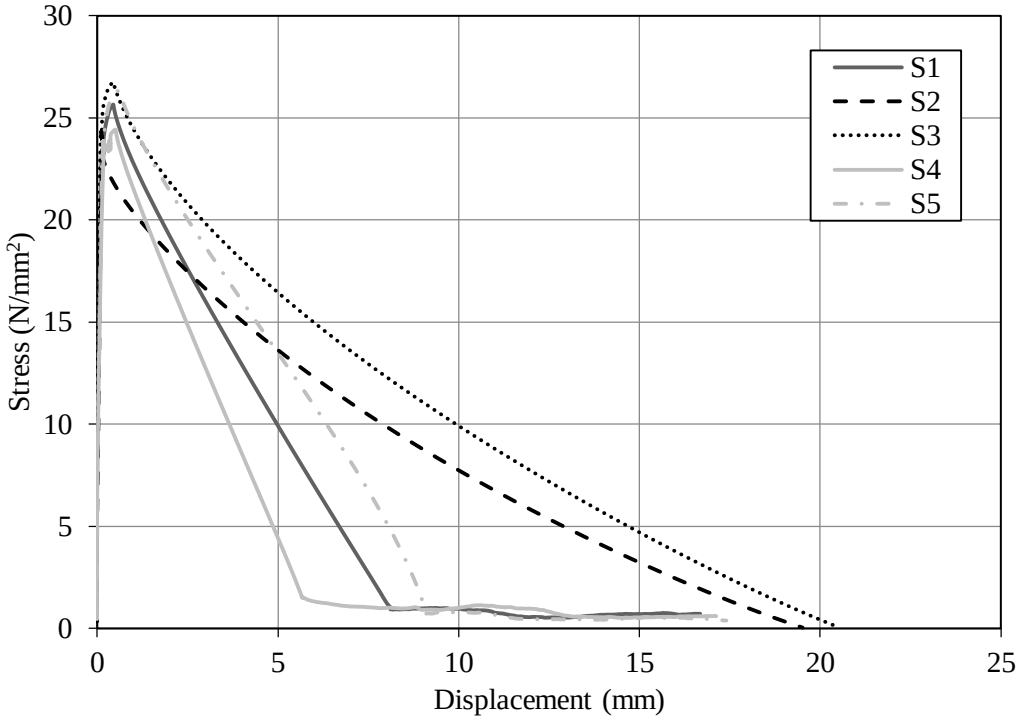

Fig. C. 7: Splitting bond stress-slip curves for carbon steel reinforcements with 10 mm diameter and 40 MPa concrete strength.

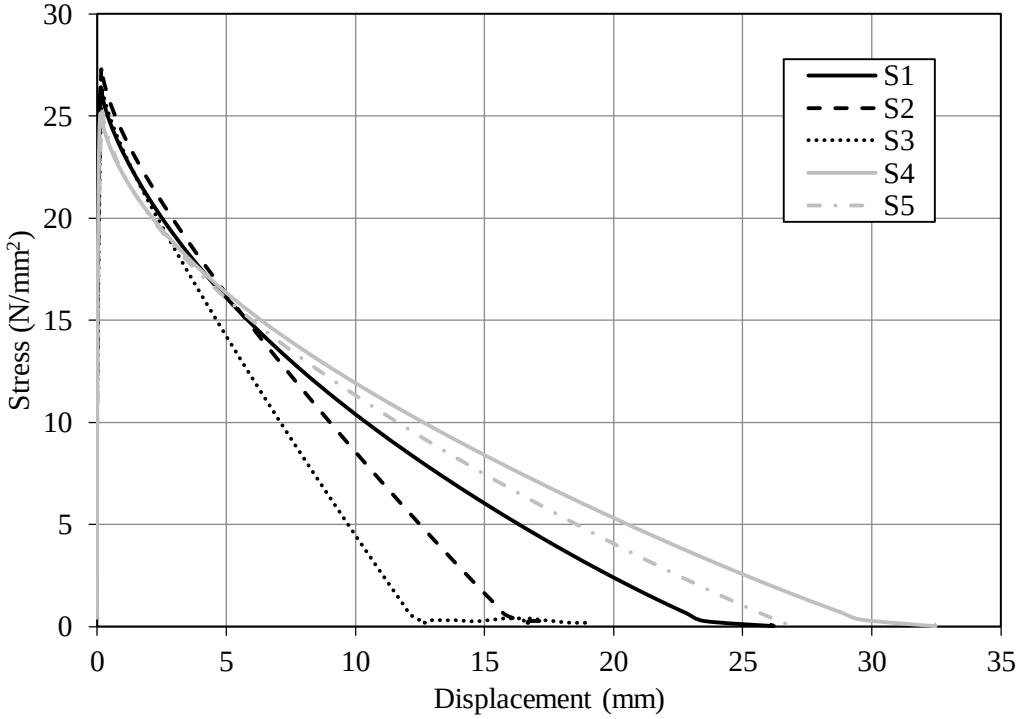

Fig. C. 8: Splitting bond stress-slip curves for carbon steel reinforcements with 12 mm diameter and 40 MPa concrete strength.

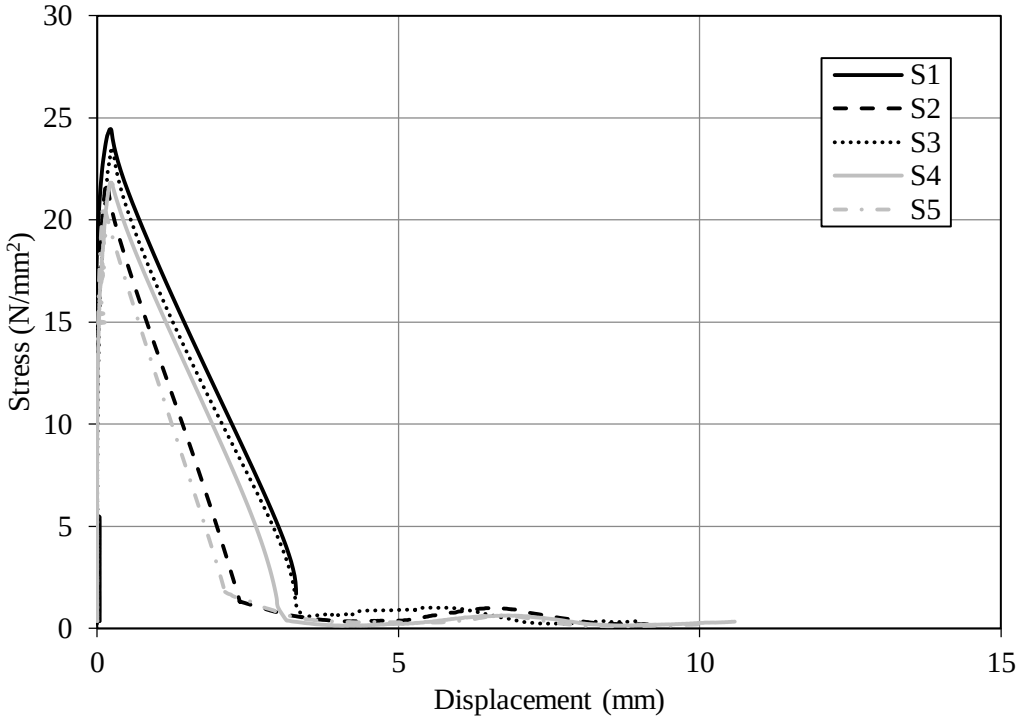

Fig. C. 9: Splitting bond stress-slip curves for stainless steel reinforcements with 10 mm diameter and 60 MPa concrete strength.

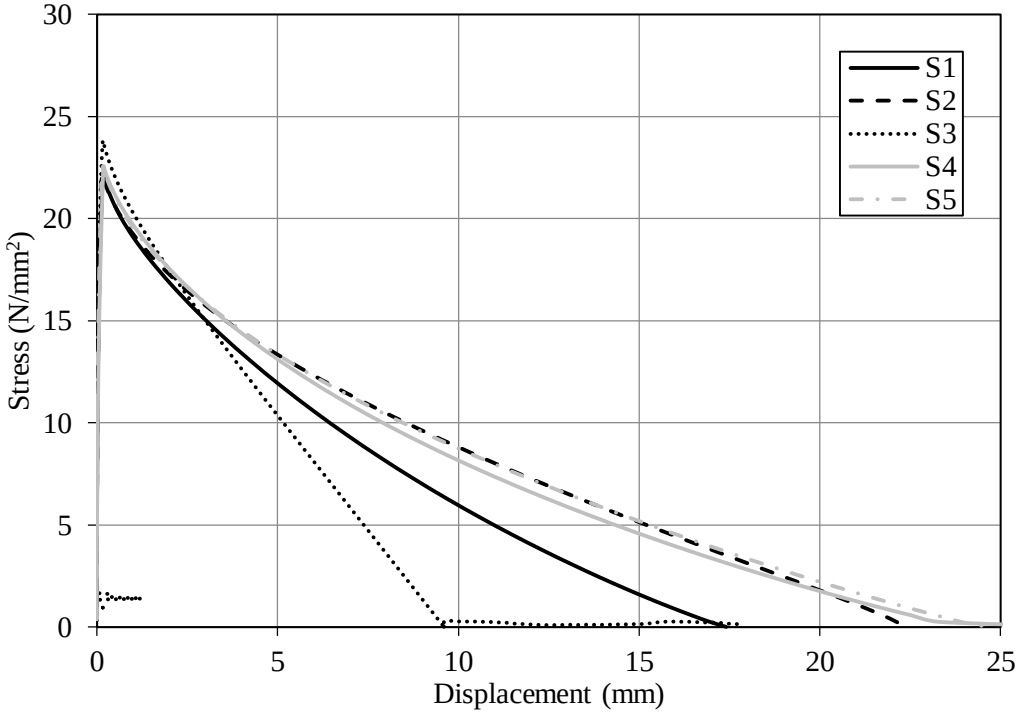

Fig. C. 10: Splitting bond stress-slip curves for stainless steel reinforcements with 12 mm diameter and 60 MPa concrete strength.

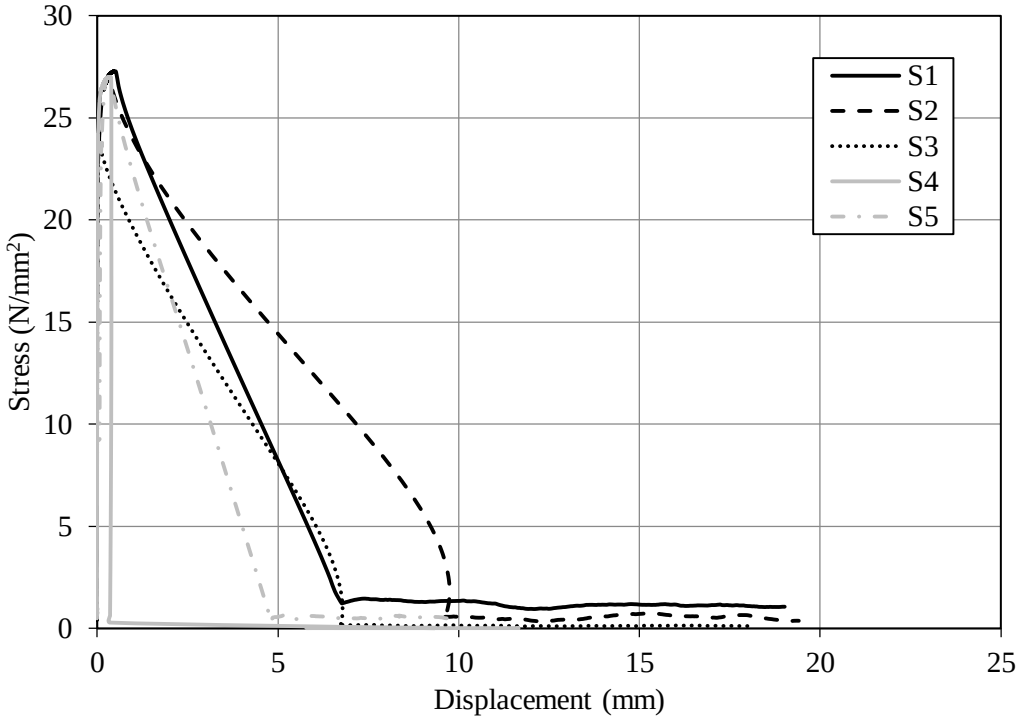

Fig. C. 11: Splitting bond stress-slip curves for carbon steel reinforcements with 10 mm diameter and 60 MPa concrete strength.

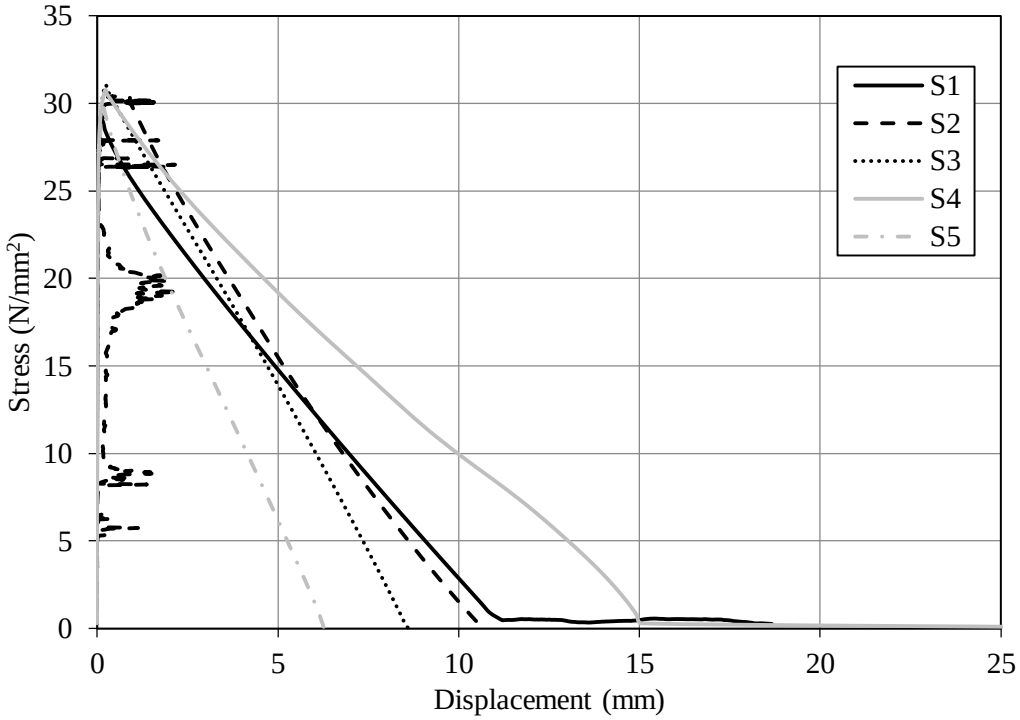

Fig. C. 12: Splitting bond stress-slip curves for carbon steel reinforcements with 12 mm diameter and 60 MPa concrete strength.

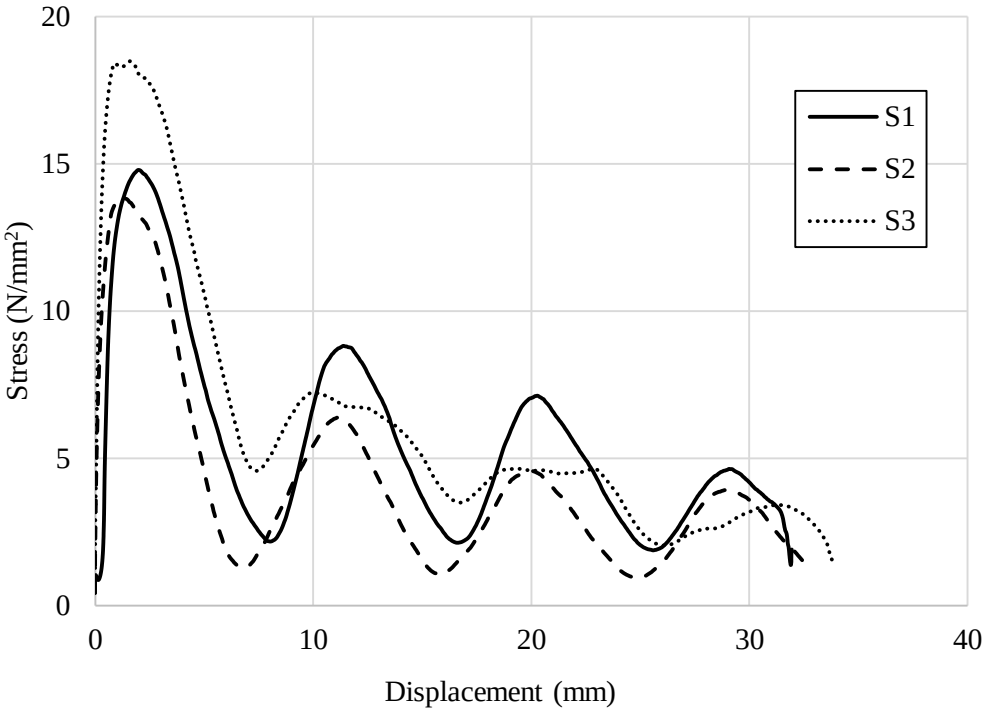

Fig. C. 13: Pull-out bond stress-slip curves for stainless steel reinforcements with 10 mm diameter and 40 MPa concrete strength.

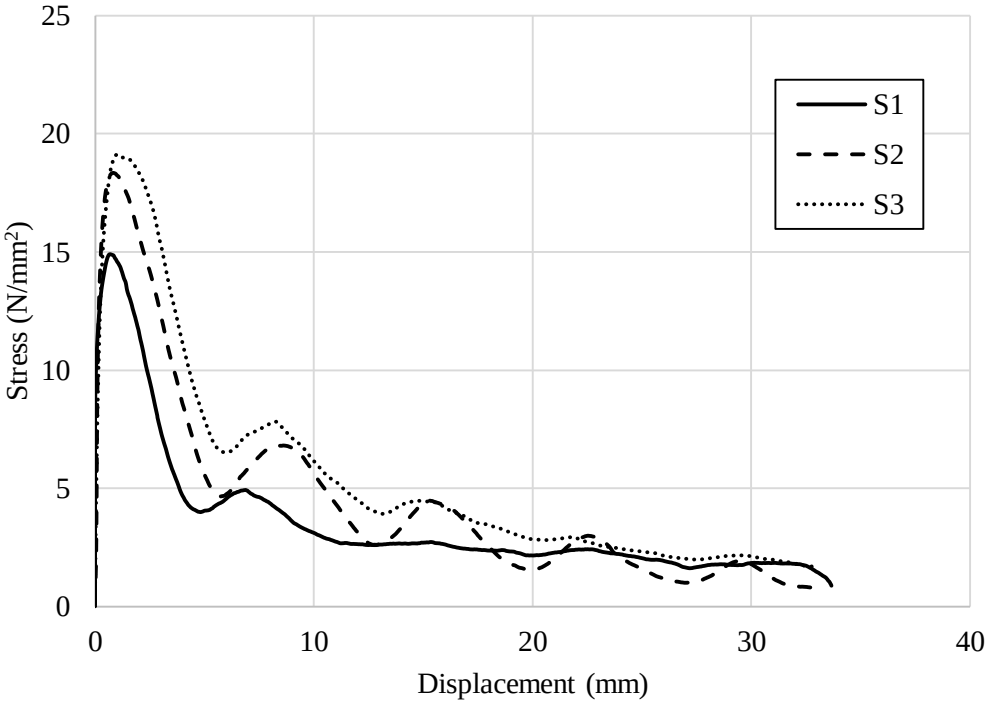

Fig. C. 14: Pull-out bond stress-slip curves for stainless steel reinforcements with 12 mm diameter and 40 MPa concrete strength.

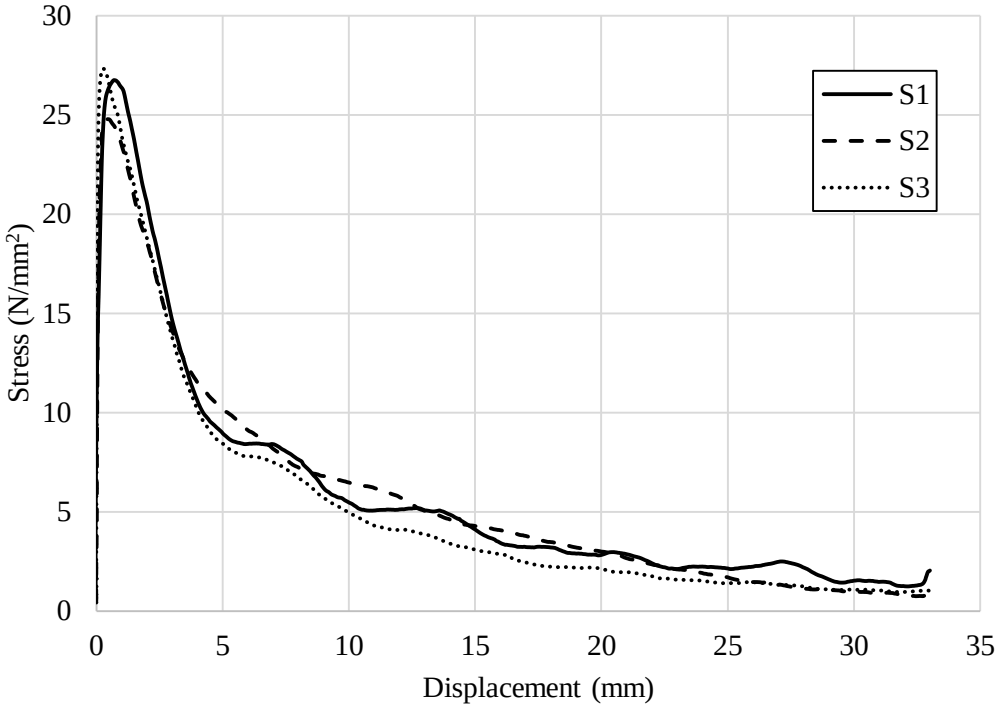

Fig. C. 15: Pull-out bond stress-slip curves for carbon steel reinforcements with 10 mm diameter and 40 MPa concrete strength.

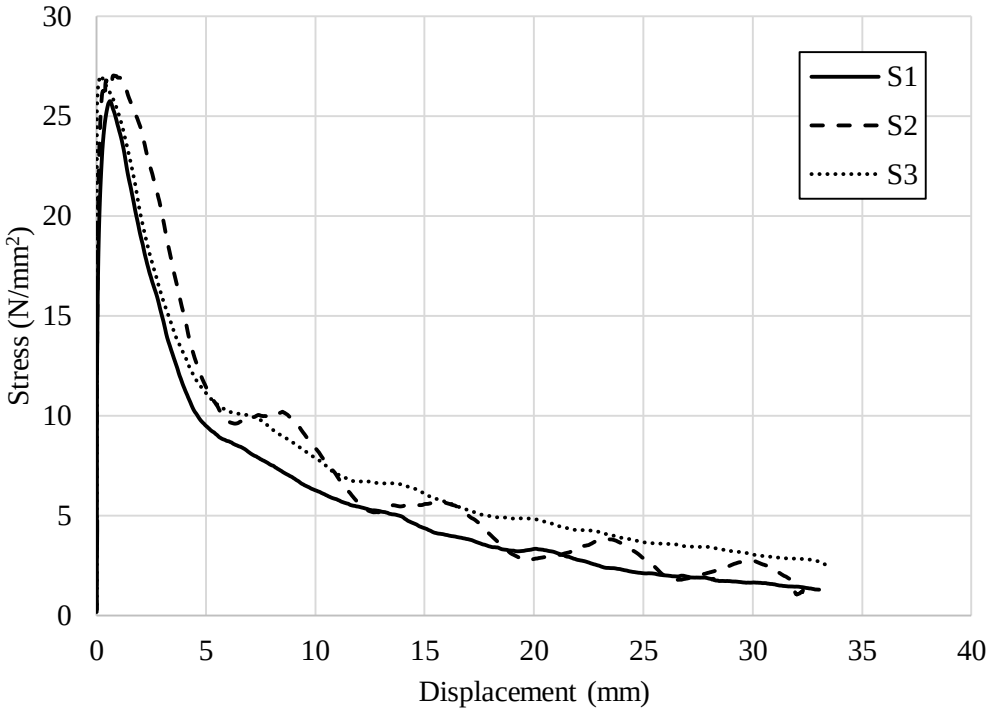

Fig. C. 16: Pull-out bond stress-slip curves for carbon steel reinforcements with 12 mm diameter and 40 MPa concrete strength.